

**Optimized non-invasive quantification of neuronal receptors
in healthy condition and psychiatric disorders
using positron emission tomography**

Doctoral thesis at the Medical University of Vienna
in the program Clinical Neurosciences
for obtaining the academic degree

Doctor of Medical Science

submitted by
Andreas Hahn, MSc.

supervision by
Rupert Lanzenberger, Assoc. Prof. PD MD

Functional, Molecular and Translational Neuroimaging Lab – PET & MRI
Department of Psychiatry and Psychotherapy
Medical University of Vienna
Waehringer Guertel 18-20, 1090 Vienna, Austria
<http://www.meduniwien.ac.at/neuroimaging/>

Vienna, July 2012

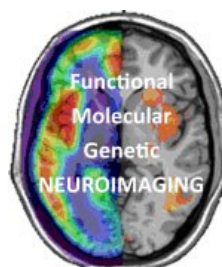


TABLE of CONTENTS

I. ABSTRACT	3
II. KURZFASSUNG	4
III. ACKNOWLEDGEMENTS	5
IV. LIST of PUBLICATIONS and PROJECT FUNDING	6
V. GLOSSARY	7
1. BACKGROUND	8
1.1. The role of serotonin in psychiatry	8
1.2. Positron emission tomography (PET)	10
1.3. Quantification of PET data	12
1.4. Arterial input function	15
1.5. Reference region models	16
1.6. Image-derived input functions	17
2. AIMS of the THESIS	18
3. SUMMARY of METHODOLOGY and RESULTS	19
3.1. Metabolite analysis of [<i>carbonyl</i> - ¹¹ C]WAY-100635	19
3.2. Image-derived input functions in healthy subjects	24
3.3. Application of image-derived input functions in patients with major depression	30
4. CONCLUSIONS and FUTURE PERSPECTIVES	35
5. REFERENCES	38
6. PUBLICATIONS	48
APPENDIX A – CURRICULUM VITAE	117

I. ABSTRACT

Positron emission tomography (PET) offers an excellent possibility to quantify proteins, such as receptors and transporters, in the living human brain. The *gold standard* for this quantification procedure is given by the arterial input function with the advantages of fewest modeling assumptions and independence of nonspecific binding. However, arterial cannulation is a laborious and demanding procedure which includes additional discomfort for the patient. Based on reference regions, several non-invasive modeling techniques have been applied with great success but their usage may be limited due to the underlying assumptions, especially within clinical comparisons and longitudinal designs. Image-derived input functions (IDIF) are extracted directly from PET images, hence, they represent a promising alternative to arterial blood sampling while maintaining independence of a reference region. However, various issues such as a robust definition of the input function and full substitution of manual arterial samples have complicated their application as a tool in clinical routine and research.

Here, we developed a novel combination of image-derived and venous input functions for the quantification of the major inhibitory serotonergic receptor (serotonin-1A, 5-HT_{1A}) with the radioligand [*carbonyl*-¹¹C]WAY-100635. The implementation of an optimized metabolite analysis showed excellent reproducibility of arterial by venous manual blood samples, enabling full independence of arterial cannulation. Quantification of 5-HT_{1A} receptor binding potentials (BP_P) resulted in strong agreement between the introduced approach and the arterial input function in healthy subjects before ($R^2=0.95$) and after 8 weeks of hormone replacement therapy ($R^2=0.93$). Subsequent application of image-derived and venous input functions on a high resolution PET scanner in patients with major depression confirmed a widespread 30% decrease in 5-HT_{1A} receptor binding (BP_{ND} and BP_P) after electroconvulsive therapy.

To summarize, the combination of image-derived and venous input functions offers quantification of 5-HT_{1A} receptor binding potentials entirely independent of arterial blood sampling. Importantly, reliable results were obtained for different study populations (healthy controls and patients with major depression), treatments (no intervention, pharmacological and electroconvulsive therapy), kinetic modeling approaches (regions of interest- and voxel-based) and PET scanners (standard and high resolution tomographs). The introduced technique offers great potential for application in clinical routine and research protocols and the thorough investigation within different settings encourages for further extension to other radioligands.

II. KURZFASSUNG

Die Positronenemissionstomographie (PET) bietet eine ausgezeichnete Möglichkeit Proteine wie Rezeptoren und Transporter im Gehirn des lebenden Menschen zu messen. Der Goldstandard für diese Quantifizierung ist die arterielle Inputfunktion, welche zwar die wenigsten Modellannahmen benötigt jedoch technisch aufwändig ist und eine zusätzliche Belastung für den Patienten darstellt. Basierend auf Referenzregionen konnten nicht-invasive Methoden bereits erfolgreich angewendet werden, wobei jedoch die zugrunde liegenden Annahmen mögliche Einschränkungen, speziell für Gruppenvergleiche und Longitudinalstudien, darstellen. Eine vielversprechende Alternative zur arteriellen Blutentnahme bei gleichzeitiger Unabhängigkeit von Referenzregionen bieten direkt aus den PET Bilddaten gewonnene Inputfunktionen. Verschiedene Probleme wie die robuste Definition dieser Inputfunktion sowie die vollständige Vermeidung arterieller Blutproben erschwerten jedoch deren Anwendung in der klinischen Routine und bei Studien.

Mit dieser Arbeit wurde eine neue Kombination von Inputfunktionen aus Bilddaten und venösen Blutproben für die Quantifizierung des wichtigsten inhibitorischen Serotoninrezeptors (Serotonin-1A, 5-HT_{1A}) mit dem Radioliganden [*carbonyl*-¹¹C]WAY-100635 entwickelt. Die Implementierung einer optimierten Metabolitenanalyse zeigte ausgezeichnete Reproduzierbarkeit von arteriellen durch venöse Blutproben und ermöglicht daher den Verzicht auf arterielle Blutentnahmen. Die Quantifizierung des 5-HT_{1A} Rezeptorbindungspotentials (BP_P) ergab eine starke Übereinstimmung zwischen dem hier neu entwickelten Ansatz und der arteriellen Inputfunktion für gesunde Probanden vor ($R^2=0.95$) und nach achtwöchiger Hormonersatztherapie ($R^2=0.93$). Die folgende Anwendung der Methode mit einem hochauflösenden PET Scanner und depressiven Patienten bestätigte eine weitgehende Verminderung der 5-HT_{1A} Rezeptorbindung um etwa 30% (BP_{ND} und BP_P) nach Elektrokonvulsionstherapie.

Zusammenfassend bietet die Kombination von Inputfunktionen aus Bilddaten und venösen Blutproben eine robuste Quantifizierung des 5-HT_{1A} Rezeptors unabhängig von arteriellen Blutproben. Die Methode ergab zuverlässige Ergebnisse für verschiedene Populationsgruppen (gesunden Probanden und depressive Patienten), Behandlungsarten (keine, pharmakologische und elektrokonvulsive Therapie), Modelle (zielregionenbasiert und voxel-weise) sowie PET Scanner (standard und hochaufgelöst). Die vorgestellte Technik bietet vielversprechende Möglichkeiten für Anwendungen in der klinischen Routine und Forschung und regt durch die vielfältige Validierung unter verschiedenen Bedingungen zur weiteren Implementierung für andere Radioliganden an.

III. ACKNOWLEDGEMENTS

This work has not been conducted alone but accomplished by a well-balanced concert of several persons. Each of them contributed with their professional expertise and continuous motivation, which altogether resulted in a great progress throughout the last years.

I would like to express my gratitude to Rupert Lanzenberger, Prof MD, for his supervision of this thesis and the possibility to contribute to the research within the *Functional, Molecular and Translational Neuroimaging Lab*, his scientific and personal support as well as countless creative discussions. In addition, I would like to thank the two members of my thesis committee, Richard Frey, Prof MD, and Wolfgang Birkfellner, Prof PhD, for their supervision and assistance regarding medical, statistical and technical issues. Furthermore, great thanks go to Siegfried Kasper, Prof MD, for the possibility to conduct research at the Department of Psychiatry and Psychotherapy. Also, I would like to acknowledge the continuous encouragement throughout my doctoral studies from the coordinator of the PhD program *Clinical Neurosciences* Johannes Hainfellner, Prof MD, Institute of Neurology.

Special thanks go to Lukas Nics, MSc, Markus Mitterhauser, Prof PhD, and Wolfgang Wadsak, Prof PhD, from the Department of Nuclear Medicine for the great collaboration and the development of the metabolite assay.

Furthermore, I would like to thank Ramin Parsey, Prof MD, Columbia University, New York, USA, for the support considering modeling, metabolite analysis and fruitful discussions.

I am grateful to the entire team of the *Functional, Molecular and Translational Neuroimaging Lab*, especially to Pia Baldinger, Christoph Kraus, Anna Höflich and Irmgard Hofer-Irmler for their medical support as well as Markus Savli and Georg Kranz for help regarding kinetic modeling and statistics, respectively.

In addition, I would like to thank the Austrian Academy of Sciences (OeAW) for the financial support and their help concerning project management.

Last but not least I would like to express my deepest gratitude to the ones who encounter my views with great understanding and constructive critics at the same time, the ones who encourage my work while helping me to keep sight of essential issues – my family and my friends.

IV. LIST of PUBLICATIONS and PROJECT FUNDING

Publications

Hahn A.*, Nics L.*, Baldinger P., Ungersböck J., Dolliner P., Frey R., Birkfellner W., Mitterhauser M., Wadsak W., Karanikas G., Kasper S., Lanzenberger R. 2012. Combining image-derived and venous input functions enables quantification of serotonin-1A receptors with [*carbonyl*-¹¹C]WAY-100635 independent of arterial sampling. *NeuroImage* 62(1): 199-206. [2011, IF: 5.895] *Contributed equally.

Hahn A., Nics L., Baldinger P., Wadsak W., Savli M., Kraus C., Birkfellner W., Ungersböck J., Haeusler D., Mitterhauser M., Karanikas G., Kasper S., Frey R., Lanzenberger R. 2012. Clinical application of image-derived and venous input functions in major depression using [*carbonyl*-¹¹C]WAY-100635. *European Journal of Nuclear Medicine and Molecular Imaging* Submitted. [2011, IF: 4.991]

Nics L., **Hahn A.**, Zeilinger M., Vraka C., Ungersboeck J., Haeusler D., Hartmann S., Wagner K-H., Dudczak R., Lanzenberger R., Wadsak W., Mitterhauser M. 2012. Quantification of the radio metabolites of the serotonin-1A receptor radioligand [*carbonyl*-¹¹C]WAY-100635 in human plasma: An HPLC-assay allowing two parallel patients. *Applied Radiation and Isotopes* Submitted. [2011, IF: 1.172]

Related publications

Hahn A., Wadsak W., Windischberger C., Baldinger P., Höflich AS., Losak J., Nics L., Philippe C., Kranz GS., Kraus C., Mitterhauser M., Karanikas G., Kasper S., Lanzenberger R. 2012. Differential modulation of self-referential processing in the default mode network via serotonin-1A receptors. *Proceedings of the National Academy of Sciences USA* 109(7): 2619-2624 [2011, IF: 9.681].

Hahn A., Lanzenberger R., Spindelegger C., Moser U., Mien L.-K., Mitterhauser M., Wadsak W., Kasper S.. 2010. Escitalopram enhances the association of serotonin-1A auto- to heteroreceptors in anxiety disorders. *Journal of Neuroscience* 30 (43): 14482-89. [2011, IF:7.115].

Lanzenberger R., Baldinger P., **Hahn A.**, Haeusler D., Mitterhauser M., Winkler D., Micskei Z., Stein P., Karanikas G., Wadsak W., Kasper S., Frey R. 2012. Global decrease of serotonin-1A receptor binding after electroconvulsive therapy in major depression revealed by PET. *Molecular Psychiatry* In Press. [2011, IF: 13.668].

Project funding

A. Hahn is recipient of a DOC-fellowship of the Austrian Academy of Sciences (OeAW) at the Department of Psychiatry and Psychotherapy. The clinical research projects were supported by grants from the Austrian National Bank (OeNB 12809 and 13219), and a grant by the Brain and Behavior Research Foundation, USA (NARSAD) to R. Lanzenberger.

V. GLOSSARY

Arterial input function (AIF) – The gold standard for the quantification of PET data with kinetic modeling. It describes the amount of intact radioligand in arterial plasma, which is available for transport across the blood brain barrier into brain tissue.

Binding potential (BP) – The ratio of receptor density and the dissociation constant, the latter being the reciprocal of the affinity. Since affinity is mostly assumed to be constant, the binding potential is an indirect measure for receptor density. The three different types of binding potential are related to free radioligand in plasma (BP_F), total radioligand in plasma (BP_P) and non-displaceable radioligand in tissue (BP_{ND}). The binding potential can also be described as the ratio of specifically bound and free radioligand.

Electroconvulsive therapy (ECT) – The application of an electric shock under short anesthesia to evoke a generalized epileptic seizure in a controlled setting. For patients suffering from treatment-resistant depression this represents an effective treatment option.

Image-derived input function (IDIF) – A non-invasive alternative to arterial blood sampling for the definition of the modeling input function required for kinetic modeling. IDIFs are usually extracted from blood vessels directly visible within the PET images.

Positron emission tomography (PET) – An imaging modality from the field of nuclear medicine. The incorporation of a positron emitting radioligand enables visualization and quantification of tissues and/or proteins through the specific binding characteristics of the radioligand.

Radioligand – The radiation source used for PET and SPECT. In addition to the positron emitting isotope, it contains the biological tracer molecule, which defines the binding characteristics for the target protein or tissue.

Serotonin (5-hydroxytryptamine, 5-HT) – A neurotransmitter of the central nervous system, which is involved in the pathophysiology and treatment of several psychiatric disorders.

Volume of distribution – Within PET quantification, it relates the radioligand concentration in a given tissue to that of blood plasma. The three different types describe the total (V_T), specific (V_S) and non-displaceable (V_{ND}) volume of distribution. Hence, V_S equals BP_P , describing the ratio of specifically bound radioligand to that in plasma.

1. BACKGROUND

1.1. The role of serotonin in psychiatry

The neurotransmitter serotonin (5-hydroxytryptamine, 5-HT) plays a key role in the regulation of several functions of the central nervous system [1]. This includes neuronal development and plasticity [2, 3] as well as basic physiological functions such as hormone release [4-6], appetite, regulation of blood pressure and body temperature. Moreover, serotonin is involved in modulation of psychological and behavioral aspects like reward modulation [7], aggression [8], perception of pain and emotional behavior [1]. These distinct physiological functions are mediated by at least 14 receptor subtypes and the serotonin transporter which have been identified within the serotonergic neurotransmitter system [9]. These receptors are grouped into 7 families according to their signaling mechanisms [10] and differ substantially in their genetic, pharmacological, functional and topological aspects [9]. An important example is given by the serotonin-1A receptor (5-HT_{1A}), the main inhibitory serotonin receptor subtype, considering its dual expression pattern within the brain (figure 1). Serotonin neurons originate in the midbrain raphe nuclei where 5-HT_{1A} receptors are mostly located on the cell bodies of these neurons [11] and hence have an autoinhibitory function [1]. Activation of these autoreceptors inhibits serotonergic cell firing [12, 13] which in turn decreases 5-HT release at terminal nerve ends [14, 15]. In the projection areas 5-HT_{1A} receptors are expressed as heteroreceptors on non-serotonergic neurons, such as glutamate and GABA neurons, and inhibit postsynaptic cell firing [1, 10]. The signaling pathways of 5-HT_{1A} receptors are defined by their coupling to inhibitory G proteins as well as activation of the growth factor pathways of mitogen-activated protein kinases (MAPK) and Akt [10].

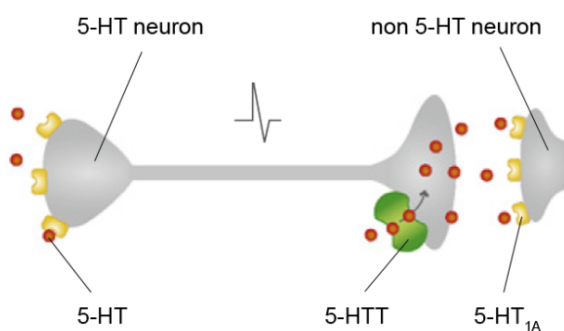


Figure 1: Schematic representation of serotonin-1A receptor (5-HT_{1A}) signaling. 5-HT_{1A} autoreceptors in the midbrain raphe nuclei are located somatodendritically on 5-HT neurons inhibiting cell firing and serotonin release. In contrast, within projection areas 5-HT_{1A} heteroreceptors are expressed on glutamate and GABA neurons where they inhibit postsynaptic cell firing. The serotonin transporter (5-HTT) serves for 5-HT reuptake into the presynaptic neuron. Figure adapted from Richardson Jones et al. [16].

Considering the variety of physiological and behavioral regulatory functions of serotonin it is not surprising that alterations of this neurotransmitter system have been associated with a variety of psychiatric and neurological disorders. Examples include but are not limited to affective [17-20] and anxiety disorders [21, 22], addiction [23] and temporal lobe epilepsy [24]. Adequate treatment of these disorders will become a major challenge in the future considering the substantial burden to the patients themselves and families but also to the society. Recent figures estimate the costs of brain disorders to almost € 800 billion per year with mood and anxiety disorders accounting for almost one quarter [25]. This estimate has doubled since 2005, whereas 40% of the costs are indirectly lost by decreased productivity of the patients. Importantly, the World Health Organization estimated the world-wide life-time incidence to exceed 25% when taking into account all mental and behavioral disorders classified by ICD-10 (international statistical classification of diseases and related health problems) [26].

The importance of research focusing on the serotonergic system in psychiatry is further reflected by the different pharmacological agents targeting the distinct binding sites. Selective serotonin reuptake inhibitors (SSRIs) represent one of the most common and effective treatment options [27, 28] with clinical improvements in affective [29-31], anxiety [32] and obsessive compulsive disorders (for review see Vaswani et al. [33]). The blockade of the serotonin transporter (5-HTT) increases the 5-HT level in the synaptic cleft. Together with the desensitization of serotonin-1A autoreceptors in the midbrain raphe nuclei [34] this leads to an increased serotonergic neurotransmission [35]. On the other hand, several other serotonin receptors are secondarily affected by SSRI treatment [36-38]. However, a sustained response may not be achieved for selected patients. One alternative for treatment-resistant patients suffering from major depressive disorder (MDD) is given by electroconvulsive therapy (ECT), which provides increased treatment efficacy [39, 40]. Interestingly, similar effects to SSRI treatment have been observed after electroconvulsive therapy regarding the serotonin-1A [41] and -2A receptors [42].

Although these treatments definitely represent important therapeutic intervention, the aforementioned findings only give first indications on the underlying biological effects whereas the exact mechanisms are far from understood. Positron emission tomography (PET) and single photon emission computed tomography (SPECT) offer the unique opportunity to quantify these neuronal binding sites in the living human brain.

1.2. Positron emission tomography (PET)

Positron emission tomography is an imaging modality from the field of nuclear medicine and molecular imaging. The main advantage of this technique is that specific functional information is obtained [43, 44]. This is achieved by incorporation of a so-called radioligand. Hence, the radiation source is inside the patient in contrast to e.g., computed tomography (CT, where an x-ray source and the corresponding detector field are rotated around the patient). The radioligand consists of two main parts, the radioactive isotope and the biological tracer [43, 44]. Within PET the first one is obviously a positron emitter which mostly exhibits a rather short half-life such as 109.8min for ^{18}F , 20.4min for ^{11}C , 10min for ^{13}N or even 2min for ^{15}O . Most of the radioligands labeled with ^{18}F can be purchased and transported, however, for the latter three isotopes an on-site cyclotron is required [43]. The emitted positron reacts with a near electron in a process called annihilation after travelling a short distance of approximately 1mm dependent on its energy (positron range) [45]. From the annihilation two photons each with an energy of 511keV are emitted in opposite directions ($180^\circ \pm 0.25^\circ$) [45]. These photons are then detected simultaneously (coincidence) by the detector ring, which is one of the main advantages in terms of sensitivity of PET compared to SPECT. The coincidence events are stored as sinograms and reconstructed to obtain the final image (figure 2) [46].

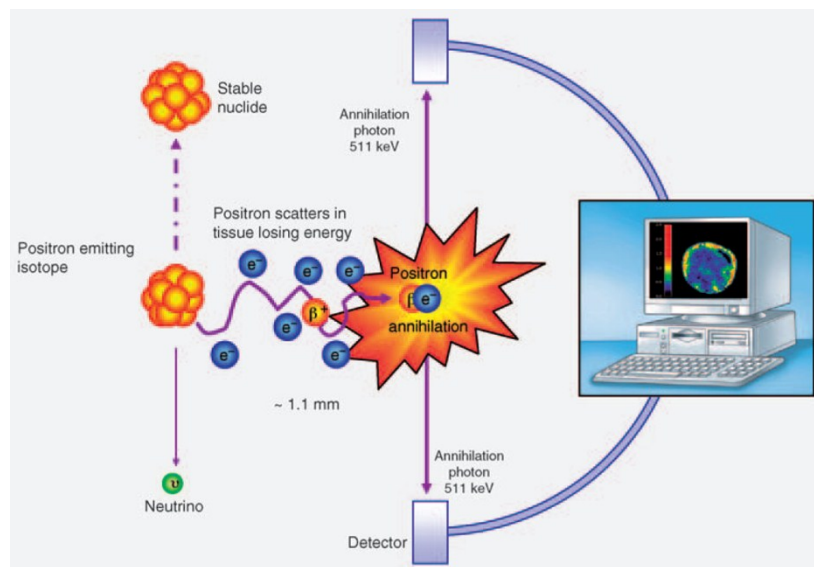


Figure 2: Measurement principle of positron emission tomography. After travelling of about 1mm (positron range) the emitted positron annihilates with a nearby electron. From this, two photons with 511keV each are emitted in opposite directions. The final image is reconstructed from the coincidence detection of these two photons by the scanner ring. Figure from Boellard [44].

In addition to the radioactive isotope, the second major part of the radioligand is the biological tracer. This determines its binding properties and can be roughly grouped into irreversible and reversible tracers. The most common example for an irreversible radioligand is [¹⁸F]FDG (2-[¹⁸F]-fluoro-2-deoxy-D-glucose). It is based on the irreversible trapping into the early reaction of the glucose metabolism and therefore represents an effective tool for tumor imaging [47] and states of altered energy consumption. However, for quantification of neuronal receptors and transporters a reversible interaction between the radioligand and binding site is desired for mathematical modeling of the binding equilibrium [48, 49] (see next section on quantification of PET data). Of note, the focus of this work concerns the quantification of neuronal binding sites within the brain, hence, the description and discussed characteristics are herein limited to radioligands used for brain imaging. The radioligand needs to meet several characteristics [48] which can be a challenging task for radiopharmacists and –chemists. First, it has to be non-toxic and cross the blood brain barrier via passive diffusion. Although useful exceptions such as [¹²³I]β-CIT for dopamine and serotonin transporter imaging exist, an ideal ligand binds to only one receptor subtype (i.e., high selectivity). The issue of affinity is somewhat more complicated. A high affinity of the radioligand to the receptor of interest is required for sufficient signal to noise ratio (1 – 0.01nM) [48]. However, increased affinity only results in improved image quality if the non-specific binding remains unchanged [48]. Use of a high affinity radioligand will also prolong the duration of the scan since the equilibrium state is reached later. This may become problematic in terms of counting statistics for isotopes with short half-life, patient comfort and the accompanying motion artifacts. Finally, a maximum of 5% receptor occupancy by the radioligand are generally considered not to violate linearity requirements for kinetic modeling (tracer doses) [48]. This is especially important for high affinity radioligands and implies that synthesis yields a sufficiently high specific activity and low mass dose. Another important parameter is the lipophilicity of the radioligand. Although certain lipophilicity is required to cross the blood brain barrier, high values will increase non-specific binding and decrease the amount of free ligand in plasma (plasma free fraction) [48]. Last but not least, it is desirable that radioligands experience slow metabolism, that radioactive metabolites do not cross the blood brain barrier or at least do not bind at the target protein.

One of the most promising radioligands for the serotonin-1A receptor is given by [*carbonyl*-¹¹C]WAY-100635 [50]. It shows sufficiently high affinity [50], specificity and selectivity [51]. The radioligand is rather insensitive to competition with endogenous serotonin [50] where only large changes may affect specific binding [52]. Compared to its forerunner [*O-methyl*-¹¹C]WAY-100635, labeling at the carbonyl site resulted in substantially increased signal to noise ratio since radioactive metabolites may not pass the blood brain barrier [53, 54] or bind

at the target receptor, if at all, only in small amounts [55]. Two disadvantages are the fast metabolism and the low plasma free fraction in humans [56]. Nevertheless, application of this ligand resulted in “exquisite delineation of 5-HT_{1A} receptors” [57, 58]. Finally, simplified techniques for synthesis of this complex radioligand have been implemented [59].

1.3. Quantification of PET data

Having established a radioligand which fulfills the aforementioned requirements, the successful PET measurement is followed by quantitative data analysis. A key term is the so-called binding potential (BP) [60] which has been introduced in 1984 [61]. It is defined by the ratio of receptor density B_{max} and the equilibrium dissociation constant K_D , whereas the latter equals the reciprocal of the affinity. Assuming K_D is constant for a given radioligand, the binding potential is directly proportional to receptor density [49]:

$$\text{Equ. 1} \quad BP = \frac{B_{max}}{K_D} = B_{max} * \textit{affinity}$$

The association comes from the Michaelis-Menten equation of *in vitro* reversible binding experiments [62]:

$$\text{Equ. 2} \quad k_{on}[L][R] = k_{off}[RL]$$

It describes the relationship between receptor R and ligand L forming the bound receptor-ligand complex RL at equilibrium with kinetic rate constants of association and dissociation k_{on} and k_{off} , respectively [49]. Equation 1 can be derived after substitution of k_{off}/k_{on} by K_D and $[R]+[RL]$ by B_{max} , rearrangement and following the assumption that the amount of incorporated radioligand L is very small compared to K_D [49]. In other words, the binding potential can also be seen as the ratio of specifically bound over free radioligand [60]. However, the aforementioned relationships are defined for the equilibrium state of association and dissociation between free ligand and receptor (equation 2). After a single bolus injection of a typical PET measurement the binding of the radioligand does usually not reach full equilibrium within the scanning time [49]. Still, the data obtained from the PET measurement contain sufficient information to infer binding parameters at earlier states using mathematical models. This is mostly done from a quasi-equilibrium, where the clearance rate of radioligand from blood plasma is the same as from tissue [63]. Figure 3 gives the compartment model used for quantification of receptor binding.

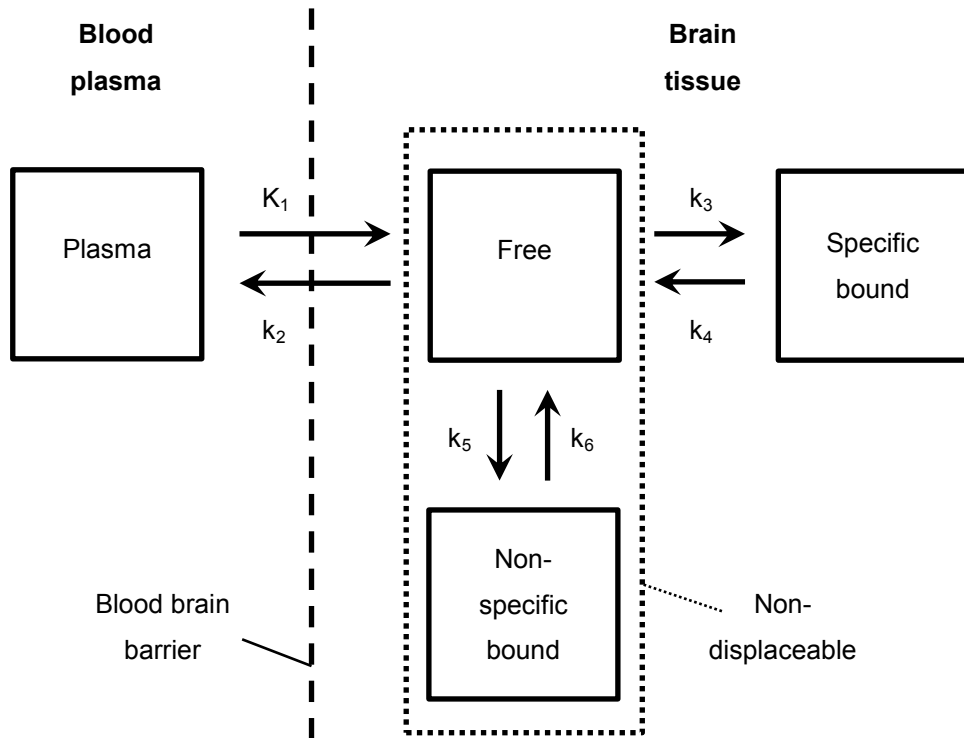


Figure 3: Compartment model configuration commonly used for kinetic modeling. The radioligand crosses the blood brain barrier from blood plasma into the brain tissue. There, it is available free within the tissue, specifically or non-specifically bound. Combination of the free and non-specific bound compartments to the non-displaceable one reduces the configuration from a three- to two-tissue compartment model. K_1 - k_6 represent rate constants which describe the transfer of the radioligand between the compartments. Figure adapted from Slifstein et al. [63].

The model shows one compartment in blood plasma and three within brain tissue. After crossing the blood brain barrier via passive diffusion [63], the radioligand binds specifically or non-specifically in the brain tissue. Specific binding sites are given by the target receptor whereas non-specific binding includes all other forms of binding to, e.g., other receptors, cell membranes, etc. Assuming that the radioligand exchange between free and non-specific compartments is considerably faster than between free and specific [63], the first ones are usually combined to the non-displaceable compartment. This reduces the configuration to a two-tissue compartment model, making it mathematically simpler and more stable since only four instead of six rate constants need to be estimated. The system can then be defined by the first-order differential equations given below, which describe the changes in radioligand concentrations across the compartments over time [49, 61, 64]:

Equ. 3
$$\frac{dC_{ND}}{dt} = K_1 * C_P - (k_2 + k_3) * C_{ND} + k_4 * C_S$$

Equ. 4
$$\frac{dC_S}{dt} = k_3 * C_{ND} - k_4 * C_S$$

C_P , C_{ND} and C_S represent the radioligand concentrations in plasma, non-displaceable and specific bound compartments, respectively. K_1 - k_4 denote the rate constants as given in figure 3. Since the binding potential is the ratio of specifically bound to free radioligand, the term volume of distribution is an important parameter for PET quantification. Adapted from pharmacology, it relates the radioligand concentration in a given tissue or compartment to that of blood plasma [60]:

Equ. 5
$$V_T = \frac{C_T}{C_P} = \frac{C_{ND}+C_S}{C_P} = \frac{C_{ND}}{C_P} + \frac{C_S}{C_P} = V_{ND} + V_S$$

with C_T and V_T being the total radioligand concentration of all compartments (i.e., $C_{ND}+C_S$) and the total volume of distribution, respectively. Analogous and as given in equation 5, the volume of distribution can be adapted to any compartment. In other words, for V_S this yields the ratio of specific bound to radioligand in plasma C_S/C_P , which in turn equals the binding potential [60]. However, in a PET scan one cannot distinguish the individual compartments as most of them are usually present in every voxel (i.e., a volume element of the PET image, the three dimensional pendant for a pixel). Instead, each time frame of the dynamic PET measurement C_{PET} is related to C_T as follows [65]:

Equ. 6
$$C_{PET} = (1 - V_B) * C_T + V_B * C_{WB}$$

with V_B and C_{WB} being the blood volume component and the radioligand concentration in whole-blood, respectively (see section on arterial input function for differences between whole-blood and plasma concentrations). Solving equations 3, 4 and 6 and fitting the measured data by non-linear regression analysis yields estimates for the rate constants K_1 - k_4 and V_B . The model is often further simplified by setting V_B to a fixed value of e.g., 5% for [*carbonyl*- ^{11}C]WAY-100635 [19, 20, 66, 67]. The rate constants can be directly used for the calculation of the binding potential [60]. At equilibrium no radioligand is transferred between the compartments, hence, the left side of equation 4 (and 3) is zero [49], where rearrangement gives

Equ. 7
$$BP_{ND} = \frac{k_3}{k_4} = \frac{C_S}{C_{ND}} = \frac{V_T - V_{ND}}{V_{ND}}$$

This is the definition of the binding potential relative to non-displaceable radioligand in tissue (BP_{ND}) [60]. It is important to distinguish the two further definitions BP_P and BP_F which denote the binding potentials relative to total radioligand in plasma and free radioligand in plasma, respectively [60]:

$$\text{Equ. 8} \quad BP_P = \frac{K_1 * k_3}{k_2 * k_4} = \frac{C_S}{C_P} = V_T - V_{ND} = V_S$$

$$\text{Equ. 9} \quad BP_F = \frac{K_1 * k_3}{f_P * k_2 * k_4} = \frac{C_S}{f_P * C_P} = \frac{V_T - V_{ND}}{f_P} = \frac{V_S}{f_P}$$

The most important differences are that BP_F reflects theoretically the most accurate estimate of the “true” binding potential B_{max}/K_D with fewest modeling assumptions. However, BP_F requires the determination of the plasma free fraction f_P , which may in turn be difficult to measure accurately [56, 60]. Hence, for small values of f_P , BP_P may be a more robust parameter. On the other hand BP_{ND} can be derived without the need for blood sampling at all but it implies several other modeling assumptions (see section on reference region models). For a detailed description and the consensus nomenclature the reader is referred to Innis et al. [60].

1.4. Arterial input function

As shown above calculation of the binding potential (at least BP_P and BP_F) requires a measure for the amount of radioligand in blood plasma which is available to cross the blood brain barrier and potentially binds at the receptor of interest [60]. The *gold standard* for this is the arterial input function (AIF) obtained simultaneously with the PET scan for each subject individually [49, 61, 63]. The initial peak of the input function is usually measured automatically during the first few minutes, which is combined with manual samples taken at later time points. This input function however still represents whole-blood activity including metabolites and radioligand bound to other cells or membranes. Hence, corrections for plasma to whole-blood ratio and radioactive metabolites are mostly necessary, with few exceptions such as [^{18}F]FDG (irreversible binding) [68] and [^{18}F]Galacto-RGD (very slow metabolism) [69]. As mentioned, receptor quantification with the arterial input function gives the most accurate estimate with fewest modeling assumption [60]. Furthermore, it is independent of variation in non-specific binding across subjects, which is an essential issue for group comparisons [49].

However, an AIF requires measurement of radioactive metabolites and plasma free fraction f_p (in case of BP_F), which may be challenging to obtain accurately, hence, may exhibit considerable variance [60]. Together this means that binding potential estimates from arterial blood sampling are more accurate but they may be less reproducible [49]. Although arterial cannulation (usually carried out at the *A. radialis*) is not particularly dangerous, it represents additional discomfort to the patient and, together with the subsequent analysis of blood samples, is a laborious procedure [70].

1.5. Reference region models

To overcome the mentioned disadvantages of arterial blood sampling several techniques for non-invasive quantification have been introduced. These are based on the use of a reference region, which represents only non-specific binding [49, 64]. This means it is devoid of the target receptor and can be described by a one-tissue compartment model (figure 3) [49]. Since C_S , k_3 and k_4 are zero, equation 3 (and 5) at equilibrium yields [49, 60]:

Equ. 10
$$\frac{K_1}{k_2} = \frac{C_{ND}}{C_P} = V_{ND} = V_T$$

The free and non-specific binding are often assumed to be constant across the brain, i.e., the same also for target regions [49, 63]. This can be used to estimate the binding potential relative to non-displaceable radioligand BP_{ND} from PET data only and hence circumvent arterial blood sampling [49, 60]. The most common reference region models are the Logan-plot [71], the simplified reference tissue model (SRTM [72, 73]) as well as the multilinear reference tissue models (MRTM [74]). These models have been applied for the quantification of neuronal receptors and transporters with great success. Despite the major advantage to avoid arterial blood sampling, reference region methods are based on several modeling assumptions [49, 63]. The most important one is that differences in non-specific binding across subjects are negligible [63]. This issue has been extensively discussed for the serotonin-1A receptor antagonist [*carbonyl*- ^{11}C]WAY-100653 [75-77]. More precisely, it has been shown that the results are dependent on the outcome parameter (BP_P vs BP_{ND}) in patients with major depression [19, 20] and bulimia nervosa [78]. Furthermore, a [^{11}C]Flumazenil study on temporal lobe epilepsy found reduced clinical sensitivity when comparing reference region with invasive modeling [79]. Taken together, reference region models provide an important and useful simplification for quantification of PET studies but the underlying assumptions and limitations associated with the outcome parameter have to be kept in mind [75].

1.6. Image-derived input functions

Image-derived input functions (IDIF) are extracted directly from blood vessels visible in the PET images (figure 4). Hence, they provide a promising non-invasive alternative to arterial blood sampling while offering quantification independent of a reference region [70]. However, IDIFs still represent whole-blood activity of the radioligand which requires further correction for plasma to whole-blood ratio and radioactive metabolites for most radioligands. This means that a full substitution of arterial cannulation and hence a less-invasive procedure is only achieved if these corrections can be carried out by other means than manual arterial blood samples. Several studies evaluating the applicability of IDIFs suggested venous instead of arterial samples [70, 80-82], however, their usage has hardly been validated (but see Chen et al. [83] for [^{18}F]FDG). This is one of the reasons why only in few occasions IDIFs have become a tool for clinical research, especially for neuroimaging and receptor quantification [70]. Their routine application is further complicated because of difficulties in blood vessel definition within the PET images (e.g., poor signal to noise ratio, partial volume effects) and since IDIF definition validated for one radioligand or scanner type may not be successfully extrapolated to different settings (e.g., different tracer kinetics and metabolism) [70]. To summarize, the application of IDIFs for quantification of neuronal binding sites is theoretically promising but is accompanied with several uncertainties which need to be carefully addressed for each radioligand separately.

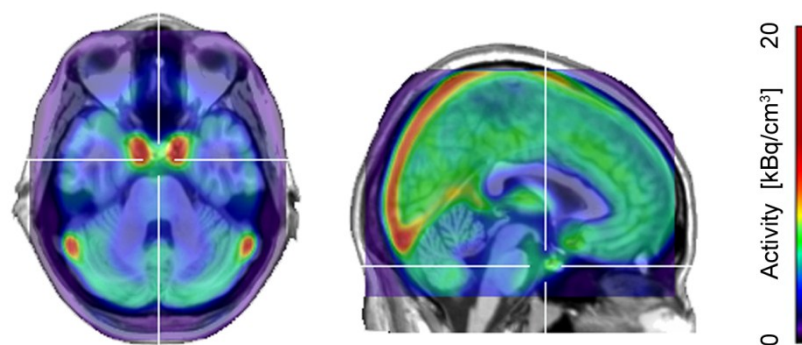


Figure 4: Distribution of the radioligand [*carbonyl*- ^{11}C]WAY-100635 within the first minute of a PET scan. Carotid arteries as well as sagittal and transversal sinus are clearly visible because of the high radioligand uptake compared to that of the surrounding tissue (i.e., high vessel to background ratio). The image represents the average of 36 healthy subjects superimposed on a T1-weighted MRI-scan.

2. AIMS of the THESIS

The *gold standard* for quantification of PET data is given by the arterial input function. Parameter estimation with arterial blood sampling requires fewest modeling assumptions but is in turn invasive and challenging which may introduce additional variance. Due to these drawbacks non-invasive methods provide useful alternatives. However, the dependency on a reference region may limit their applicability, especially in group comparisons as well as longitudinal and interventional designs.

Based on these circumstances the primary aim of this thesis is to develop, implement and validate a method for quantification of neuronal binding sites with PET. The introduced technique is designed to yield robust binding estimates while using minimally invasive measures and maintaining independence of a reference region. Image-derived input functions represent a promising solution for the given requirements. However, several issues have complicated earlier attempts for successful routine applications. These include among others the reliable definition of the input function and the substitution of manual arterial blood samples.

Therefore, the aims of this thesis can be split up in detail as follows:

- The implementation of a new method for the robust automated extraction of modeling input functions directly from cerebral blood vessels of PET imaging data.
- The complete substitution of arterial blood samples by use of image-derived input functions and by carrying out the required corrections only with venous blood samples.
- The validation of the introduced approach in healthy subjects with the *gold standard* for quantification (i.e., arterial input function) by direct comparison of receptor binding potentials.
- A second verification step where this comparison with arterial blood sampling is carried out after treatment of healthy women with hormone replacement therapy.
- The final application of the technique in a longitudinal design of patients with major depressive disorder before and after treatment to evaluate the practicability of the method as a routine tool for quantification in clinical research.

3. SUMMARY of METHODOLOGY and RESULTS

The studies were designed and conducted by the Functional, Molecular and Translational Neuroimaging Lab, Department of Psychiatry and Psychotherapy, Medical University of Vienna. All measurements were carried out at the PET Center, Department of Nuclear Medicine, Medical University of Vienna, using the radioligand [*carbonyl*-¹¹C]WAY-100635 which is a specific and selective antagonist for the serotonin-1A receptor [50, 51]. The importance of this major inhibitory serotonergic receptor subtype in psychiatry and the advantages of the radioligand have been highlighted in the background section.

3.1. Metabolite analysis of [*carbonyl*-¹¹C]WAY-100635

The radioligand [*carbonyl*-¹¹C]WAY-100635 experiences fast metabolism with only 10% of the parent compound available at 10min post injection [66] (see also figure 6). The main radioactive metabolites comprise [*carbonyl*-¹¹C]desmethyl-WAY-100635, [*carbonyl*-¹¹C]cyclohexanecarboxylic acid and more polar compounds [55]. Of those, only the first shows specific binding to the 5-HT_{1A} receptor, but the overall fraction of this compound is less than 2% in humans [53, 55, 58]. Nevertheless, the fast metabolism of the radioligand requires an accurate determination of the parent fraction for each PET measurement when using input function modeling, usually obtained by at least 6 samples [56, 66]. To enable full independence of arterial blood sampling through image-derived input functions, the metabolite correction needs to be carried out with an alternative measure [70]. Hence, the direct comparison between arterial and venous blood samples requires sampling of both ideally in the same subject and within a single scan (i.e., 2x6 samples). The available approaches for the metabolite analysis of [*carbonyl*-¹¹C]WAY-100635 take 7.5-16min per sample for the analysis with high performance liquid chromatography (HPLC) excluding the time for preparation [55, 56, 58, 77]. Considering the fast metabolism of the radioligand, paired with the short half-life of ¹¹C (20.4min) and the requirement to take twice the amount of samples, this would result in rather low counting statistics for late time points when using the available methods. These issues required the development of a new method for metabolite analysis of [*carbonyl*-¹¹C]WAY-100635, which has been resolved in the following manuscript:

Nics L., **Hahn A.**, Zeilinger M., Vracka C., Ungersboeck J., Haeusler D., Hartmann S., Wagner K.-H., Dudczak R., Lanzenberger R., Wadsak W., Mitterhauser M., 2012. Quantification of the serotonin-1A receptor radioligand [carbonyl-¹¹C]WAY-100635 and its radio-metabolites in human plasma: An HPLC-assay allowing two parallel patients. *Applied Radiation and Isotopes Submitted.*

In this study we aimed to optimize the determination of the radiometabolites of [carbonyl-¹¹C]WAY-100635 in terms of analysis time and logistics while maintaining measurement accuracy. The most common methods for metabolite assessment were evaluated in pilot measurements which included liquid-liquid extraction, solid phase extraction (SPE), and HPLC. Generally, all three types of analyses aim for the separation of molecules according to their hydrophilic/lipophilic properties, whereas the different underlying procedures of each method define the separation accuracy [84].

Liquid-liquid extraction is based on the separation of an organic (lipophilic) from an aqueous (hydrophilic) phase. The approach for the radioligand [carbonyl-¹¹C]WAY-100635 has been adapted from the [¹⁸F]-labeled analogue FCWAY [85]. A liquid solvent phase of KCl-NaOH buffer and hexane:ethyl acetate (4:1) was added to the plasma sample. Phase separation was achieved by centrifugation (2500g for 5min), followed by freezing the aqueous phase in a -80°C fridge and pouring off the organic phase. This procedure already took approximately 20min (10min until the aqueous phase was completely frozen) to separate cyclohexanecarboxylic acid and more polar compounds from the two WAY fractions. Hence, a further HPLC step would be required to segregate desmethyl-WAY-100635 from the parent compound due to their similar lipophilic characteristics [55]. Also, the time for freezing represents a considerable problem with ¹¹C considering the short half-life as opposed to ¹⁸F.

Within the two methods of SPE and HPLC the separation is based on the interaction of the sample with a stationary and mobile phase [84]. In SPE the plasma sample is loaded onto a pre-conditioned cartridge containing the stationary phase. This comprises particles (also called the chromatographic packing material) which provide a certain resistance to flow. The successive application of liquid solvent phases with different lipophilic properties yields the elution of the different fractions. In other words, the optimal combination of stationary and mobile phases determines which components are eluted by a certain solvent or remain in the cartridge. Adapted from Ma et al. [85] we used 5% methanol in 0.1N ammonium formate (pH 6.5, hydrophilic) and acetonitrile (lipophilic) to separate cyclohexanecarboxylic acid from the two WAY compounds which took approximately 4min. Again, another HPLC step would be required to isolate the parent compound from its metabolite desmethyl-WAY-100635.

Considering the additional expenditure of time and logistic effort by an additional HPLC processing step, liquid-liquid extraction and solid phase extraction methods were not further used for the metabolite analysis of [*carbonyl*-¹¹C]WAY-100635. Instead, we aimed to apply a single HPLC step to separate the parent compound from the metabolite fractions, more precisely using a reversed-phase radio-HPLC system. In contrast to SPE, HPLC columns (i.e., the stationary phase) comprise smaller particles and the mobile phase is applied with a considerably higher pressure. The different molecules are then separated by their affinity to the mobile phase yielding specific retention times for each compound [84]. Here, we modified an existing procedure based on Parsey et al. which originally takes 12min per sample [56]. Although other studies reported faster HPLC assays [55, 58, 77] these methods used gradient systems, i.e., varying compositions of the mobile phase with different lipophilicity. This however requires a more complex setup and a certain time for equilibration of the system from the end of the last sample (more lipophilic mobile phase) to the start of the next one (more hydrophilic mobile phase). Hence, the isocratic approach [56] was chosen, also because of similar facilities in our laboratory and due to great support and continuous personal communication with Prof. R. Parsey (Columbia University, New York, USA).

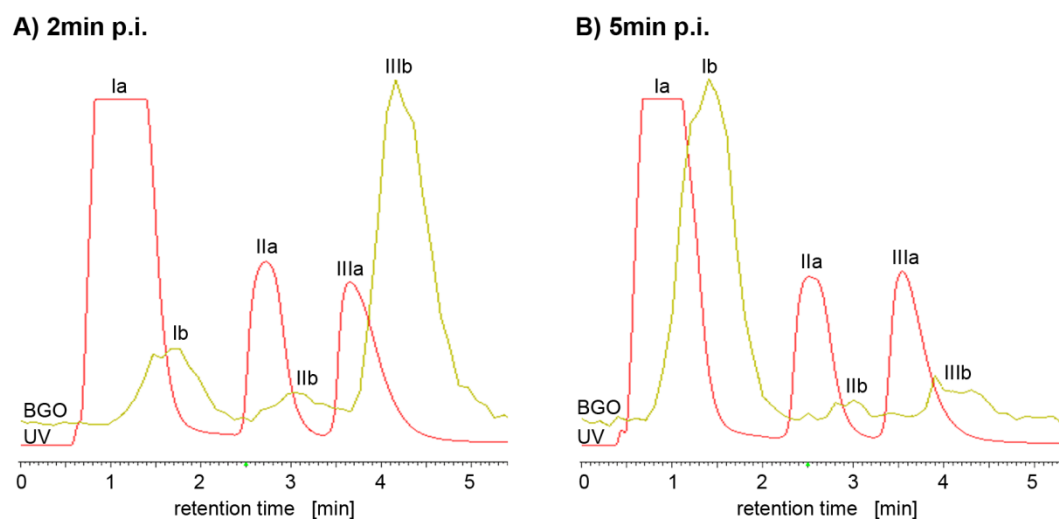


Figure 5: Representative HPLC chromatograms obtained 2min (**A**) and 5min (**B**) post injection (p.i.) of the radioligand [*carbonyl*-¹¹C]WAY-100635. The two lines show the ultraviolet (UV, red, Ia-IIIa) and radiodetector channels (BGO, green, Ib-IIIb). The identified molecules comprise the [*carbonyl*-¹¹C]-labelled compounds cyclohexanecarboxylic acid and more polar molecules (Ia-b), desmethyl-WAY-100635 (IIa-b) and WAY-100635 (IIIa-b). The comparison of 2min (**A**) with 5min (**B**) shows the rapid metabolism of the radioligand with intact WAY-100635 (IIIb) representing the highest fraction at 2min but almost the lowest at 5min. Figure adapted from Nics et al. [86].

The sample processing and the developed HPLC assay is described as follows: After centrifugation of the whole blood (1800g for 7min), 830 μ l plasma were precipitated with acetonitrile at a ratio of plasma:acetonitrile of 42:58 [56]. This was additionally spiked with non-radioactive standards of WAY-100635 and the metabolites cyclohexanecarboxylic acid and desmethyl-WAY-100635. After another centrifugation step (23000g, 4min) 2ml of the supernatant were injected into the HPLC system (Merck Hitachi, Sigma-Aldrich, St. Louis, MO, USA). The system was equipped with an ultraviolet (UV)-detector set at 220nm and a downstream connected radiodetector (bismuth germanium oxide (BGO)-crystal). The main modifications to the existing assay [56] concerned the stationary and mobile phase. We used a 4x4mm LiChrospher[®] LiChroCART[®] pre-column and a 125x4mm LiChrospher[®] LiChroCART[®] analytical column both reversed phase (RP-18) columns with 5 μ m particle size (Merck, Darmstadt, Germany). The mobile phase comprised a mixture of 25mM phosphate buffer (pH 7.0) and acetonitrile at a ratio of 42:58 applied isocratic at a flow rate of 2ml/min. For a more accurate assessment of the parent compound and its metabolites, two fractions were obtained by a fraction collector (one with the metabolite fractions, the other containing intact radioligand) and measured in the gamma counter. The parent fraction was determined by the ratio of intact radioligand to both fractions. The metabolite profile across time was assessed during 15 PET measurements each with 2x6 samples obtained at 2, 5, 10, 20, 35 and 50min post injection and fitted with a Hill-type function [53, 66] (figure 6).

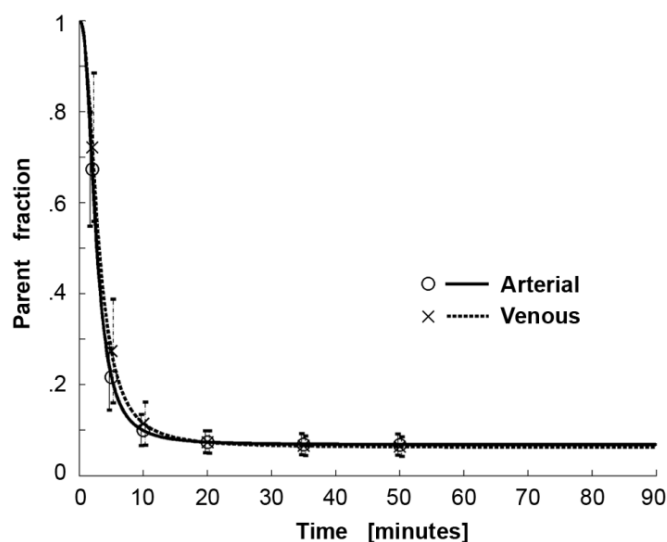


Figure 6: Parent fraction of the radioligand [*carbonyl*-¹¹C]WAY-100635 obtained from 6 arterial (solid line, circles) and 6 venous samples (dotted line, crosses) of 15 PET scans. Manual samples at 2, 5, 10, 20, 35 and 50min were fitted with a Hill-type function. Bars represent standard deviation and are intentionally shifted on the abscissa to distinguish arterial from venous samples. Figure from Hahn et al. [87].

The obtained retention times for [*carbonyl*-¹¹C]cyclohexanecarboxylic acid (including other polar compounds), [*carbonyl*-¹¹C]desmethyl-WAY-100635 and [*carbonyl*-¹¹C]WAY-100635 were 1.6±0.05min, 3.0±0.01min and 4.1±0.12min, respectively (figure 5). The three compounds were baseline separated and the total HPLC run time was 5.3min per sample. For 12 consecutive samples (6 arterial, 6 venous) this yields a total analysis time of 64min and 115min without and with sample preparation and workup, respectively.

Considering that the HPLC is the time limiting factor [85], the introduced approach requires 30% less time than the fastest assay so far [55, 58]. This corresponds to 26min for the total analysis time, which in turn is more than one half-life of ¹¹C. Although the limitation of the HPLC could be circumvented by a second HPLC system, this may cause additional measurement uncertainties. Furthermore, the use of multiple HPLCs requires additional personnel and cross-calibration, which may still not fully account for the differences across systems. Therefore, we aimed to use a single HPLC in order to avoid potential errors.

To summarize, we developed a new approach for fast (5.3min/sample) and accurate (baseline separation of compounds) determination of the parent fraction of [*carbonyl*-¹¹C]WAY-100635. Since the introduced method is 30% faster compared to previous techniques it enables reliable measurements also for late time points, while using a single HPLC system with isocratic operation mode.

3.2. Image-derived input functions in healthy subjects

Proceeding from the successful implementation of a fast and robust metabolite assay which allows parallel analysis of arterial and venous samples, the next step concerned the extraction and application of image-derived input functions for the quantification of [*carbonyl*-¹¹C]WAY-100635. This represents the most important but also the most challenging part of this work for several reasons. First, previous investigations of IDIFs for this radioligand are missing and extrapolation of available methods from other tracers does not necessarily prove to be useful [70]. Next, it is currently unknown if manual venous blood samples are actually suitable for the substitution of arterial ones. This concerns whole-blood activity, whereas the time for arterio-venous equilibrium has not yet been identified, plasma to whole-blood ratio and the parent fraction. A further problem arises from the latter issue since the radioligand [*carbonyl*-¹¹C]WAY-100635 is rapidly metabolized (<10% parent compound from 10min onward) [66]. Such a high metabolite fraction substantially decreases the tail of the input function since the time course of the radioligand in arterial plasma is multiplied by the parent fraction to obtain the final modeling input function (figure 7) [88].

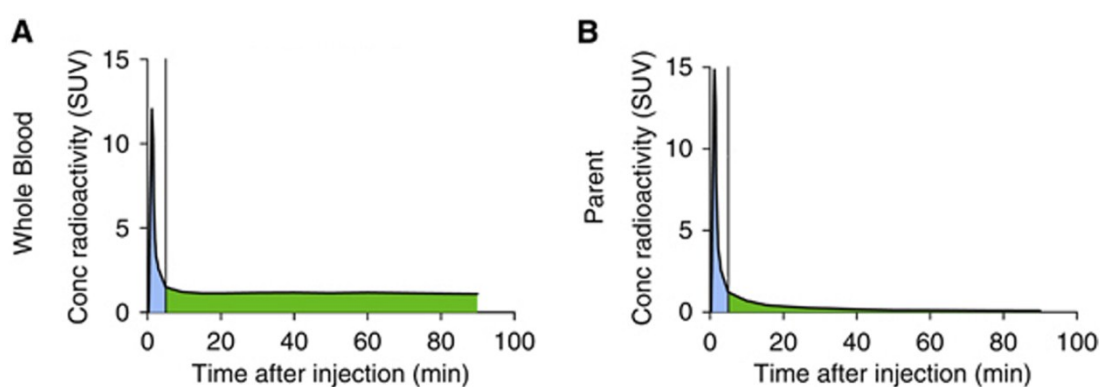


Figure 7: The impact of the metabolite fraction on the input function for radioligands with fast metabolism such as [¹¹C]PBR28 shown here and [*carbonyl*-¹¹C]WAY-100635. The tail of the whole blood curve (**A**, shaded in green) is substantially reduced after correction for radioactive metabolites (**B**). Since graphical modeling approaches use the integral of the input function the area under the peak (shaded in blue) becomes more important for these radioligands. A potential problem emerges for image-derived input functions as accurate peak estimation may be difficult to obtain. Figure adapted from Zanotti-Fregonara et al. [70].

The main issue with IDIFs is that input function peaks may be difficult to determine accurately as opposed to arterial blood sampling, however, the performance of the kinetic modeling procedure is dependent on the shape of input function [70]. This becomes even more important as graphical methods are mostly used [68, 81, 89] and recommended [70] for modeling with IDIFs. Graphical modeling approaches such as the Logan-plot [90] use the area under the curve (i.e., the integral) of the input function rather than estimating individual rate constants. For radioligands with slow metabolism an unreliable estimation of the peak is less problematic since it represents only a small part of the total area. However, the mentioned decrease of the input function tail by a high metabolite fraction makes the integral dependent on the peak (figure 7) [70, 88]. To summarize, graphical methods are the recommended approach for IDIF modeling but they may not provide stable results for radioligands with fast metabolites. On the other hand, compartment modeling represents the method of choice when using input functions for [*carbonyl*-¹¹C]WAY-100635 [20, 66, 77]. However, the binding potentials obtained with this method are calculated from individual rate constants (see background section), whose estimation accuracy in turn depend on the shape of the input function [70]. Taken together, these issues require an even more robust definition of the image-derived input function and a careful evaluation of outcome parameters. These problems have been addressed in the following publication:

Hahn A.*, Nics L.*, Baldinger P., Ungersböck J., Dolliner P., Frey R., Birkfellner W., Mitterhauser M., Wadsak W., Karanikas G., Kasper S., Lanzenberger R., 2012. *Combining image-derived and venous input functions enables quantification of serotonin-1A receptors with [*carbonyl*-¹¹C]WAY-100635 independent of arterial sampling*. *NeuroImage* 62: 199-206 [Epub May 2nd 2012]. *Contributed equally.

In this study we aimed for an accurate extraction of image-derived input functions from cerebral blood vessels to be further applied for quantification of serotonin-1A receptor binding. For complete independence of arterial samples the use of venous blood was evaluated for plasma to whole-blood ratios and metabolite correction. The approach was then compared to the current *gold standard* of quantification, i.e., the arterial input function. This last validation step was carried out in healthy postmenopausal women at baseline (n=8) and after 8 weeks of hormone replacement therapy (n=7) to assess the usefulness of the approach in a treatment setting.

Delineating regions of interest (ROI) of cerebral blood vessels represents the first step for IDIF definition (except for algorithms like independent component analysis). Most of the approaches use the sum of early time frames of the PET scan to identify cerebral blood vessels [80, 89, 91], however, we observed important details during the implementation. For different voxels of the blood vessel ROIs the peaks do not only vary in their maximum values but also in temporal occurrences (figure 8). This implies that simple averaging of all voxels of the ROI lowers and widens the IDIF peak, which may result in less accurate input function definition especially when using a fixed volume [89, 91]. Therefore, the first ROI delineation is followed by a refinement step. We used an automated method (linear discriminant analysis, LDA) for the initial coarse ROI definition [92]. LDA is a supervised classification algorithm which assigns a tissue class to each voxel of the test set (i.e., the PET scan) based on a discriminant function obtained with the training set. The training set was created from an average of 36 healthy subjects used in previous studies of our group [93, 94]. The tissue classes of gray matter, white matter and cerebrospinal fluid are given by tissue probability maps of SPM (statistical parametric mapping, The Wellcome Trust Centre for Neuroimaging, <http://www.fil.ion.ucl.ac.uk/spm/>). The carotid arteries of the training set were defined manually.

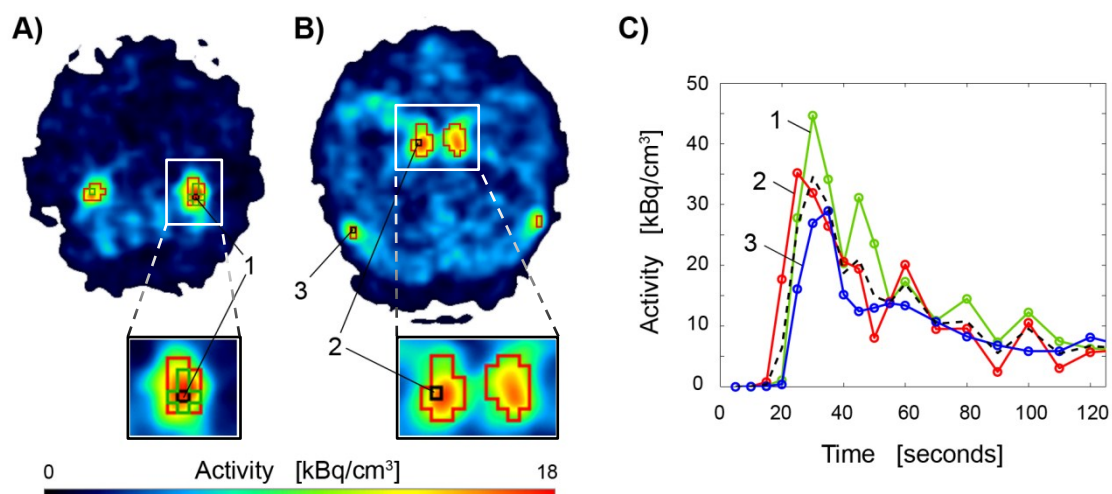


Figure 8: Extraction of image-derived input functions (IDIF) from cerebral blood vessels of a representative subject. Axial slices at height of the cerebellum (**A**, **B**) show the average activity of a [*carbonyl*- ^{11}C]WAY-100635 PET scan during the first minute. High activity is observed in cerebral vessels such as the jugular veins (**A**) as well as carotid arteries and transversal sinus (**B**). Zoom shows regions of interest as identified by linear discriminant analysis (red), which are further refined (green) by a height threshold (0.66 times maximum) within the time frame when the peak activity is observed. Voxels 1-3 (black) denote areas for the time activity curves (TACs) given in **C**. These TACs highlight the importance to refine the IDIF region since both the peak activity and the time of the peak vary across voxels. Simple averaging of the three voxels would therefore considerably decrease and widen the peak of the input function (dashed black line). Figures **A-B** adapted from Hahn et al. [87].

Voxel classification within individual PET scans was carried out with the voxel intensities (rather than spatial location) using a standard Matlab algorithm ('classify' as implemented in MatlabR2010a, The Mathworks, Natick, MA, USA). Although this first part of the ROI definition may yield comparable results across different algorithms, the crucial issue is the following refinement and correction for partial volume effects [95]. Considering the variation of TACs between different voxels (figure 8C) we aimed to refine the initial ROI to obtain a blood pool with more homogenous kinetic characteristics. Here, the maximum activity and the associated time frame when the peak occurs were identified first. The final ROI used for IDIF definition was then restricted to those voxels, which comprise at least 0.66 times the maximum activity within the determined time frame of the peak (figure 8A-B). Interestingly, the vast majority of cerebral vessels obtained from this automated algorithm comprised venous blood pool (96% of 29.4 ± 18.3 voxels). Although IDIF extraction from arteries would in theory be more intuitive [70] our findings point toward higher signal to noise ratio from the venous vessels. This may result from a less pronounced partial volume effect since venous vessels comprise a larger diameter and more voxels from venous blood pool are captured within the PET field of view. Furthermore, the definition of a blood pool with homogenous kinetic characteristics is more important for IDIF extraction than its actual location [96-98].

The next step concerns the correction for partial volume effects, i.e., spill-out to and spill-in from the adjacent tissue of the blood vessels. Although scaling of IDIF with manual blood samples [68] has been recommended for IDIF peak recovery [70], a high variability in IDIF peaks was observed with this method. Possible reasons for this may include that IDIFs exhibit considerable noise at later time points (figure 9) and that a single IDIF may not give an accurate representation of the peak *and* the tail of the input function [70].

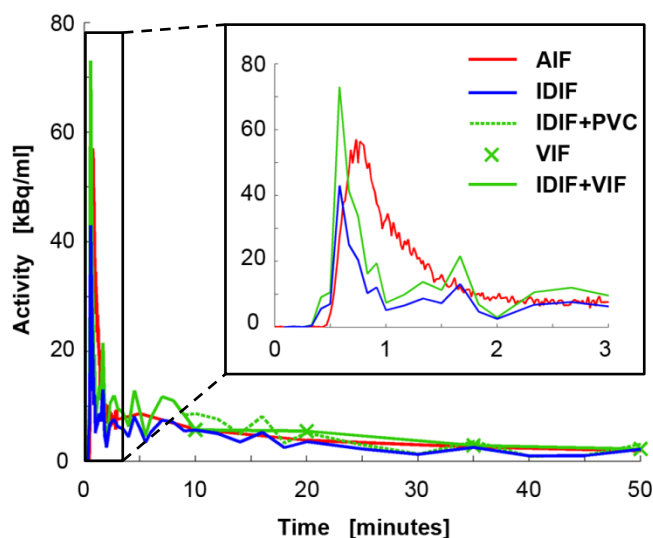


Figure 9: Whole blood activities for different modeling input functions from a single subject. Compared to the arterial input function (AIF, red) the image-derived input function (IDIF, blue) shows good recovery of the peak after partial volume correction (PVC, green). Due to increasing noise of the IDIF at late time points (green dotted line), venous blood samples (green crosses) were used for the tail of the input function (IDIF+VIF, green solid line). Figure adapted from Hahn et al. [87].

Therefore, the peak of the input function was recovered by conventional partial volume effects correction (PVC) on a ROI-basis [99] using the software package PMOD 3.3 (PMOD Technologies Ltd, Zurich, Switzerland, www.pmod.com). This showed a consistent PVC magnitude of 1.75 ± 0.2 defined as the ratio of IDIF peak values after/before PVC (figure 9). Furthermore, IDIF peaks were not significantly different from those obtained by the arterial input function ($p > 0.1$). The tail of the input function was then defined by whole-blood activity of manual venous samples from 10min onward yielding a combination of image-derived and venous input functions (IDIF+VIF, figure 9). This is feasible since venous whole-blood activities were not significantly different from arterial ones after 10min ($p > 0.4$) and hence may represent a more accurate estimate than an IDIF for late time points.

Concerning the remaining parameters obtained from manual venous samples, plasma to whole-blood ratios did not differ from those of arterial samples ($p > 0.4$). Although parent fractions were significantly higher for venous samples for 2, 5 and 10min ($p < 0.05$) the values were still within the reported test-retest variability [56, 77]. No differences were observed for the remaining parent fractions (20, 35, 50min, $p > 0.12$). For the final input function, the whole-blood IDIF+VIF was corrected for plasma to whole-blood ratio and radioactive metabolites using only venous blood. Similarly, the arterial input function (AIF) was corrected for these parameters with arterial samples. Hence, IDIF+VIF were obtained completely independent from arterial blood samples.

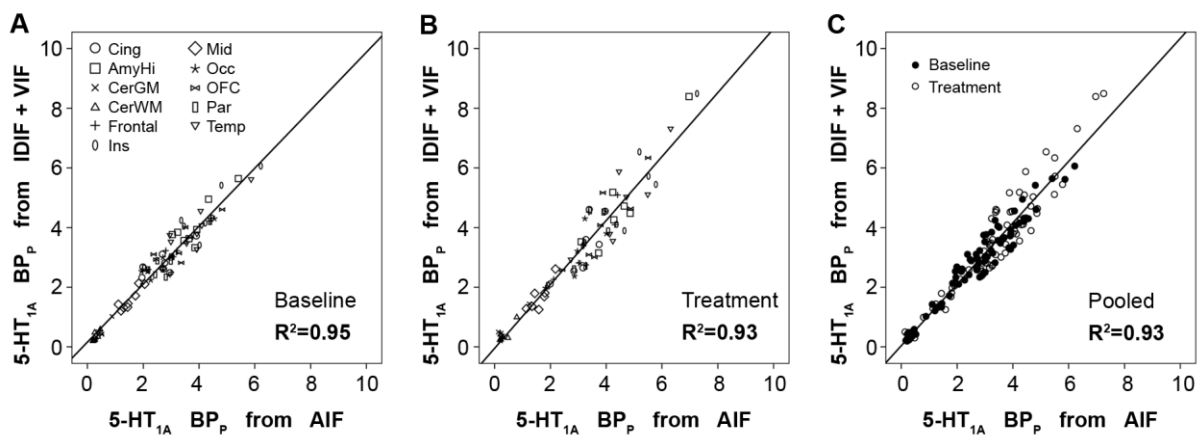


Figure 10: Comparison of serotonin-1A (5-HT_{1A}) receptor binding potentials (BP_p) obtained from the combination of image-derived and venous input functions (IDIF+VIF) and arterial input functions (AIF). Regression analysis indicates strong match between the two independent approaches at baseline (A), after treatment (B) and when pooling all scans (C). The symbols denote different regions of interest (A, B) or baseline and treatment scans (C). AmyHi: amygdala-hippocampus complex; Ins: insula; Cing, Frontal, Occ, OFC, Par, Temp: cingulate, frontal, occipital, orbitofrontal parietal and temporal cortices; Mid: midbrain; CerWM, CerGM: cerebellar white and gray matter. Figure adapted from Hahn et al. [87].

Serotonin-1A receptor binding potentials (BP_P) were then quantified independently for the combination of image-derived and venous input functions and the arterial input function. We used a two-tissue compartment model according to established procedures for this radioligand [20, 77]. Here, the ratio of rate constants K_1/k_2 was fixed to that of cerebellar white matter. Quantification was carried out on a region of interest basis [20, 77] and voxel-wise [100] using PMOD 3.3. The direct comparison of 5-HT_{1A} BP_P resulted in excellent agreement of IDIF+VIF with the *gold standard* (AIF). More precisely, regression analysis showed $R^2=0.95$ for healthy subjects at baseline ($n=8$), $R^2=0.93$ after 8 weeks of treatment ($n=7$) and $R^2=0.93$ when pooling all scans ($n=15$) (figure 10). Intercepts ranged from -0.05 to 0.16 and slopes from 0.97 to 1.07. These results are further supported by repeated measures ANOVA showing no significant differences in 5-HT_{1A} BP_P between IDIF+VIF and AIF ($F_{1,43}=2.4$, $p>0.1$, method and ROI=fixed effects, subject=random effect [101]). Similarly, voxel-wise quantification showed virtually identical results for the two input functions with small differences only observable in regions with lowest receptor binding (occipital cortex and non-brain areas, figure 11).

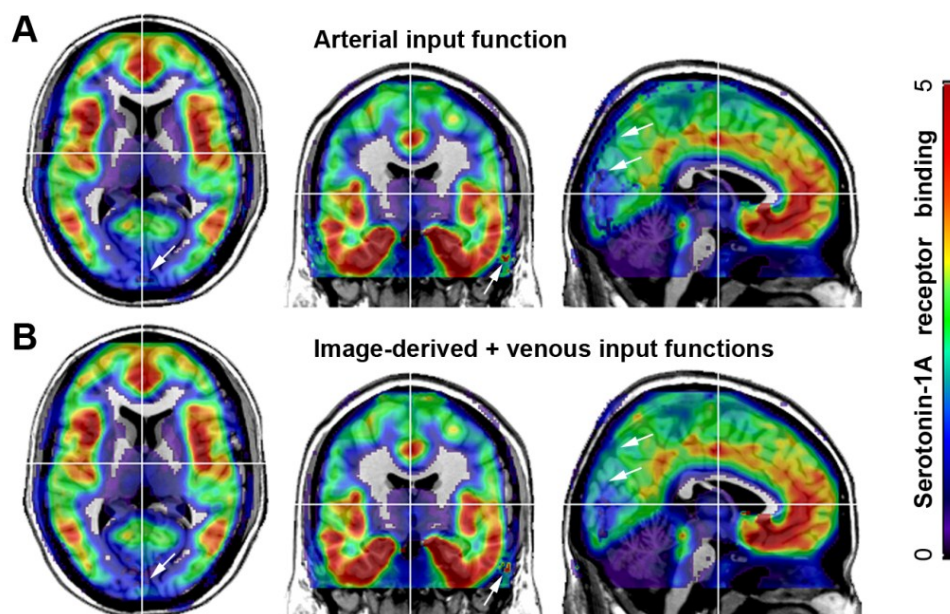


Figure 11: Single subject voxel-wise quantification of the serotonin-1A receptor binding potential (BP_P) using the arterial input function (A) and the combination of image-derived and venous input functions (B). The resulting maps are virtually identical whereas small differences are only observable in regions with lowest receptor binding (occipital cortex) and non-brain areas. Figure adapted from Hahn et al. [87].

To summarize, we introduced a novel combination of image-derived and venous input functions for the quantification of serotonin-1A receptor binding potentials with the radioligand [carbonyl-¹¹C]WAY-100635. The approach yields strong agreement with the gold standard for quantification on a ROI- and voxel-wise basis. The direct comparison between venous and arterial manual blood samples enables full independence of the technique from arterial cannulation despite the fast metabolism of the radioligand. Finally, the robust results at baseline and after 8 weeks of hormone replacement therapy indicate great potential for the routine application of the approach in clinical research protocols and treatment studies.

3.3. Application of image-derived input functions in patients with major depression

Having established and validated the combination of image-derived and venous input functions for 5-HT_{1A} receptor quantification in healthy subjects, the final step of this work was to evaluate the application of the introduced approach in an independent patient population. IDIFs have been successfully used for different radioligands in healthy subjects but the routine application in clinical research protocols is largely missing [70]. Most IDIF studies with patients concern tumor evaluation [69, 102-106], whereas only few studies have been carried out in the field of neuroscience. These include patients with dream-enactment behavior [107] and Alzheimer's disease [108, 109] using the radioligands [¹⁸F]FDG and [¹¹C]PIB. In the aforementioned studies metabolite correction was omitted [69, 102, 107, 108] or based on a population average because of slow metabolism [103-106, 109]. IDIFs were further used for the evaluation of patients with multiple sclerosis, however, the kinetic modeling results were not satisfactory because of the fast metabolism of the radioligand [¹¹C]PBR [88]. These results highlight the importance to extend IDIF methods to patient studies with a longitudinal or treatment design but also for radioligands with more complex metabolic behavior. As shown above, the 5-HT_{1A} receptor antagonist [carbonyl-¹¹C]WAY-100635 exhibits such a fast metabolism. Interestingly, 5-HT_{1A} quantification results differ between reference region and input function models in patients with depression [19, 20] and bulimia nervosa [78], further underlining the need for accurate but minimally invasive modeling procedures. Finally, the successful application of IDIFs may not only vary for different radioligands but also between scanner types, such as standard and high resolution tomographs. High resolution scanners have the advantage of reduced partial volume effects [110-113], however, within the application of IDIFs additional scaling [114] or correction [115] was still required to obtain accurate modeling results. One alternative to subsequent partial volume correction is to

model the point spread function directly during image reconstruction. This has been proven useful for imaging of small brain structures [112] whereas IDIF extraction has been successful for a standard PET scanner [82] but not a high resolution tomograph [114]. These discrepancies for different scanners, modeling approaches and the general lack of IDIF studies in patient populations were the motivation for the following study:

Hahn A., Nics L., Baldinger P., Wadsak W., Savli M., Kraus C., Birkfellner W., Ungersböck J., Haeusler D., Mitterhauser M., Karanikas G., Kasper S., Frey R., Lanzenberger R. 2012. Clinical application of image-derived and venous input functions in major depression using [*carbonyl*-¹¹C]WAY-100635. European Journal of Nuclear Medicine and Molecular Imaging Submitted.

The aim of this study was to apply the previously established approach of 5-HT_{1A} receptor quantification with the combination of IDIF+VIF in a patient sample with major depressive disorder (MDD). Since patients underwent PET before and after electroconvulsive therapy (ECT), we further aimed to assess treatment effects in a longitudinal study design. This represents an important step to evaluate the practicability of the technique as tool in clinical research and routine protocols. Finally, two algorithms for the correction of partial volume effects were compared in order to obtain a robust IDIF definition on a high resolution PET scanner.

Eleven PET scans were acquired from 5 MDD patients using the radioligand [*carbonyl*-¹¹C]WAY-100635 and a Siemens Biograph 64 True Point PET/CT scanner. This included 5 measurements at baseline, 3 before and 3 after ECT. In other words, test-retest data was available for 3 patients and the evaluation of treatment effects for another 3 subjects. Data preprocessing was generally carried out as described above [87]. To reduce noise and scatter from high resolution scanners [70], images were additionally smoothed with a Gaussian kernel of 6mm full-width at half-maximum [110, 111, 114] for IDIF extraction. Furthermore, the field of view was restricted by 13.5m and 27mm in cranial and caudal directions, respectively. These steps are feasible since the delineation of the cerebral blood vessels and IDIF extraction were established with PET data from a standard camera (GE Advance PET scanner) [87].

Cerebral blood vessels were defined as described previously [87]. This includes coarse classification of vessels by linear discriminant analysis and further refinement (0.66 times the maximum activity within the peak time frame). For the recovery of IDIF peaks two different

methods were applied. Using the previously established approach [87], images were reconstructed with a standard ordered subsets expectation maximization (OSEM) algorithm. Hence, subsequent correction for partial volume effects was done on a ROI-basis [99] as implemented in PMOD 3.3 (OSEM+PVC). Second, the point spread function was modeled during image reconstruction using a Siemens-specific reconstruction algorithm (TrueX) [112, 116]. Hence, IDIFs were extracted from the blood vessel ROI without any further corrections. For the final input function IDIF peaks were combined with manual venous blood samples starting at 10min (IDIF+VIF) and further corrected for plasma to whole-blood ratio and radioactive metabolites.

Arterial blood sampling was omitted to minimize patient burden and since the use of IDIF+VIF for the radioligand [*carboxyl*- ^{11}C]WAY-100635 was already validated in our previous work [87]. Still, we aimed for an indirect comparison of the approach with a reference region model in this clinical setting. Kinetic modeling was carried out with PMOD 3.3 using a two-tissue compartment model again on a ROI-basis [20, 77] and voxel-wise [100], yielding binding potentials relative to total radioligand in plasma (BP_P) and to non-displaceable radioligand in tissue (BP_ND). Furthermore, the multilinear reference tissue model 2 (MRTM2 [74]) was used as reference region model (BP_ND).

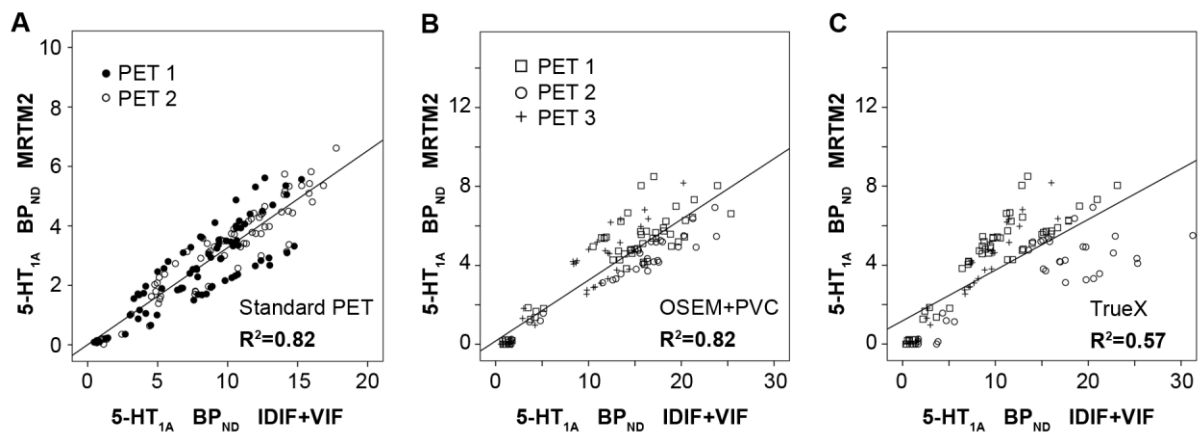


Figure 12: Comparison of serotonin-1A ($5\text{-HT}_{1\text{A}}$) receptor binding potentials (BP_ND) obtained from the multilinear reference tissue model 2 (MRTM2, [74]) and the combination of image-derived and venous input functions (IDIF+VIF). Compared to our previous findings obtained in healthy subjects with a standard PET camera (A, [87]), we found essentially the same relationship in the independent sample of patients with major depression on a high resolution scanner when defining IDIFs from subsequent partial volume correction (B, OSEM+PVC). In contrast, modeling the point spread function during image reconstruction with the TrueX algorithm shows considerably weaker agreement and higher bias (C). Figure adapted from Hahn et al. [87] and Hahn et al. [117].

The ROI-based comparison of the two approaches resulted in good agreement with $R^2=0.82$ and intercept=0.17 when using OSEM+PVC (figure 12B). The slope of 0.31 indicates an underestimation 5-HT_{1A} receptor binding with the reference region model, which is in line with previous reports [56, 66]. More importantly, the obtained parameters are almost identical to those from our previous sample of healthy subjects ($R^2=0.82$, slope=0.33, intercept=0.01, figure 12A) [87]. However, using TrueX image reconstruction for IDIF peak recovery resulted in a decreased association and increased bias ($R^2=0.57$, slope=0.26, intercept=1.18, figure 12C). This is further reflected by significantly lower IDIF peak values (mean difference $\Delta=19.11\pm 9.05$ kBq/ml, $p<0.001$) and a trend towards worse model fits (repeated measures ANOVA $F_{1,27}=3.72$, $p=0.065$) for IDIFs from TrueX compared to OSEM+PVC.

Regarding treatment effects in MDD patients, the use of IDIF+VIF for input function modeling confirms a 23-35% decrease in 5-HT_{1A} BP_P and BP_{ND} [41] when using OSEM+PVC (figure 13). On the other hand, for IDIFs obtained from TrueX image reconstruction the 5-HT_{1A} decreases induced by ECT were similar for BP_P (26-29%) but overestimated with BP_{ND} (20-55%).

Interestingly, one subject showed markedly different results dependent on the model, input function and outcome parameter. More precisely, a 47% *increase* in 5-HT_{1A} BP_{ND} was observed after ECT with the reference region model MRTM2, whereas no change was obtained with IDIF from OSEM+PVC for BP_{ND} (-2%) and BP_P (7%). In contrast, using IDIF from TrueX resulted in an increase for BP_P (17%) and a decrease for BP_{ND} (-47%).

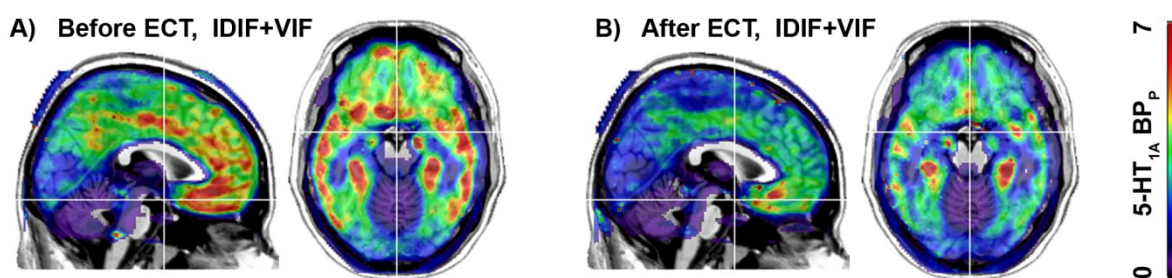


Figure 13: Serotonin-1A (5-HT_{1A}) receptor binding potentials (BP_P) for a representative patient before (A) and after (B) electroconvulsive therapy (ECT). Voxel-wise computation was carried out using the combination of image-derived and venous input functions (IDIF+VIF) obtained from conventional image reconstruction and subsequent partial volume correction (OSEM+PVC). Compared to the pretreatment scans (A), widespread reductions in 5-HT_{1A} BP_P were observed after ECT (B), which confirms previous results [41] also with input function modeling. Figure adapted from Hahn et al. [117].

A detailed analysis of this patient revealed that this inconsistency was caused by an unreliable estimation of the non-specific binding V_{ND} for IDIF defined by TrueX image reconstruction. Here, V_{ND} was 2.4 times lower for the pretreatment scan (i.e., PET 2) with $0.14\text{ml}/\text{cm}^3$ as compared to $0.34\pm 0.08\text{ml}/\text{cm}^3$ for the remaining patients. Since V_{ND} enters the calculation of BP_{ND} in the denominator (Equ. 7 [60]) small variations of this parameter lead to considerable uncertainties of the outcome [19, 20, 78]. For comparison, V_{ND} was robustly estimated by IDIF from OSEM+PVC with $0.19\text{ml}/\text{cm}^3$ for this patient and $0.20\pm 0.07\text{ml}/\text{cm}^3$ for the remaining subjects. Regarding the clinical implications, the differences for the one patient suggest that the effect of our previously reported ECT-induced decreases in 5-HT_{1A} BP_{ND} [41] were at the worst underestimated.

Together, the lower IDIF peak values as well as reduced agreement and higher variation in receptor bindings indicate considerable uncertainties in input function definition by TrueX reconstruction. This most probably caused unreliable estimation of the outcome parameter. Despite the successful application of such algorithms for the modeling of small brain structures [112] it seems that further corrections are still required for IDIF definition on high resolution scanners [88, 115]. Similarly, transfer of a validated IDIF approach from a standard [82] to a high resolution tomograph [114] was only realized by scaling with manual arterial blood samples.

To summarize, the combination of image-derived and venous input functions was successfully applied for the quantification of serotonin-1A receptor binding with [carbonyl- ^{11}C]WAY-100635 in patients with major depression. Hence, we confirm a decrease of 5-HT_{1A} binding after electroconvulsive therapy also with input function modeling. However and in contrast to the theoretical improvement, the findings do not generally support the definition of image-derived input functions by modeling of the point spread function during image reconstruction with TrueX for high resolution PET scanners.

4. CONCLUSIONS and FUTURE PERSPECTIVES

In this work we implemented and validated a minimally invasive technique for the quantification of serotonin-1A receptor binding potentials using the radioligand [*carbonyl*-¹¹C]WAY-100635. The approach maintains the possibility for compartmental quantification without arterial blood sampling or the dependency on a reference region. In detail, this was achieved by defining a modeling input function within the following steps (see workflow diagram in figure 14):

The development of an optimized method for fast and reliable determination of the radioligand's parent fraction enabled the direct comparison of manual venous blood samples with arterial ones. To extract image-derived input functions from a blood pool with homogenous kinetic characteristics we implemented an automated algorithm for the individual definition of cerebral blood vessels including subsequent refinement. Full independence of arterial cannulation was then achieved by combining image-derived and venous input functions and by carrying out the required corrections only using venous blood samples.

The validation with the *gold standard* for quantification showed excellent agreement of serotonin-1A receptor binding potentials between the introduced approach and the arterial input function. In a second verification step this was confirmed for healthy women undergoing 8 weeks continuous treatment with hormone replacement therapy. Finally, within the successful application of the approach in a patient sample suffering from major depression we confirmed a decrease in serotonin-1A receptor binding after electroconvulsive therapy using input function modeling. The evaluation of different reconstruction algorithms provides further information for the optimal definition of image-derived input functions when using a high resolution PET scanner.

Taken together, the combination of image-derived and venous input functions seems to represent a reliable technique for the quantification of serotonin-1A receptor binding potentials with [*carbonyl*-¹¹C]WAY-100635. Importantly, this holds true independent of the study population (healthy subjects and patients with major depression), treatment (no intervention, pharmacological and electroconvulsive therapy), kinetic modeling approach (regions of interest- and voxel-based) and PET scanner (standard and high resolution tomograph) but not modeling of the point spread function (subsequent partial volume correction vs. TrueX during image reconstruction) [87, 117]. Hence, the approach offers

great potential for application in clinical routine and research protocols including the evaluation of patients in a longitudinal study design.

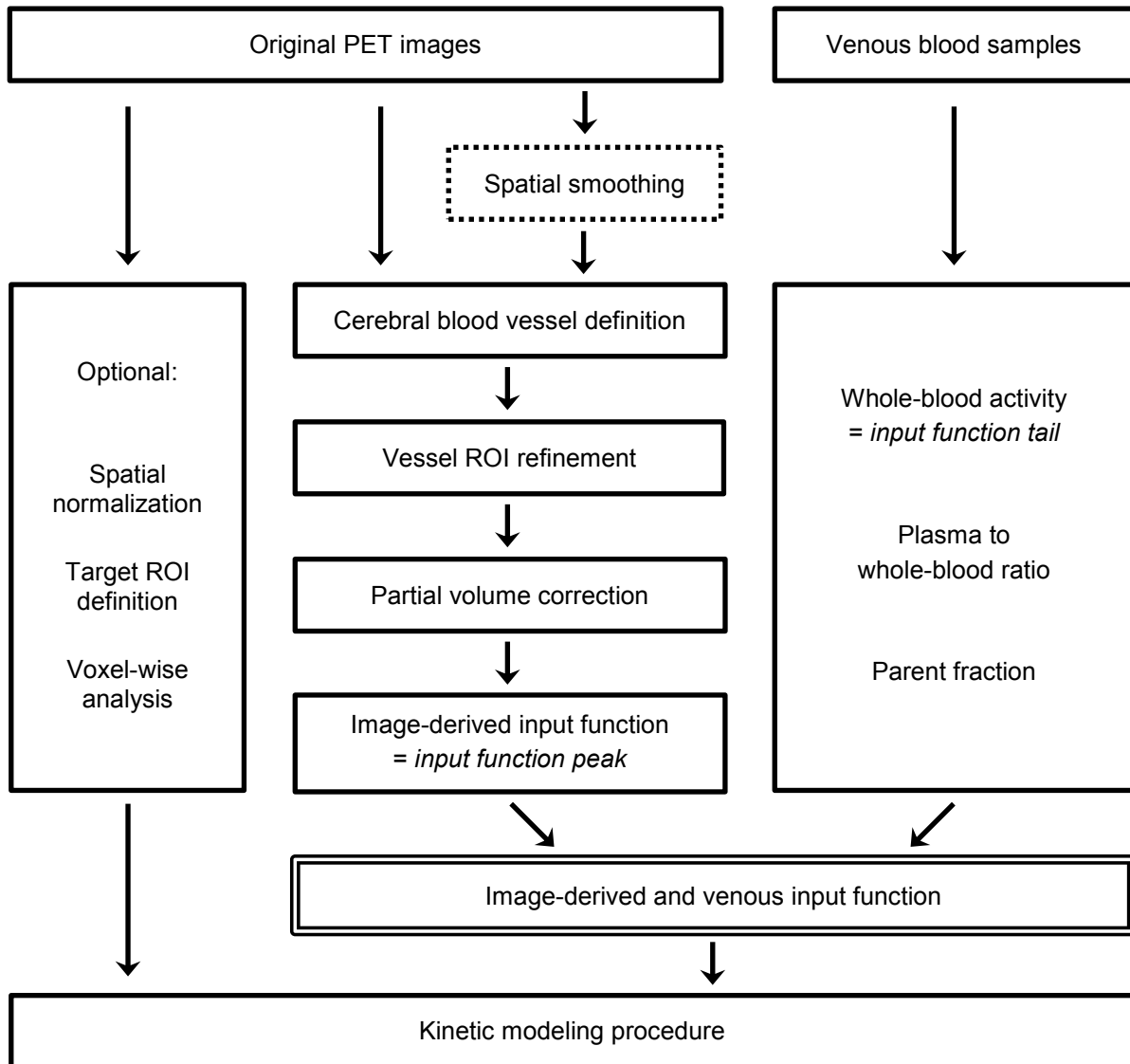


Figure 14: Recommended workflow for the quantification of [*carbonyl*-¹¹C]WAY-100635 PET data using the combination of image-derived and venous input functions. Cerebral blood vessels are extracted from original PET images [92] (including spatial smoothing for high resolution scanners [117]) and further refined regarding the peak values and time of peak occurrence [87, 117]. The obtained blood vessel ROIs are then used to correct for partial volume effects [99], hence, to recover the input function peak. The tail of the input function is in turn defined by whole blood activity of venous manual blood samples [70, 87, 117]. Correction for plasma to whole-blood ratio and radioactive metabolites [86] yields the final plasma input function. This enables quantification of serotonin-1A receptor binding potentials by kinetic modeling with a constrained standard two-tissue compartment model [20, 77] for both ROI-based and voxel-wise [100] analyses.

The next step will be to extrapolate the introduced method for usage with other radioligands, especially those with different kinetic characteristics. Although distinct radioligands may require different techniques to realize modeling with image-derived input functions [70] the successful application of the proposed method in different settings encourages further extension. This is also supported by the fact that no other radioligand (except [^{18}F]FDG) has been evaluated in that detail for the use of image-derived input functions. Furthermore, important issues such as the improved extraction of cerebral blood vessels, the substitution of arterial samples by venous ones despite the fast metabolism of the radioligand and treatment evaluation in a patient sample have been resolved in this work, hence, are available for future applications. Still, the results are limited to binding potential relative to total radioligand in plasma (BP_p) [60], since the free fraction of the radioligand was not determined in the current studies. However, this parameter is rather small for [*carbonyl*- ^{11}C]WAY-100635 (approximately 8%) and therefore may be difficult to estimate robustly [56, 60].

An important future application of the technique concerns radioligands lacking areas which comprise only nonspecific binding, hence where reference region models cannot be applied, and therefore, arterial blood sampling represents the only choice for quantification. One example of such a radioligand is [^{11}C]Harmine [118]. It binds specifically at monoamine oxidase-A, which is responsible for the metabolic inactivation of the neurotransmitters serotonin, dopamine and noradrenaline [119]. More importantly, it is ubiquitously distributed across the entire brain which implies that no region without specific binding is available and an arterial input function is required for quantification [119]. Hence, application of image-derived input functions may provide an essential simplification for the modeling of such radioligands. That is, the implementation of the introduced approach could completely circumvent arterial blood sampling which in turn reduces patient burden as well as expenditure in terms of staff, time and technical demands.

Finally, image-derived input functions may not only be useful for psychiatry or neuroscience but can be extended to any clinical field where PET imaging adds important information, including neurology, cardiology and oncology. The absolute quantification of binding proteins in these settings may provide important information such as longitudinal patient evaluation, tumor assessment and therapeutic efficacy.

5. REFERENCES

1. Fink KB, Gothert M. 5-HT receptor regulation of neurotransmitter release. *Pharmacol Rev.* 2007;59:360-417.
2. Gross C, Zhuang X, Stark K, Ramboz S, Oosting R, Kirby L, et al. Serotonin1A receptor acts during development to establish normal anxiety-like behaviour in the adult. *Nature.* 2002;416:396-400.
3. Zatorre RJ, Fields RD, Johansen-Berg H. Plasticity in gray and white: neuroimaging changes in brain structure during learning. *Nat Neurosci.* 2012;15:528-36.
4. Lanzenberger R, Wadsak W, Spindelegger C, Mitterhauser M, Akimova E, Mien LK, et al. Cortisol plasma levels in social anxiety disorder patients correlate with serotonin-1A receptor binding in limbic brain regions. *Int J Neuropsychopharmacol.* 2010;13:1129-43.
5. Moser U, Wadsak W, Spindelegger C, Mitterhauser M, Mien LK, Bieglmayer C, et al. Hypothalamic serotonin-1A receptor binding measured by PET predicts the plasma level of dehydroepiandrosterone sulfate in healthy women. *Neurosci Lett.* 2010;476:161-5.
6. Lanzenberger R, Mitterhauser M, Kranz GS, Spindelegger C, Wadsak W, Stein P, et al. Progesterone level predicts serotonin-1a receptor binding in the male human brain. *Neuroendocrinology.* 2011;94:84-8.
7. Kranz GS, Kasper S, Lanzenberger R. Reward and the serotonergic system. *Neuroscience.* 2010;166:1023-35.
8. Witte AV, Floel A, Stein P, Savli M, Mien LK, Wadsak W, et al. Aggression is related to frontal serotonin-1A receptor distribution as revealed by PET in healthy subjects. *Hum Brain Mapp.* 2009;30:2558-70.
9. Saulin A, Savli M, Lanzenberger R. Serotonin and molecular imaging in humans using PET. *Amino Acids.* 2011;Epub ahead of print.
10. Polter AM, Li X. 5-HT1A receptor-regulated signal transduction pathways in brain. *Cell Signal.* 2010;22:1406-12.
11. Hornung JP. The Neuroanatomy of the Serotonergic System. In: Müller CP, Jacobs BL, editors. *Handbook of the Behavioral Neurobiology of Serotonin.* London: Academic Press; 2010.
12. Hajos M, Hoffmann WE, Tetko IV, Hyland B, Sharp T, Villa AE. Different tonic regulation of neuronal activity in the rat dorsal raphe and medial prefrontal cortex via 5-HT(1A) receptors. *Neurosci Lett.* 2001;304:129-32.

13. Evans AK, Reinders N, Ashford KA, Christie IN, Wakerley JB, Lowry CA. Evidence for serotonin synthesis-dependent regulation of in vitro neuronal firing rates in the midbrain raphe complex. *Eur J Pharmacol.* 2008;590:136-49.
14. Parsons LH, Kerr TM, Tecott LH. 5-HT(1A) receptor mutant mice exhibit enhanced tonic, stress-induced and fluoxetine-induced serotonergic neurotransmission. *J Neurochem.* 2001;77:607-17.
15. Bundgaard C, Larsen F, Jorgensen M, Gabrielsson J. Mechanistic model of acute autoinhibitory feedback action after administration of SSRIs in rats: application to escitalopram-induced effects on brain serotonin levels. *Eur J Pharm Sci.* 2006;29:394-404.
16. Richardson-Jones JW, Craige CP, Guiard BP, Stephen A, Metzger KL, Kung HF, et al. 5-HT1A Autoreceptor Levels Determine Vulnerability to Stress and Response to Antidepressants. *Neuron.* 2010;65:40-52.
17. Drevets WC, Frank E, Price JC, Kupfer DJ, Holt D, Greer PJ, et al. PET imaging of serotonin 1A receptor binding in depression. *Biol Psychiatry.* 1999;46:1375-87.
18. Meyer JH, Houle S, Sagrati S, Carella A, Hussey DF, Ginovart N, et al. Brain serotonin transporter binding potential measured with carbon 11-labeled DASB positron emission tomography: effects of major depressive episodes and severity of dysfunctional attitudes. *Arch Gen Psychiatry.* 2004;61:1271-9.
19. Hirvonen J, Karlsson H, Kajander J, Lepola A, Markkula J, Rasi-Hakala H, et al. Decreased brain serotonin 5-HT1A receptor availability in medication-naive patients with major depressive disorder: an in-vivo imaging study using PET and [carbonyl-11C]WAY-100635. *Int J Neuropsychopharmacol.* 2008;11:465-76.
20. Parsey RV, Ogden RT, Miller JM, Tin A, Hesselgrave N, Goldstein E, et al. Higher serotonin 1A binding in a second major depression cohort: modeling and reference region considerations. *Biol Psychiatry.* 2010;68:170-8.
21. Lanzenberger RR, Mitterhauser M, Spindelegger C, Wadsak W, Klein N, Mien L-K, et al. Reduced serotonin-1A receptor binding in social anxiety disorder. *Biol Psychiatry.* 2007;61:1081-9.
22. Neumeister A, Bain E, Nugent AC, Carson RE, Bonne O, Luckenbaugh DA, et al. Reduced serotonin type 1A receptor binding in panic disorder. *J Neurosci.* 2004;24:589-91.
23. Martinez D, Slifstein M, Gil R, Hwang DR, Huang Y, Perez A, et al. Positron emission tomography imaging of the serotonin transporter and 5-HT(1A) receptor in alcohol dependence. *Biol Psychiatry.* 2009;65:175-80.

24. Assem-Hilger E, Lanzenberger R, Savli M, Wadsak W, Mitterhauser M, Mien LK, et al. Central serotonin 1A receptor binding in temporal lobe epilepsy: a [carbonyl-(11)C]WAY-100635 PET study. *Epilepsy Behav.* 2010;19:467-73.
25. Smith K. Trillion-dollar brain drain. *Nature.* 2011;478:15.
26. WHO. The World Health Report 2001 - Mental Health: New Understanding, New Hope.; 2001.
27. Bandelow B, Zohar J, Hollander E, Kasper S, Moller HJ. World Federation of Societies of Biological Psychiatry (WFSBP) guidelines for the pharmacological treatment of anxiety, obsessive-compulsive and posttraumatic stress disorders. *World J Biol Psychiatry.* 2002;3:171-99.
28. Kasper S, Stein DJ, Loft H, Nil R. Escitalopram in the treatment of social anxiety disorder: randomised, placebo-controlled, flexible-dosage study. *Br J Psychiatry.* 2005;186:222-6.
29. Blier P, de Montigny C. Serotonin and drug-induced therapeutic responses in major depression, obsessive-compulsive and panic disorders. *Neuropsychopharmacology.* 1999;21:91S-8S.
30. Sheline YI, Barch DM, Donnelly JM, Ollinger JM, Snyder AZ, Mintun MA. Increased amygdala response to masked emotional faces in depressed subjects resolves with antidepressant treatment: an fMRI study. *Biol Psychiatry.* 2001;50:651-8.
31. Di Simplicio M, Norbury R, Harmer CJ. Short-term antidepressant administration reduces negative self-referential processing in the medial prefrontal cortex in subjects at risk for depression. *Mol Psychiatry.* 2011;Epub ahead of print.
32. Sanchez C, Bergqvist PB, Brennum LT, Gupta S, Hogg S, Larsen A, et al. Escitalopram, the S-(+)-enantiomer of citalopram, is a selective serotonin reuptake inhibitor with potent effects in animal models predictive of antidepressant and anxiolytic activities. *Psychopharmacology (Berl).* 2003;167:353-62.
33. Vaswani M, Linda FK, Ramesh S. Role of selective serotonin reuptake inhibitors in psychiatric disorders: a comprehensive review. *Prog Neuropsychopharmacol Biol Psychiatry.* 2003;27:85-102.
34. Dawson LA, Nguyen HQ, Smith DI, Schechter LE. Effects of chronic fluoxetine treatment in the presence and absence of (+/-)pindolol: a microdialysis study. *Br J Pharmacol.* 2000;130:797-804.
35. Blier P, Pineyro G, el Mansari M, Bergeron R, de Montigny C. Role of somatodendritic 5-HT autoreceptors in modulating 5-HT neurotransmission. *Ann N Y Acad Sci.* 1998;861:204-16.

36. Meyer JH, Kapur S, Eisefeld B, Brown GM, Houle S, DaSilva J, et al. The effect of paroxetine on 5-HT_{2A} receptors in depression: an [(18)F]setoperone PET imaging study. *Am J Psychiatry*. 2001;158:78-85.
37. Le Poul E, Boni C, Hanoun N, Laporte AM, Laaris N, Chauveau J, et al. Differential adaptation of brain 5-HT_{1A} and 5-HT_{1B} receptors and 5-HT transporter in rats treated chronically with fluoxetine. *Neuropharmacology*. 2000;39:110-22.
38. Spindelegger C, Lanzenberger R, Wadsak W, Mien LK, Stein P, Mitterhauser M, et al. Influence of escitalopram treatment on 5-HT_{1A} receptor binding in limbic regions in patients with anxiety disorders. *Mol Psychiatry*. 2009;14:1040-50.
39. Bauer M, Bschor T, Pfennig A, Whybrow PC, Angst J, Versiani M, et al. World Federation of Societies of Biological Psychiatry (WFSBP) Guidelines for Biological Treatment of Unipolar Depressive Disorders in Primary Care. *World J Biol Psychiatry*. 2007;8:67-104.
40. Husain MM, Rush AJ, Fink M, Knapp R, Petrides G, Rummans T, et al. Speed of response and remission in major depressive disorder with acute electroconvulsive therapy (ECT): a Consortium for Research in ECT (CORE) report. *J Clin Psychiatry*. 2004;65:485-91.
41. Lanzenberger R, Baldinger P, Hahn A, Ungersboeck J, Mitterhauser M, Winkler D, et al. Global decrease of serotonin-1A receptor binding after electroconvulsive therapy in major depression measured by PET. *Mol Psychiatry*. 2012;In Press. doi:10.1038/mp.2012.93.
42. Strome EM, Clark CM, Zis AP, Doudet DJ. Electroconvulsive shock decreases binding to 5-HT₂ receptors in nonhuman primates: an in vivo positron emission tomography study with [18F]setoperone. *Biol Psychiatry*. 2005;57:1004-10.
43. Wadsak W, Mitterhauser M. Basics and principles of radiopharmaceuticals for PET/CT. *Eur J Radiol*. 2010;73:461-9.
44. Boellaard R. Obtaining cardiac images from positron emission tomography, computed tomography, and magnetic resonance imaging: physical principles. *Heart and Metabolism*; 2007. p. 33-7.
45. Cherry SR. The 2006 Henry N. Wagner Lecture: Of mice and men (and positrons)--advances in PET imaging technology. *J Nucl Med*. 2006;47:1735-45.
46. Fahey FH. Data acquisition in PET imaging. *J Nucl Med Technol*. 2002;30:39-49.
47. Facey K, Bradbury I, Laking G, Payne E. Overview of the clinical effectiveness of positron emission tomography imaging in selected cancers. *Health Technol Assess*. 2007;11:iii-iv, xi-267.

48. Laruelle M, Slifstein M, Huang Y. Relationships between radiotracer properties and image quality in molecular imaging of the brain with positron emission tomography. *Mol Imaging Biol.* 2003;5:363-75.
49. Ichise M, Meyer JH, Yonekura Y. An introduction to PET and SPECT neuroreceptor quantification models. *J Nucl Med.* 2001;42:755-63.
50. Passchier J, van Waarde A. Visualisation of serotonin-1A (5-HT_{1A}) receptors in the central nervous system. *Eur J Nucl Med.* 2001;28:113-29.
51. Martel JC, Leduc N, Ormiere AM, Faucillon V, Danty N, Culie C, et al. WAY-100635 has high selectivity for serotonin 5-HT_{1A} versus dopamine D₄ receptors. *Eur J Pharmacol.* 2007;574:15-9.
52. Hume S, Hirani E, Opacka-Juffry J, Myers R, Townsend C, Pike V, et al. Effect of 5-HT on binding of [(11)C] WAY 100635 to 5-HT_{1A} receptors in rat brain, assessed using in vivo microdialysis and PET after fenfluramine. *Synapse.* 2001;41:150-9.
53. Wu S, Ogden RT, Mann JJ, Parsey RV. Optimal metabolite curve fitting for kinetic modeling of 11C-WAY-100635. *J Nucl Med.* 2007;48:926-31.
54. Pike VW. PET radiotracers: crossing the blood-brain barrier and surviving metabolism. *Trends Pharmacol Sci.* 2009;30:431-40.
55. Osman S, Lundkvist C, Pike VW, Halldin C, McCarron JA, Swahn CG, et al. Characterisation of the appearance of radioactive metabolites in monkey and human plasma from the 5-HT_{1A} receptor radioligand, [carbonyl-11C]WAY-100635-- explanation of high signal contrast in PET and an aid to biomathematical modelling. *Nucl Med Biol.* 1998;25:215-23.
56. Parsey R, Slifstein M, Hwang DR, Abi-Dargham A, Simpson N, Mawlawi O, et al. Validation and reproducibility of measurement of 5-HT_{1A} receptor parameters with [carbonyl-11C]WAY-100635 in humans: comparison of arterial and reference tissue input functions. *J Cereb Blood Flow Metab.* 2000;20:1111-33.
57. Pike VW, McCarron JA, Lammertsma AA, Osman S, Hume SP, Sargent PA, et al. Exquisite delineation of 5-HT_{1A} receptors in human brain with PET and [carbonyl-11 C]WAY-100635. *Eur J Pharmacol.* 1996;301:R5-7.
58. Farde L, Ito H, Swahn CG, Pike VW, Halldin C. Quantitative analyses of carbonyl-carbon-11-WAY-100635 binding to central 5-hydroxytryptamine-1A receptors in man. *J Nucl Med.* 1998;39:1965-71.
59. Wadsak W, Mien LK, Ettliger DE, Lanzenberger R, Haeusler D, Dudczak R, et al. Simple and fully automated preparation of [carbonyl-11C]WAY-100635. *Radiochimica Acta.* 2007;95:417-22.

60. Innis RB, Cunningham VJ, Delforge J, Fujita M, Gjedde A, Gunn RN, et al. Consensus nomenclature for in vivo imaging of reversibly binding radioligands. *J Cereb Blood Flow Metab.* 2007;27:1533-9.
61. Mintun MA, Raichle ME, Kilbourn MR, Wooten GF, Welch MJ. A quantitative model for the in vivo assessment of drug binding sites with positron emission tomography. *Ann Neurol.* 1984;15:217-27.
62. Michaelis L, Menten ML. Die Kinetik der Invertinwirkung. *Biochem Z.* 1913;49:333-6.
63. Slifstein M, Laruelle M. Models and methods for derivation of in vivo neuroreceptor parameters with PET and SPECT reversible radiotracers. *Nucl Med Biol.* 2001;28:595-608.
64. Heiss WD, Herholz K. Brain Receptor Imaging. *The Journal of Nuclear Medicine.* 2006;47:302-12.
65. Lammertsma AA. Chapter 8: Receptor kinetics - modelling and practical approach. In: Dittrich S, van den Hoff J, Maguire RP, editors. *PET Pharmacokinetics Course Manual.* Loch Lomond, Scotland; 2010.
66. Gunn RN, Sargent PA, Bench CJ, Rabiner EA, Osman S, Pike VW, et al. Tracer kinetic modeling of the 5-HT_{1A} receptor ligand [carbonyl-¹¹C]WAY-100635 for PET. *Neuroimage.* 1998;8:426-40.
67. Bose SK, Mehta MA, Selvaraj S, Howes OD, Hinz R, Rabiner EA, et al. Presynaptic 5-HT_{1A} is Related to 5-HTT Receptor Density in the Human Brain. *Neuropsychopharmacology.* 2011;36:2258-65.
68. Chen K, Bandy D, Reiman E, Huang SC, Lawson M, Feng D, et al. Noninvasive quantification of the cerebral metabolic rate for glucose using positron emission tomography, ¹⁸F-fluoro-2-deoxyglucose, the Patlak method, and an image-derived input function. *J Cereb Blood Flow Metab.* 1998;18:716-23.
69. Beer AJ, Grosu AL, Carlsen J, Kolk A, Sarbia M, Stangier I, et al. [¹⁸F]galacto-RGD positron emission tomography for imaging of alphavbeta3 expression on the neovasculature in patients with squamous cell carcinoma of the head and neck. *Clin Cancer Res.* 2007;13:6610-6.
70. Zanotti-Fregonara P, Chen K, Liow JS, Fujita M, Innis RB. Image-derived input function for brain PET studies: many challenges and few opportunities. *J Cereb Blood Flow Metab.* 2011;31:1986-98.
71. Logan J, Fowler JS, Volkow ND, Wang GJ, Ding YS, Alexoff DL. Distribution volume ratios without blood sampling from graphical analysis of PET data. *J Cereb Blood Flow Metab.* 1996;16:834-40.
72. Lammertsma AA, Hume SP. Simplified reference tissue model for PET receptor studies. *Neuroimage.* 1996;4:153-8.

73. Wu Y, Carson RE. Noise reduction in the simplified reference tissue model for neuroreceptor functional imaging. *J Cereb Blood Flow Metab.* 2002;22:1440-52.
74. Ichise M, Liow JS, Lu JQ, Takano A, Model K, Toyama H, et al. Linearized reference tissue parametric imaging methods: application to [¹¹C]DASB positron emission tomography studies of the serotonin transporter in human brain. *J Cereb Blood Flow Metab.* 2003;23:1096-112.
75. Slifstein M, Parsey RV, Laruelle M. Derivation of [(11)C]WAY-100635 binding parameters with reference tissue models: effect of violations of model assumptions. *Nucl Med Biol.* 2000;27:487-92.
76. Parsey RV, Arango V, Olvet DM, Oquendo MA, Van Heertum RL, John Mann J. Regional heterogeneity of 5-HT_{1A} receptors in human cerebellum as assessed by positron emission tomography. *J Cereb Blood Flow Metab.* 2005;25:785-93.
77. Hirvonen J, Kajander J, Allonen T, Oikonen V, Nagren K, Hietala J. Measurement of serotonin 5-HT_{1A} receptor binding using positron emission tomography and [carbonyl-(11)C]WAY-100635-considerations on the validity of cerebellum as a reference region. *J Cereb Blood Flow Metab.* 2007;27:185-95.
78. Bailer UF, Bloss CS, Frank GK, Price JC, Meltzer CC, Mathis CA, et al. 5-HT_{1A} receptor binding is increased after recovery from bulimia nervosa compared to control women and is associated with behavioral inhibition in both groups. *Int J Eat Disord.* 2011;44:477-87.
79. Hammers A, Panagoda P, Heckemann RA, Kelsch W, Turkheimer FE, Brooks DJ, et al. [¹¹C]Flumazenil PET in temporal lobe epilepsy: do we need an arterial input function or kinetic modeling? *J Cereb Blood Flow Metab.* 2008;28:207-16.
80. Sanabria-Bohorquez SM, Maes A, Dupont P, Bormans G, de Groot T, Coimbra A, et al. Image-derived input function for [¹¹C]flumazenil kinetic analysis in human brain. *Mol Imaging Biol.* 2003;5:72-8.
81. Liptrot M, Adams KH, Martiny L, Pinborg LH, Lonsdale MN, Olsen NV, et al. Cluster analysis in kinetic modelling of the brain: a noninvasive alternative to arterial sampling. *Neuroimage.* 2004;21:483-93.
82. Mourik JE, Lubberink M, Klumpers UM, Comans EF, Lammertsma AA, Boellaard R. Partial volume corrected image derived input functions for dynamic PET brain studies: methodology and validation for [¹¹C]flumazenil. *Neuroimage.* 2008;39:1041-50.
83. Chen K, Chen X, Renaut R, Alexander GE, Bandy D, Guo H, et al. Characterization of the image-derived carotid artery input function using independent component analysis for the quantitation of [¹⁸F] fluorodeoxyglucose positron emission tomography images. *Phys Med Biol.* 2007;52:7055-71.

84. Snyder LR, Kirkland JJ, Dolan JW. Introduction to Modern Liquid Chromatography. Hoboken, New Jersey: John Wiley and Sons, Inc.; 2010.
85. Ma Y, Kiesewetter DO, Lang L, Der M, Huang B, Carson RE, et al. Determination of [18F]FCWAY, [18F]FP-TZTP, and their metabolites in plasma using rapid and efficient liquid-liquid and solid phase extractions. *Nucl Med Biol.* 2003;30:233-40.
86. Nics L, Hahn A, Zeilinger M, Vranka C, Ungersboeck J, Haeusler D, et al. Quantification of the radio metabolites of the serotonin-1A receptor radioligand [carbonyl-11C]WAY-100635 in human plasma: An HPLC-assay allowing two parallel patients. *Appl Radiat Isotopes.* 2012;Submitted.
87. Hahn A, Nics L, Baldinger P, Ungersboeck J, Dolliner P, Frey R, et al. Combining image-derived and venous input functions enables quantification of serotonin-1A receptors with [carbonyl-11C]WAY-100635 independent of arterial blood sampling. *NeuroImage.* 2012;62:199-206.
88. Zanotti-Fregonara P, Liow JS, Fujita M, Dusch E, Zoghbi SS, Luong E, et al. Image-derived input function for human brain using high resolution PET imaging with [C](R)-rolipram and [C]PBR28. *PLoS One.* 2011;6:e17056.
89. Mourik JE, Lubberink M, Schuitemaker A, Tolboom N, van Berckel BNM, Lammertsma AA, et al. Image-derived input functions for PET brain studies. *Eur J Nucl Med Mol Imaging.* 2009;36:463-71.
90. Logan J, Fowler JS, Volkow ND, Wolf AP, Dewey SL, Schlyer DJ, et al. Graphical analysis of reversible radioligand binding from time-activity measurements applied to [N-11C-methyl]-(-)-cocaine PET studies in human subjects. *J Cereb Blood Flow Metab.* 1990;10:740-7.
91. Zanotti-Fregonara P, Zoghbi SS, Liow JS, Luong E, Boellaard R, Gladding RL, et al. Kinetic analysis in human brain of [11C](R)-rolipram, a positron emission tomographic radioligand to image phosphodiesterase 4: a retest study and use of an image-derived input function. *Neuroimage.* 2011;54:1903-9.
92. Hahn A, Savli M, Spindelegger C, Haeusler D, Wadsak W, Mitterhauser M, et al. Segmentation of [11C]DASB and [carbonyl-11C]WAY-100635 PET Brain Images using Linear Discriminant Analysis. *Neuroimage.* 2010;52:S155-S6.
93. Stein P, Savli M, Wadsak W, Mitterhauser M, Fink M, Spindelegger C, et al. The serotonin-1A receptor distribution in healthy men and women measured by PET and [carbonyl-11C]WAY-100635. *Eur J Nucl Med Mol Imaging.* 2008;35:2159-68.
94. Fink M, Wadsak W, Savli M, Stein P, Moser U, Hahn A, et al. Lateralization of the serotonin-1A receptor distribution in language areas revealed by PET. *Neuroimage.* 2009;45:598-605.

95. Zanotti-Fregonara P, Fadaili el M, Maroy R, Comtat C, Souloumiac A, Jan S, et al. Comparison of eight methods for the estimation of the image-derived input function in dynamic [(18)F]-FDG PET human brain studies. *J Cereb Blood Flow Metab.* 2009;29:1825-35.
96. Naganawa M, Kimura Y, Ishii K, Oda K, Ishiwata K, Matani A. Extraction of a plasma time-activity curve from dynamic brain PET images based on independent component analysis. *IEEE Trans Biomed Eng.* 2005;52:201-10.
97. Turkheimer FE, Edison P, Pavese N, Roncaroli F, Anderson AN, Hammers A, et al. Reference and target region modeling of [11C]-(R)-PK11195 brain studies. *J Nucl Med.* 2007;48:158-67.
98. Tomasi G, Edison P, Bertoldo A, Roncaroli F, Singh P, Gerhard A, et al. Novel reference region model reveals increased microglial and reduced vascular binding of 11C-(R)-PK11195 in patients with Alzheimer's disease. *J Nucl Med.* 2008;49:1249-56.
99. Rousset OG, Ma Y, Evans AC. Correction for partial volume effects in PET: principle and validation. *J Nucl Med.* 1998;39:904-11.
100. Byrtek M, O'Sullivan F, Muzi M, Spence AM. An adaptation of ridge regression for improved estimation of kinetic model parameters from PET studies. *IEEE T Nucl Sci.* 2005;52:63-8.
101. Ogden RT, Zanderigo F, Choy S, Mann JJ, Parsey RV. Simultaneous estimation of input functions: an empirical study. *J Cereb Blood Flow Metab.* 2010;30:816-26.
102. Wang W, Lee NY, Georgi JC, Narayanan M, Guillem J, Schoder H, et al. Pharmacokinetic analysis of hypoxia (18)F-fluoromisonidazole dynamic PET in head and neck cancer. *J Nucl Med.* 2010;51:37-45.
103. Schiepers C, Chen W, Cloughesy T, Dahlbom M, Huang SC. 18F-FDOPA kinetics in brain tumors. *J Nucl Med.* 2007;48:1651-61.
104. Schiepers C, Chen W, Dahlbom M, Cloughesy T, Hoh CK, Huang SC. 18F-fluorothymidine kinetics of malignant brain tumors. *Eur J Nucl Med Mol Imaging.* 2007;34:1003-11.
105. Schiepers C, Hoh CK, Nuyts J, Seltzer M, Wu C, Huang SC, et al. 1-11C-acetate kinetics of prostate cancer. *J Nucl Med.* 2008;49:206-15.
106. Backes H, Ullrich R, Neumaier B, Kracht L, Wienhard K, Jacobs AH. Noninvasive quantification of 18F-FLT human brain PET for the assessment of tumour proliferation in patients with high-grade glioma. *Eur J Nucl Med Mol Imaging.* 2009;36:1960-7.
107. Caselli RJ, Chen K, Bandy D, Smilovici O, Boeve BF, Osborne D, et al. A preliminary fluorodeoxyglucose positron emission tomography study in healthy adults reporting dream-enactment behavior. *Sleep.* 2006;29:927-33.

108. Reiman EM, Chen K, Alexander GE, Caselli RJ, Bandy D, Osborne D, et al. Functional brain abnormalities in young adults at genetic risk for late-onset Alzheimer's dementia. *Proc Natl Acad Sci U S A*. 2004;101:284-9.
109. Lopresti BJ, Klunk WE, Mathis CA, Hoge JA, Ziolkowski SK, Lu X, et al. Simplified quantification of Pittsburgh Compound B amyloid imaging PET studies: a comparative analysis. *J Nucl Med*. 2005;46:1959-72.
110. Leroy C, Comtat C, Trebossen R, Syrota A, Martinot JL, Ribeiro MJ. Assessment of ¹¹C-PE2I binding to the neuronal dopamine transporter in humans with the high-spatial-resolution PET scanner HRRT. *J Nucl Med*. 2007;48:538-46.
111. van Velden FH, Kloet RW, van Berckel BN, Buijs FL, Luurtsema G, Lammertsma AA, et al. HRRT versus HR+ human brain PET studies: an interscanner test-retest study. *J Nucl Med*. 2009;50:693-702.
112. Varrone A, Sjöholm N, Eriksson L, Gulyas B, Halldin C, Farde L. Advancement in PET quantification using 3D-OP-OSEM point spread function reconstruction with the HRRT. *Eur J Nucl Med Mol Imaging*. 2009;36:1639-50.
113. Schain M, Toth M, Cselenyi Z, Stenkrona P, Halldin C, Farde L, et al. Quantification of serotonin transporter availability with [¹¹C]MADAM--a comparison between the ECAT HRRT and HR systems. *Neuroimage*. 2012;60:800-7.
114. Mourik JE, van Velden FH, Lubberink M, Kloet RW, van Berckel BN, Lammertsma AA, et al. Image derived input functions for dynamic High Resolution Research Tomograph PET brain studies. *Neuroimage*. 2008;43:676-86.
115. Fung EK, Planeta-Wilson B, Mulnix T, Carson RE. A Multimodal Approach to Image-Derived Input Functions for Brain PET. *IEEE Nucl Sci Symp Conf Rec (1997)*. 2009;2009:2710-4.
116. Casey M. Point spread function reconstruction in PET. Siemens Molecular Imaging; 2007.
117. Hahn A, Nics L, Baldinger P, Wadsak W, Savli M, Kraus C, et al. Clinical application of image-derived and venous input functions in major depression using [carbonyl-¹¹C]WAY-100635. *Eur J Nucl Med Mol Imaging*. 2012;Submitted.
118. Bergstrom M, Westerberg G, Langstrom B. ¹¹C-harmine as a tracer for monoamine oxidase A (MAO-A): in vitro and in vivo studies. *Nucl Med Biol*. 1997;24:287-93.
119. Ginovart N, Meyer JH, Boovariwala A, Hussey D, Rabiner EA, Houle S, et al. Positron emission tomography quantification of [¹¹C]-harmine binding to monoamine oxidase-A in the human brain. *J Cereb Blood Flow Metab*. 2006;26:330-44.

6. PUBLICATIONS

Quantification of the radio-metabolites of the serotonin-1A receptor radioligand [*carbonyl*-¹¹C]WAY-100635 in human plasma: An HPLC-assay allowing two parallel patients

Lukas Nics^{1,2}, **Andreas Hahn**³, Markus Zeilinger^{1,4}, Chrysoula Vraka^{1,2},
Johanna Ungersboeck^{1,5}, Daniela Haeusler¹, Sabine Hartmann¹, Karl-Heinz Wagner²,
Robert Dudczak¹, Rupert Lanzenberger³, Wolfgang Wadsak^{1,5}, Markus Mitterhauser,^{1,6,7 *}

¹ *Department of Nuclear Medicine, Medical University of Vienna, Austria*

² *Department of Nutritional Sciences, University of Vienna, Austria*

³ *Department of Psychiatry and Psychotherapy, Medical University of Vienna, Austria*

⁴ *University of Applied Sciences, Wiener Neustadt, Austria*

⁵ *Department of Inorganic Chemistry, University of Vienna, Austria*

⁶ *Department of Pharmaceutical Technology and Biopharmaceutics, University of Vienna, Austria*

⁷ *Hospital Pharmacy of the General Hospital of Vienna, Austria*

For submission to: **Applied Radiation and Isotopes**

Word count	78	Abstract
	2265	Main section
Tables: 2, Figures: 4, References 20		

* Correspondence to: PD. Dr. Markus Mitterhauser
Radiochemistry and Biomarker Development Unit
Department of Nuclear Medicine
Medical University of Vienna
Waehringer Guertel 18-20
A-1090 Vienna, Austria
tel.: +43 1 40400 1557
fax.: +43 1 40400 1559
e-mail: markus.mitterhauser@meduniwien.ac.at

Keywords:

WAY100635, 5-HT, serotonin-1A, carbon-11, PET, metabolites

ABSTRACT

[*Carbonyl*-¹¹C]WAY-100635 is a potent and effective antagonist for the 5-HT_{1A} receptor subtype. We aimed to assess the status of [*carbonyl*-¹¹C]WAY-100635 and its main radio-metabolites, [*carbonyl*-¹¹C]desmethyl-WAY-100635 and [*carbonyl*-¹¹C]Cyclohexanecarboxylic acid, on the basis of an improved radio-HPLC method. Common methods were characterized by preparative HPLC columns with long runtimes and/or high flow rates. Considering the short half-life of C-11, we developed a more rapid and solvent saving HPLC assay, allowing a fast, efficient and reliable quantification of these major metabolites.

INTRODUCTION

The serotonin-1A receptor (5-HT_{1A}) shows highest densities in the cerebral cortex, hippocampus, amygdala and in the raphe nuclei (Hall et al., 1997; Ito et al., 1999). With this receptor subtype being the predominant inhibitory receptor it has been gaining considerable interest in the field of pathophysiology of neuropsychiatric disorders such as anxiety (Gunn et al., 1998; Lanzenberger et al., 2007), schizophrenia and depression (Hirvonen et al., 2007; Parsey et al., 2005). As for the quantitative assessment of these receptors with positron emission tomography (PET) and kinetic modelling of these data an input function is required. Essential prerequisites are therefore an accurate determination and the correction of radioactive metabolites. [*Carbonyl*-¹¹C]WAY-100635 (N-(2-(4-(2-methoxyphenyl)piperazin-1-yl)ethyl)-N-(pyridin-2-yl)cyclohexane[¹¹C]carboxamide) is an antagonist of the 5-HT_{1A} receptor and particularly suitable for its quantification (Forster et al., 1995; Gunn et al., 1998; Ito et al., 1999; Parsey et al., 2000; Pike et al., 2000; Sargent et al., 2000). However, it shows very fast metabolism (Pike et al., 1996; Wu et al., 2007) to form non radioactive WAY-100634 (N-(2-(4-(2-methoxyphenyl)piperazin-1-yl)ethyl)pyridin-2-amine) as well as [*carbonyl*-¹¹C]cyclohexanecarboxylic acid and other polar metabolites in high amounts but much minor metabolism to form [*carbonyl*-¹¹C]desmethyl-WAY-100635 (N-(2-(4-(2-hydroxyphenyl)piperazin-1-yl)ethyl)-N-(pyridin-2-yl)cyclohexane [¹¹C]carbox-amide) and methanol in low amounts (see figure 1). Additionally, due to the short half-life of C-11 (20.3 min), it is a daunting challenge to achieve robust data with sufficient counting statistics; this is especially true for late time points (> 20min), which are still important for adequate curve-fitting and calculation of 5-HT_{1A} binding potentials. Although accurate methods for metabolite analysis have already been introduced, they may be limited to few samples due to long runtimes of the high-performance liquid-chromatography (HPLC) system. Hence, we aimed to develop a fast and robust radio-HPLC method, which allows:

- (1) a maximum of perpetuate analyses and, as a consequence,
- (2) an improved determination of late data points.

METHODS

Materials

All chemicals and solvents were obtained from commercial sources with analytical grade and used without further purification. Acetonitrile (AcN) CHROMASOLV[®] (for HPLC) CAS [75-05-8], methanol CHROMASOLV[®] (for HPLC) CAS [67-56-1], ammonium formate (for HPLC) CAS [540-69-2], triethylamine (TEA) CAS [121-44-8], thionyl chloride CAS [7719-09-7], tetrahydrofuran (THF) anhydrous CAS [109-99-9], cyclohexyl magnesium chloride in diethylether CAS [931-51-1] were purchased from Sigma Aldrich (Vienna, Austria). Sodiumdihydrogenphosphat monohydrat (for molecular biology), CAS [10049-21-5] and cyclohexanecarboxylic acid (for synthesis), CAS [98-89-5] were purchased from Merck (Darmstadt, Germany). Disodiumhydrogenphosphate dihydrate (puriss), CAS [10028-24-7] was purchased from Fluka (Neu-Ulm, Germany). WAY-100635 (reference standard for [*carbonyl*-¹¹C]WAY-100635), desmethyl-WAY-100635 (reference standard for radio-metabolite [*carbonyl*-¹¹C]desmethyl-WAY-100635) and WAY-100634 (precursor for radiosynthesis of [*carbonyl*-¹¹C]WAY-100635) were all purchased from ABX (Radeberg, Germany). Preparative HPLC column Phenomenex[®] Gemini C18, 250x10 mm (10 μm) was purchased from Phenomenex, Inc. (Torrance, USA). Analytical HPLC columns LiChrospher[®] LichroCART[®] 125x4 mm, RP-18 (5 μm) and pre-column Lichrospher[®] LichroCART[®] 4x4mm, RP-18 (5 μm) were purchased from Merck (Darmstadt, Germany).

Radiochemical Preparation

Radiosynthesis was performed according to an optimized procedure as described elsewhere (Wadsak et al., 2007). Briefly, [¹¹C]CO₂ (68.9-87.7 GBq) was obtained from a cyclotron and passed through a synthesis loop containing cyclohexylmagnesium chloride in THF. [¹¹C]cyclohexylcarboxylic acid was eluted with thionyl chloride and added to 3.5 mg WAY100634 in TEA and THF. After 4 min at 70°C, the product was purified by preparative HPLC (column: Phenomenex[®] Gemini C18, 250x10 mm (10 μm); mobile phase: 0.1 N ammonium formate, methanol, 30:70 with 0.3% triethylamine; flow at 8 ml/min; UV detection at 254 nm) and solid phase extraction (SPE). Yields were 4.3 ± 2.7 GBq with specific radioactivities of 292 ± 130 GBq/μmol (n=16).

Instruments

All analytical HPLC analyses were performed on a single Merck Hitachi system equipped with an Interface D-6000, Intelligent Pump L-6220 and an UV- Detector L-4000 adjusted at 220 nm. The online radio-detection was obtained using a Packard flow scintillation analyzer with a BGO crystal, Radiomatic Flo-One Beta 150TR (Canberra, Canada). Solvent fractions

were separated using a fraction-collector Teledyne ISCO Foxy Jr. (Lincoln, USA). Measurement of all activities was performed using an automatic Wizard² 3" 2480 (Waltham, USA) gamma-counter from Perkin Elmer.

Metabolite analysis

After radiotracer injection, blood samples were collected at 2, 5, 10, 20, 35 and 50 minutes. Three millilitres of whole blood were first measured in the gamma-counter and followed by a further centrifugation step (1800 g, 7 min, 14°C) to separate plasma fractions. Plasma aliquots of 830 µl were then precipitated with acetonitrile and spiked with standards of WAY-100635, desmethyl-WAY-100635 and cyclohexanecarboxylic acid to achieve a final plasma:AcN ratio of 42:58 (Parsey et al., 2000). Plasma activity was measured in another gamma-counting step and the precipitate was obtained by renewed centrifugation (23.000 g, 4 min, 20°C). Ultimately two millilitres of the supernatant were injected into the radio-HPLC. The mobile phase was prepared by mixing acetonitrile and 25 mM phosphate buffer (pH 7.0) in a ratio of 58:42, degassed by an ultrasonic system. An isocratic HPLC method was established with a flow of 2 ml/min and the UV detector set at 220 nm. Following HPLC quantification, two fractions with intact [*carbonyl*-¹¹C]WAY-100635 and its metabolites were collected by a fraction collector and re-measured in the Gamma-Counter to obtain an even more accurate assessment of metabolites (Nics et al., 2010).

Data processing

Fractions were then corrected for radioactive decay and background activity. For each sample, the parent fraction was calculated as the ratio of intact [*carbonyl*-¹¹C]WAY-100635 to total activity from both fractions. The final profile of the unmetabolized radioligand over time was obtained by fitting a Hill-type function (Gunn et al., 1998) to the six parent fractions (see figure 2):

$$\text{parent fraction (t)} = 1 - \frac{\alpha * t^{\beta}}{t^{\beta} + \gamma}$$

The model parameters α , β and γ were estimated with a standard non-linear least squares fitting procedure implemented in Matlab R2010a (The MathWorks, Natick, MA, USA).

RESULTS

The amount of intact [*carbonyl*-¹¹C]WAY-100635 and metabolites derived from blood samples as well as retention times and retention factors are given in table 1 (n=16). The compounds eluted from the HPLC-column in the following order: [*carbonyl*-¹¹C]cyclohexanecarboxylic acid and other polar metabolites (1.6 ± 0.05 min), followed by [*carbonyl*-¹¹C]desmethyl-WAY-100635 (3.0 ± 0.01 min) and [*carbonyl*-¹¹C]WAY-100635 (4.1 ± 0.12 min, see figure 4). Metabolism was very rapid: after 5min already 74 ± 10.33% of the parent compounds were metabolized (see table 2 and figure 2). The total analysis time of the HPLC was 5.3 minutes per sample. The suitability of the method could be proved by 16 patients so far. No failures due to technical or analytical malfunctions were observed.

DISCUSSION

We have introduced here an improved HPLC-assay to quantify the metabolic fate of the 5-HT_{1A} antagonist [*carbonyl*-¹¹C]WAY-100635 *in vivo*. The method allows for the determination of 12 blood samples in less than 115 minutes using a single HPLC-system. The arterial input function represents the gold standard for quantification of neuronal receptors and transporters with PET (Innis et al., 2007). This implies exact determination of the metabolite fraction across time. In the case of [*carbonyl*-¹¹C]WAY-100635 it is known that metabolism is fast. Four major methods (Farde et al., 1998; Hirvonen et al., 2007; Osman et al., 1998; Parsey et al., 2000) have been introduced so far to quantify the metabolites of this radioligand. All described approaches as well as the one introduced here were capable to distinguish between [*carbonyl*-¹¹C]WAY-100635 and [*carbonyl*-¹¹C]desmethyl-WAY-100635.

In-vitro, several more hydrophilic metabolites were found in microsomal experiments using LC-MS/MS for detection (Laven et al., 2006). Furthermore, Osman et al. observed another significant polar metabolite, [*carbonyl*-¹¹C]cyclohexanecarboxylic acid along with some other metabolites that were even more hydrophilic in human studies (Osman et al., 1998). Still, Wu et al concluded that, with the exception of [*carbonyl*-¹¹C]desmethyl-WAY-100635, no metabolites are expected to bind specifically to the 5-HT_{1A} receptor (Wu et al., 2007).

Confronted with the requirement to establish such a method in our institution, we have compared the methods suggested in the literature so far, and observed that we had to adjust the setup to our prerequisites: analyses of blood samples derived from two patients simultaneously (parallel analyses). However, the fastest assays so far (Farde et al., 1998; Osman et al., 1998) have been used with gradient HPLC-methods. Analysing 7 samples

(Farde et al., 1998) would take 52.5 min (HPLC runtime excluding workup). We determined to use an isocratic HPLC method because of the far better signal to noise ratio, less baseline-drift (both not applicable to radio-channel) and the possibility to immediately inject the follow-up-sample to the system without having to wait for column equilibration. The use of two HPLC systems simultaneously would minimize the overall analysis time but may in turn lead to different results between the systems. Although cross-calibration limits internal differences across systems, even small errors result in considerable inaccuracies especially at late time points characterized by low counting rates. In comparison to the fastest isocratic method we were able to finish the same amount of samples in only 37 ± 1.03 min (see figure 3). Hence, the fastest assay described so far is about 40% slower than the method described in this manuscript. That enables us to analyse 10 samples (i.e., 10 different time points) within the same timeframe, allowing a more reliable curve fitting and hence input function modelling. When taking blood samples of two patients (parallel analyses, 6 samples per patient), our assay is still fast enough to ensure that the radiosignals of the final samples have a sufficient counting statistic for robust curve fitting. This improvement is essential because the counting rate at late time points is strongly diminished due to rapid radioactive decay of C-11 labelled compounds; but it is absolutely pivotal to get sufficient signal for an accurate unmetabolized radioligand quantification. A brief comparison of our method to the four standard approaches is also given in figure 3.

Apart from HPLC, some other methods, such as solid phase extraction (SPE) and liquid-liquid extraction, were described to assess the metabolism of F-18 [*carbonyl*-¹¹C]WAY-100635 analogues (Ma et al., 2003; Ma et al., 2001). Since the major *in-vivo* metabolites of [¹⁸F]FCWAY in man are two very hydrophilic compounds, namely [¹⁸F]parafluorocyclohexylcarboxylic acid and [¹⁸F]fluoride, they can be easily separated using SPE methods. However, with [*carbonyl*-¹¹C]WAY-100635, we have to focus on the lipophilic metabolite [*carbonyl*-¹¹C]desmethyl-WAY-100635, which is known to bind to the 5-HT_{1A} receptor. Using these published SPE methods (Ma et al., 2003; Ma et al., 2001), we were not able to isolate [*carbonyl*-¹¹C]WAY-100635 and [*carbonyl*-¹¹C]desmethyl-WAY-100635 quantitatively due to the lower separating capacity of the cartridges. Hence, SPE was only effective to separate of the main hydrophilic metabolite, [*carbonyl*-¹¹C]cyclohexanecarboxylic acid but was not able to distinguish between [*carbonyl*-¹¹C]WAY-100635 and [*carbonyl*-¹¹C]desmethyl-WAY-100635. Therefore, an additional HPLC would have been required, yielding in even longer analytical protocols.

On the basis of a liquid-liquid extraction method (Ma et al., 2003), we found out that overall expenditure for a single sample (including sample preparation and gamma counting)

demanded 5.0 ± 0.5 min more analysis time compared to our HPLC method. Moreover, the quantitative separation of [*carbonyl*- ^{11}C]WAY-100635 and [*carbonyl*- ^{11}C]desmethyl-WAY-100635 was also unsatisfactory.

That motivated us to consider a method efficient enough to separate [*carbonyl*- ^{11}C]WAY-100635, [*carbonyl*- ^{11}C]desmethyl-WAY-100635 and [*carbonyl*- ^{11}C]cyclohexanecarboxylic acid quantitatively in a minimum period of time. Based on these experiences, HPLC evinced as the only suitable method in our case (NB: this must not be generalized; using other tracers, e.g. [^{18}F]FCWAY, [^{18}F]MPPF, different methods might still be applicable). Hence, the direct comparison with other methods (see figure 3) was limited to the published HPLC-approaches.

Total number of analyses

The method allowing the highest number of analyses (based on HPLC time consumption, excluding workup) in the literature is given by Osman et al. (1998), allowing 8 analyses in 128 minutes, followed by Farde et al. (1998) with 7 analyses in 52.5 minutes. Since we had to analyze 12 samples these methods may not allow for a sufficient signal-to-noise ratio at late time points. Additionally and in contrast to the approaches available, we administered a maximum of 3.08 ± 0.16 MBq/kg body weight (patient total amount: 206.01 ± 28.79 MBq compared to 325.6-391 MBq (Hirvonen et al., 2007; Osman et al., 1998; Parsey et al., 2000) due to regulatory issues regarding radiation protection for repetitive patient scans. Hence, our injected activity was considerably lower (36.7 to 47.4%) compared to the previously described methods (Hirvonen et al., 2007; Osman et al., 1998; Parsey et al., 2000). Thus, we had to establish a faster method compensating for the lower available activities in blood samples especially at late time points.

System requirements

Methods based on preparative HPLC systems are characterized by larger column size (Farde et al., 1998; Hirvonen et al., 2007; Osman et al., 1998; Parsey et al., 2000) and higher flow rates (Farde et al., 1998; Hirvonen et al., 2007; Osman et al., 1998) (see figure 3). Our aim was to use a conventional single analytical HPLC system, also widely used for routine quality control of radiopharmaceuticals. The use of a single HPLC-system provides the advantage avoiding potential systemic errors, which can occur using two or more systems in parallel, even if they are identical in construction and cross-calibrated. That could have significant effects on results. The appropriateness and good resolution of the system is shown in figures 4a+b. Radiometabolites are baseline-separated and easily integrated/collected by the fraction collector.

CONCLUSION

The proposed HPLC system allows the reliable quantification of the metabolic status of [*carbonyl*-¹¹C]WAY-100635 of two parallel patients simultaneously. The assay is realized with an analytical HPLC system with baseline separated metabolites. Total analysis time of two parallel patients (12 samples) is <64 minutes (excluding workup) and <115 minutes (including workup), respectively. The fastest assay so far (Farde et al., 1998; Osman et al., 1998) is about 40% slower in comparison to the herewith presented method. This improvement provides the advantage to achieve more accurate counting statistics with late samples for robustly modelling the metabolite-corrected input function.

ACKNOWLEDGEMENTS

Andreas Hahn is recipient of a DOC-fellowship of the Austrian Academy of Sciences. This study is part of the doctoral thesis of Lukas Nics at the University of Vienna and Andreas Hahn at the Medical University of Vienna. The authors are grateful to Georgios Karanikas, Peter Dolliner, Matthias Schuetz, and Pia Baldinger for blood sampling and clinical support. We are especially indebted to Bettina Reiterits, Ingrid Leitinger, Friedrich Girschele, Rainer Bartosch, Thomas Zenz and Andreas Krcal for their technical assistance.

REFERENCES

- Farde, L., Ito, H., Swahn, C.G., Pike, V.W., Halldin, C., 1998. Quantitative analyses of carbonyl-carbon-11-WAY-100635 binding to central 5-hydroxytryptamine-1A receptors in man. *J Nucl Med* 39, 1965-1971.
- Forster, E.A., Cliffe, I.A., Bill, D.J., Dover, G.M., Jones, D., Reilly, Y., Fletcher, A., 1995. A pharmacological profile of the selective silent 5-HT_{1A} receptor antagonist, WAY-100635. *European journal of pharmacology* 281, 81-88.
- Gunn, R.N., Sargent, P.A., Bench, C.J., Rabiner, E.A., Osman, S., Pike, V.W., Hume, S.P., Grasby, P.M., Lammertsma, A.A., 1998. Tracer kinetic modeling of the 5-HT_{1A} receptor ligand [carbonyl-¹¹C]WAY-100635 for PET. *NeuroImage* 8, 426-440.
- Hall, H., Lundkvist, C., Halldin, C., Farde, L., Pike, V.W., McCarron, J.A., Fletcher, A., Cliffe, I.A., Barf, T., Wikstrom, H., Sedvall, G., 1997. Autoradiographic localization of 5-HT_{1A} receptors in the post-mortem human brain using [³H]WAY-100635 and [¹¹C]way-100635. *Brain research* 745, 96-108.
- Hirvonen, J., Kajander, J., Allonen, T., Oikonen, V., Nagren, K., Hietala, J., 2007. Measurement of serotonin 5-HT_{1A} receptor binding using positron emission tomography and [carbonyl-(¹¹C)]WAY-100635-considerations on the validity of cerebellum as a reference region. *J Cereb Blood Flow Metab* 27, 185-195.
- Innis, R.B., Cunningham, V.J., Delforge, J., Fujita, M., Gjedde, A., Gunn, R.N., Holden, J., Houle, S., Huang, S.C., Ichise, M., Iida, H., Ito, H., Kimura, Y., Koeppe, R.A., Knudsen, G.M., Knutti, J., Lammertsma, A.A., Laruelle, M., Logan, J., Maguire, R.P., Mintun, M.A., Morris, E.D., Parsey, R., Price, J.C., Slifstein, M., Sossi, V., Suhara, T., Votaw, J.R., Wong, D.F., Carson, R.E., 2007. Consensus nomenclature for in vivo imaging of reversibly binding radioligands. *J Cereb Blood Flow Metab* 27, 1533-1539.
- Ito, H., Halldin, C., Farde, L., 1999. Localization of 5-HT_{1A} receptors in the living human brain using [carbonyl-¹¹C]WAY-100635: PET with anatomic standardization technique. *J Nucl Med* 40, 102-109.

Lanzenberger, R.R., Mitterhauser, M., Spindelegger, C., Wadsak, W., Klein, N., Mien, L.K., Holik, A., Attarbaschi, T., Mossaheb, N., Sacher, J., Geiss-Granadia, T., Kletter, K., Kasper, S., Tauscher, J., 2007. Reduced serotonin-1A receptor binding in social anxiety disorder. *Biological psychiatry* 61, 1081-1089.

Laven, M., Itsenko, O., Markides, K., Langstrom, B., 2006. Determination of metabolic stability of positron emission tomography tracers by LC-MS/MS: an example in WAY-100635 and two analogues. *Journal of pharmaceutical and biomedical analysis* 40, 943-951.

Ma, Y., Kiesewetter, D.O., Lang, L., Der, M., Huang, B., Carson, R.E., Eckelman, W.C., 2003. Determination of [¹⁸F]FCWAY, [¹⁸F]FP-TZTP, and their metabolites in plasma using rapid and efficient liquid-liquid and solid phase extractions. *Nuclear medicine and biology* 30, 233-240.

Ma, Y., Lang, L., Kiesewetter, D.O., Jagoda, E., Sassaman, M.B., Der, M., Eckelman, W.C., 2001. Liquid chromatography-tandem mass spectrometry identification of metabolites of two 5-HT_{1A} antagonists, N-[2-[4-(2-methoxyphenyl)piperazino]ethyl]-N-(2-pyridyl) trans- and cis-4-fluorocyclohexanecarboxamide, produced by human and rat hepatocytes. *Journal of chromatography* 755, 47-56.

Nics, L., Hartmann, S., Hahn, A., Haeusler, D., Ungersboeck, J., Mien, L.K., Wadsak, W., Lanzenberger, R., Wagner, K.H., Dudczak, R., Kletter, K., Mitterhauser, M., 2010. Quantification of radioactive metabolites of the 5-HT_{1A} receptor radioligand [carbonyl ¹¹C]-WAY-100635 in human plasma: An improved HPLC-assay. *European journal of nuclear medicine and molecular imaging* 37, S242.

Osman, S., Lundkvist, C., Pike, V.W., Halldin, C., McCarron, J.A., Swahn, C.G., Farde, L., Ginovart, N., Luthra, S.K., Gunn, R.N., Bench, C.J., Sargent, P.A., Grasby, P.M., 1998. Characterisation of the appearance of radioactive metabolites in monkey and human plasma from the 5-HT_{1A} receptor radioligand, [carbonyl-¹¹C]WAY-100635--explanation of high signal contrast in PET and an aid to biomathematical modelling. *Nuclear medicine and biology* 25, 215-223.

Parsey, R.V., Arango, V., Olvet, D.M., Oquendo, M.A., Van Heertum, R.L., John Mann, J., 2005. Regional heterogeneity of 5-HT_{1A} receptors in human cerebellum as assessed by positron emission tomography. *J Cereb Blood Flow Metab* 25, 785-793.

Parsey, R.V., Slifstein, M., Hwang, D.R., Abi-Dargham, A., Simpson, N., Mawlawi, O., Guo, N.N., Van Heertum, R., Mann, J.J., Laruelle, M., 2000. Validation and reproducibility of measurement of 5-HT_{1A} receptor parameters with [carbonyl-¹¹C]WAY-100635 in humans: comparison of arterial and reference tissue input functions. *J Cereb Blood Flow Metab* 20, 1111-1133.

Pike, V.W., Halldin, C., Wikstrom, H., Marchais, S., McCarron, J.A., Sandell, J., Nowicki, B., Swahn, C.G., Osman, S., Hume, S.P., Constantinou, M., Andree, B., Farde, L., 2000. Radioligands for the study of brain 5-HT(1A) receptors in vivo--development of some new analogues of way. *Nuclear medicine and biology* 27, 449-455.

Pike, V.W., McCarron, J.A., Lammertsma, A.A., Osman, S., Hume, S.P., Sargent, P.A., Bench, C.J., Cliffe, I.A., Fletcher, A., Grasby, P.M., 1996. Exquisite delineation of 5-HT_{1A} receptors in human brain with PET and [carbonyl-¹¹C]WAY-100635. *European journal of pharmacology* 301, R5-7.

Sargent, P.A., Kjaer, K.H., Bench, C.J., Rabiner, E.A., Messa, C., Meyer, J., Gunn, R.N., Grasby, P.M., Cowen, P.J., 2000. Brain serotonin_{1A} receptor binding measured by positron emission tomography with [¹¹C]WAY-100635: effects of depression and antidepressant treatment. *Archives of general psychiatry* 57, 174-180.

Wadsak, W., Mien, L.-K., Ettliger, D.E., Lanzenberger, R., Haeusler, D., Dudczak, R., Kletter, K., Mitterhauser, M., 2007. Simple and fully automated preparation of [carbonyl-¹¹C]WAY-100635. *Radiochim Acta* 95, 417-422.

Wu, S., Ogden, R.T., Mann, J.J., Parsey, R.V., 2007. Optimal metabolite curve fitting for kinetic modeling of ¹¹C-WAY-100635. *J Nucl Med* 48, 926-931.

FIGURES

Figure 1: Main radiometabolites and non-radioactive metabolites of [*carbonyl-¹¹C*]WAY-100635.

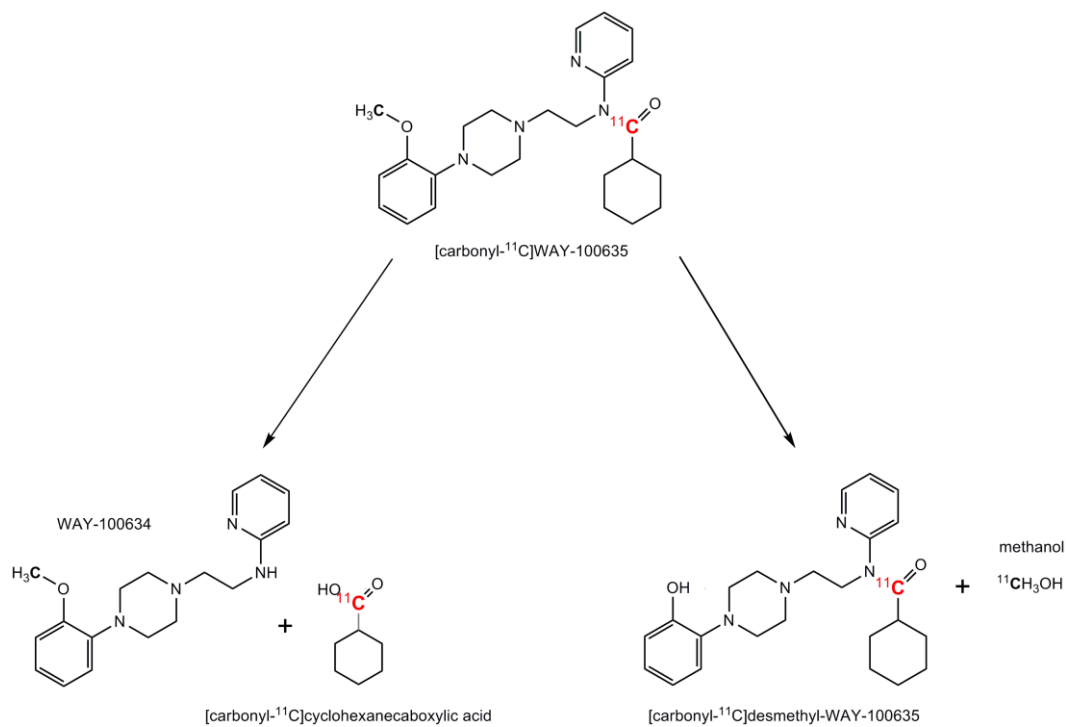


Figure 2: profile of the unmetabolized radioligand over time, obtained by a fitted Hill-type function. Bars show mean±SD (n=16).

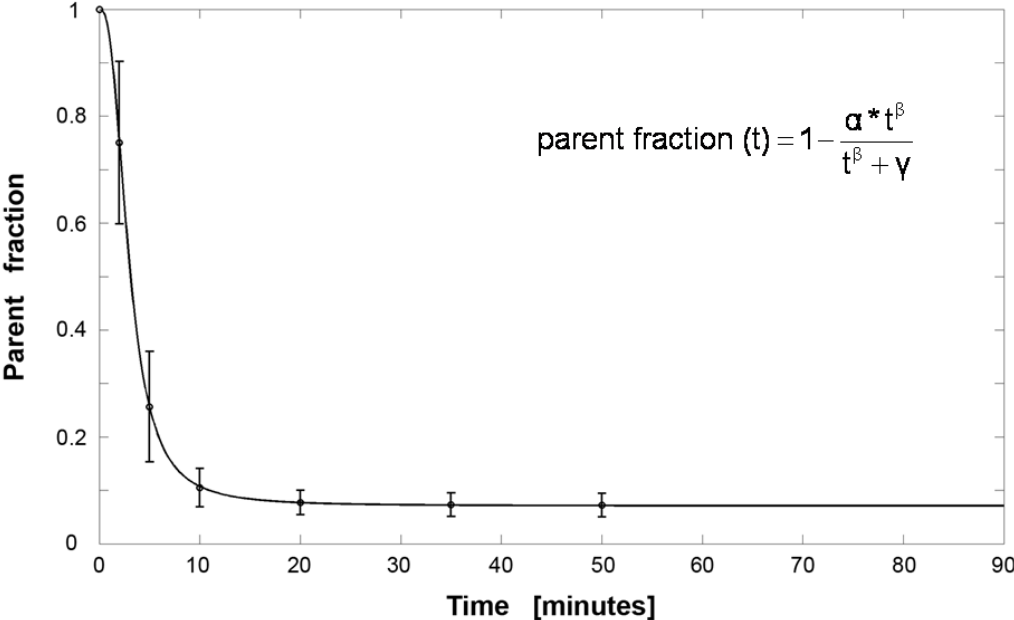


Figure 3: comparison of five major HPLC-methods (isocratic and gradient) previously described and our optimized method showing the runtime of a single sample, the HPLC-pump-flow of the mobile phase and the number of samples analyzed during one experimental setup

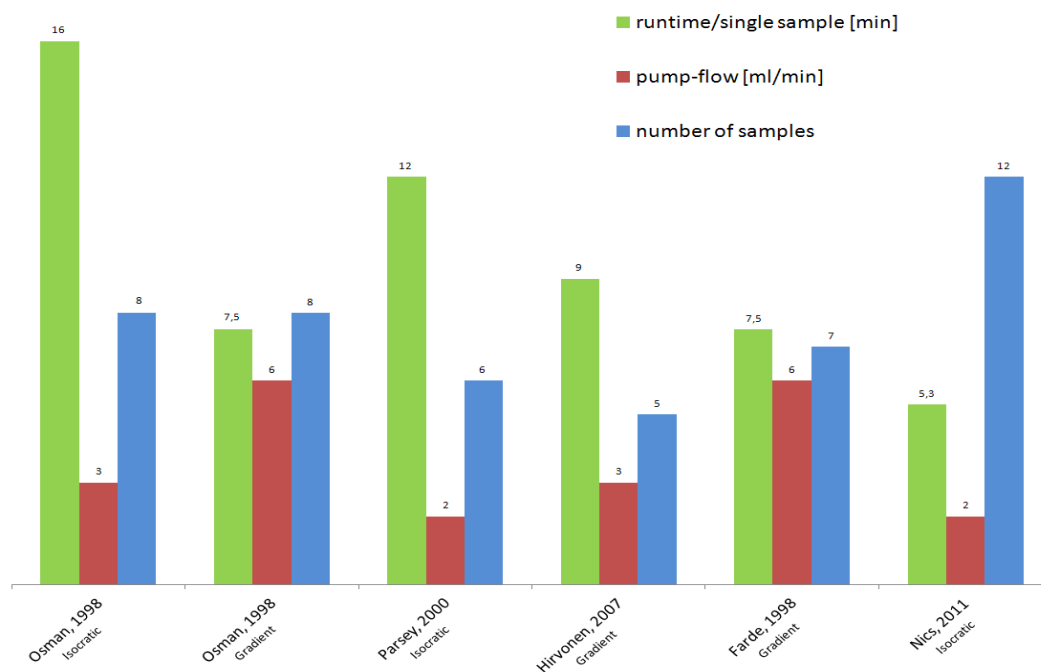
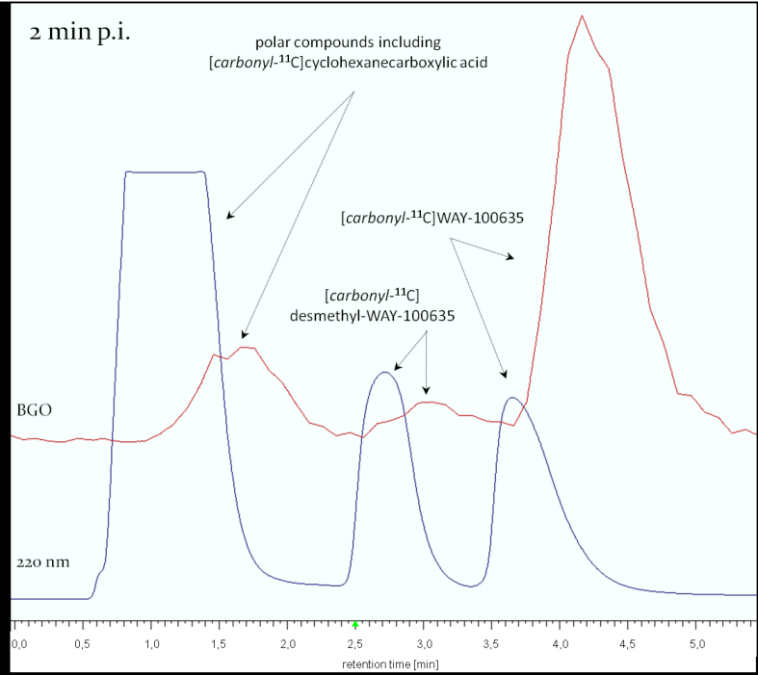
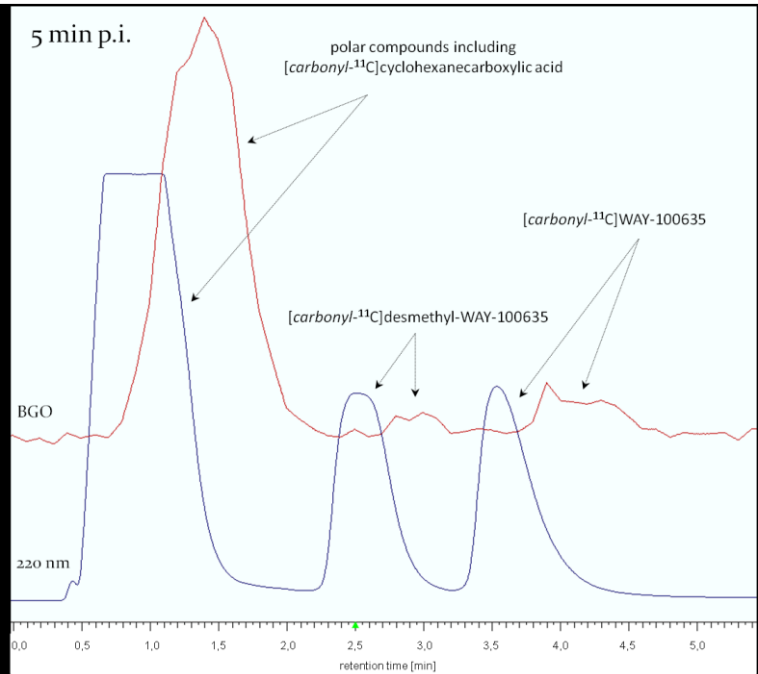


Figure 4: HPLC-Chromatogram 2 minutes (A) and 5 minutes (B) after radiotracer injection.

A



B



TABLES

Table 1: retention times (Rt), retention factors (k') of intact tracer and metabolites of all blood samples over time (mean±SD, n=16)

	molecule	Rt (min)	k'
hydrophilic metabolites	polar compounds including [carbonyl-¹¹C]cyclohexanecarboxylic acid	1.6±0.05	1.7±0.03
metabolite	[carbonyl-¹¹C]desmethyl-WAY-100635	3.0±0.01	3.6±0.16
radiotracer	[carbonyl-¹¹C]WAY-100635	4.1±0.12	5.3±0.25

Table 2: metabolic status of radiotracer and metabolites after time (minutes past injection (mean±SD, n=16))

	molecule	% 2min p.i.	% 5min p.i.	% 10min p.i.	% 20min p.i.	% 35min p.i.	% 50min p.i.
metabolites *	[carbonyl-¹¹C]cyclohexanecarboxylic acid	24.98±15.18	74.35±10.33	89.47±3.59	92.29±2.28	92.70±2.19	92.78±2.19
	[carbonyl-¹¹C]desmethyl-WAY-100635						
radiotracer	[carbonyl-¹¹C]WAY-100635	75.02±15.18	25.65±10.33	10.53±3.59	7.71±2.28	7.30±2.19	7.22±2.19

* [carbonyl-¹¹C]desmethyl-WAY-100635 was detected only in 2 of 16 patients after 2min (1.33±0.55 % of total amount) and 5min (3.50±0.66 % of total amount)

Combining image-derived and venous input functions enables quantification of serotonin-1A receptors with [*carbonyl*-¹¹C]WAY-100635 independent of arterial sampling

Andreas Hahn^{a#}, Lukas Nics^{b,d#}, Pia Baldinger^a, Johanna Ungersböck^b, Peter Dolliner^b, Richard Frey^a, Wolfgang Birkfellner^c, Markus Mitterhauser^b, Wolfgang Wadsak^b, Georgios Karanikas^b, Siegfried Kasper^a, Rupert Lanzenberger^{a*}

^a Department of Psychiatry and Psychotherapy, Medical University of Vienna, Austria

^b Department of Nuclear Medicine, Medical University of Vienna, Austria

^c Center for Medical Physics and Biomedical Engineering, Medical University of Vienna, Austria

^d Department of Nutritional Sciences, University of Vienna

NeuroImage 62 (1): 199-206, 2012

Word count	409	Abstract
	4634	Main section
Tables: 1, Figures: 5, References 48, Supplement		

These authors contributed equally.

* Correspondence to: Rupert Lanzenberger, A/Prof. PD MD
Functional, Molecular and Translational Neuroimaging Lab
Permanent address: Department of Psychiatry and Psychotherapy
Medical University of Vienna
Waehringer Guertel 18-20, 1090 Vienna, AUSTRIA
Phone: +43-1-40400-3825
Fax: +43-1-40400-3099
rupert.lanzenberger@meduniwien.ac.at
<http://www.meduniwien.ac.at/neuroimaging/>
Present address: Queensland Brain Institute
Visiting academic
University of Queensland
St. Lucia, QLD 4072, AUSTRALIA

ABSTRACT

Image-derived input functions (IDIFs) represent a promising technique for a simpler and less invasive quantification of PET studies as compared to arterial cannulation. However, a number of limitations complicate the routine use of IDIFs in clinical research protocols and the full substitution of manual arterial samples by venous ones has hardly been evaluated. This study aims for a direct validation of IDIFs and venous data for the quantification of serotonin-1A receptor binding (5-HT_{1A}) with [*carbonyl*-¹¹C]WAY-100635 before and after hormone treatment.

Methods

Fifteen PET measurements with arterial and venous blood sampling were obtained from 10 healthy women, 8 scans before and 7 after eight weeks of hormone replacement therapy. Image-derived input functions were derived automatically from cerebral blood vessels, corrected for partial volume effects and combined with venous manual samples from 10min onward (IDIF+VIF). Corrections for plasma/whole-blood ratio and metabolites were done separately with arterial and venous samples. 5-HT_{1A} receptor quantification was achieved with arterial input functions (AIF) and IDIF+VIF using a two-tissue compartment model.

Results

Comparison between arterial and venous manual blood samples yielded excellent reproducibility. Variability (VAR) was less than 10% for whole-blood activity ($p > 0.4$) and below 2% for plasma to whole-blood ratios ($p > 0.4$). Variability was slightly higher for parent fractions (VAR_{max}=24% at 5min, $p < 0.05$ and VAR<13% after 20min, $p > 0.1$) but still within previously reported values. IDIFs after partial volume correction had peak values comparable to AIFs (mean difference $\Delta = -7.6 \pm 16.9$ kBq/ml, $p > 0.1$), whereas AIFs exhibited a delay ($\Delta = 4 \pm 6.4$ s, $p < 0.05$) and higher peak width ($\Delta = 15.9 \pm 5.2$ s, $p < 0.001$). Linear regression analysis showed strong agreement for 5-HT_{1A} binding as obtained with AIF and IDIF+VIF at baseline ($R^2 = 0.95$), after treatment ($R^2 = 0.93$) and when pooling all scans ($R^2 = 0.93$), with slopes and intercepts in the range of 0.97 to 1.07 and -0.05 to 0.16, respectively. In addition to the region of interest analysis, the approach yielded virtually identical results for voxel-wise quantification as compared to the AIF.

Conclusions

Despite the fast metabolism of the radioligand, manual arterial blood samples can be substituted by venous ones for parent fractions and plasma to whole-blood ratios. Moreover, the combination of image-derived and venous input functions provides a reliable

quantification of 5-HT_{1A} receptors. This holds true for 5-HT_{1A} binding estimates before and after treatment for both regions of interest-based and voxel-wise modeling. Taken together, the approach provides less invasive receptor quantification by full independence of arterial cannulation. This offers great potential for the routine use in clinical research protocols and encourages further investigation for other radioligands with different kinetics characteristics.

KEYWORDS

image-derived input function

[*carbonyl*-¹¹C]WAY-100635

serotonin-1A

arterial input function

venous blood

kinetic analysis

INTRODUCTION

Positron emission tomography (PET) provides an excellent opportunity to quantify neuronal receptors in the living human brain. In addition to insights in basic human brain function, this has led to important investigations of psychiatric and neurological disorders such as depression (Drevets et al., 2007; Hirvonen et al., 2008; Parsey et al., 2010), anxiety disorders (Lanzenberger et al., 2007; Spindelegger et al., 2009) and Alzheimer's disease (Devanand et al., 2010). The gold standard for receptor quantification is the arterial input function, describing the amount of intact radioligand in plasma which is available for transport into tissue (Ichise et al., 2001; Mintun et al., 1984; Slifstein and Laruelle, 2001). However, arterial cannulation is an invasive and technically demanding technique, which discourages study participation and may lead to drop-out if cannulation fails or clots (Ogden et al., 2010; Zanotti-Fregonara et al., 2011a).

Several non-invasive techniques have been introduced on the basis of reference regions, which are devoid of specific receptor binding (Hume et al., 1992; Ichise et al., 2003; Lammertsma and Hume, 1996; Logan et al., 1996). These methods have been applied with great success in the majority of PET receptor studies. Still, the applicability of these models may be limited by the underlying assumptions and to tracers where a reliable reference region exists (Ichise et al., 2001; Slifstein and Laruelle, 2001). For instance, previous work reported reduced clinical sensitivity (Hammers et al., 2008) and differences in outcome parameters when using non-invasive models (Parsey et al., 2010). Notably, the two studies mention a high intersubject variability regarding blood flow and/or low but considerable specific receptor binding in the reference region. Especially for the serotonin-1A receptor antagonist [*carbonyl*-¹¹C]WAY-100635, the violation of modeling assumptions may cause a bias in binding estimates (Parsey et al., 2000; Slifstein et al., 2000).

Recently, image-derived input functions (IDIFs) have received growing attention (Zanotti-Fregonara et al., 2011a). Extracted directly from the PET images, IDIFs represent a non-invasive alternative to arterial blood sampling while being independent from a reference region. The use of IDIFs has been evaluated for several radioligands to quantify receptors (Liptrot et al., 2004) and other neuronal binding sites (Mourik et al., 2009; Sanabria-Bohorquez et al., 2003; Zanotti-Fregonara et al., 2011b), but only in a few scenarios has this become a routine clinical tool (Zanotti-Fregonara et al., 2011a). Image-derived input functions represent the activity in whole-blood and hence, the majority of radioligands require correction for metabolites and plasma to whole-blood ratio. This implies that IDIFs only result in a less-invasive procedure for the patient if manual arterial blood samples for these corrections can be avoided. The most obvious alternative would be the substitution by

venous samples (Zanotti-Fregonara et al., 2011a), but despite several suggestions of this kind (Liptrot et al., 2004; Mourik et al., 2009; Sanabria-Bohorquez et al., 2003), corrections with venous blood have hardly been used or even validated. Few exceptions include the application in a brain study using [^{18}F]FDG (Chen et al., 2007) as well as abdomen (Visvikis et al., 2004) and animal studies (Iida et al., 1992; Schroeder et al., 2007). In addition, differences between arterial and venous samples in whole-blood activity and parent fraction may further complicate successful substitution (Zanotti-Fregonara et al., 2011a). The validation of venous blood may be an even more important issue for radioligands with fast metabolism, such as [^{11}C]-PBR28 (Zanotti-Fregonara et al., 2011b) and [*carbonyl*- ^{11}C]WAY-100635 (Gunn et al., 1998).

Therefore, the aims of this study were, i) to evaluate the combination of image-derived and venous input functions for the quantification of serotonin-1A (5-HT_{1A}) receptor binding with [*carbonyl*- ^{11}C]WAY-100635. ii) To obtain a less-invasive method for quantification, the required corrections of the IDIFs for plasma to whole-blood ratio and metabolites were carried out using only venous samples. iii) The validation of the introduced approach was assessed by direct comparison with arterial blood sampling. iv) Finally, the applicability of the method was further evaluated in two independent measurement series of healthy subjects at baseline and after 8 weeks of hormone treatment.

MATERIALS and METHODS

Subjects and treatment

Ten healthy women from a clinical project participated in this study (mean age \pm sd = 54.5 \pm 3.1 years). All subjects underwent standard medical examinations, electrocardiogram, routine laboratory tests and the Structural Clinical Interview for DSM-IV Diagnoses (SCID) to rule out physical, psychiatric and neurological disorders. Further exclusion criteria were past or current substance abuse, intake of psychotropic medication or hormonal treatment. All participants were postmenopausal women, since the clinical project assessed serotonin-1A binding before and after hormone replacement therapy in a randomized, double-blind, longitudinal study. Hence, subjects underwent PET before and after 8 weeks of treatment with either A) 17 β -estradiol and progesterone, B) 17 β -estradiol or C) placebo. For this study, 15 PET scans with full blood sampling were available, 8 before and 7 after treatment. According to the randomization of the clinical project, 3, 1 and 3 subjects with post-treatment scans received A, B and C, respectively. The treatment was monitored by experienced physicians and hormonal status was confirmed by blood tests at the screening visit and the days of the PET measurements. Subjects provided written informed consent after detailed explanation of the study protocol and received reimbursement for their participation. This study was approved by the Ethics Committee of the Medical University of Vienna and the General Hospital of Vienna.

Positron emission tomography (PET)

All measurements were carried out with a GE Advance PET scanner (General Electric Medical Systems, Waukesha, WI, USA) at the Department of Nuclear Medicine, Medical University of Vienna, and are essentially described elsewhere (Hahn et al., 2010a; Lanzenberger et al., 2007; Spindelegger et al., 2009). Briefly, the subject's head was placed in a cushioned polyurethane mold and head movement was minimized with additional straps around the forehead. Following a 5min tissue attenuation scan (retractable ⁶⁸Ge rod sources, segmented attenuation approach), the 3D dynamic emission measurement started synchronously with the bolus injection of the radioligand [*carbonyl*-¹¹C]WAY-100635 (mean injected dose \pm sd = 210.2 \pm 28.1 MBq, for synthesis see Wadsak et al. (2007)). In order to capture the initial peak of the image-derived input function, 50 consecutive frames were acquired with short timing at the beginning (12x5s, 6x10s, 3x20s, 6x30s, 4x1min, 5x2min, 14x5min). Total scan time was 90min and reconstructed images comprised a spatial resolution of 4.36mm full-width at half-maximum (FWHM, determined by manufacturer's performance procedure according to NEMA NU 2-1994 standard) at the center of the field of view (matrix 128x128, 35 slices, voxel size = 3.125 x 3.125 x 4.25mm).

Blood sampling

Arterial blood samples were taken automatically for the first 3 minutes using an automated blood sampling system (ABSS, Allogg, Mariefred, Sweden). Pump rate was 4ml/min and a pre-existing cross-calibration measured according to manufacturer's recommendations was used. Manual arterial (A. radialis) and venous (V. cubitalis) blood samples were taken simultaneously by two staff members (physician supported by nurse/medical technician) at 2, 5, 10, 20, 35 and 50min post injection, 3ml each.

All manual blood samples were analyzed by two chemists/pharmacists as described previously (Nics et al., 2011). After measuring whole-blood activity in a gamma-counter (Wizard² 3" 2480, Perkin Elmer, Waltham, MA, USA), plasma was separated by centrifugation (1800g, 7min). As the plasma to whole-blood ratio is assumed to be temporally invariant for WAY-100635 (Parsey 2010, personal communication), plasma activity was measured for 3 samples (5, 10, 20min) to calculate plasma to whole-blood ratio, which were averaged for further analysis. Plasma aliquots of 830µl were then precipitated with acetonitrile (Parsey et al., 2000) and spiked with standards of WAY-100635 and its main metabolites, Desmethyl-WAY-100635 and cyclohexanecarboxylic acid. Following a second centrifugation (23000g, 4min), 2ml of the supernatant were injected into a high performance liquid chromatography system (HPLC, Merck Hitachi, Sigma-Aldrich, St. Louis, MO, USA) equipped with a BGO-crystal and a UV-detector. To enable analysis of 12 blood samples (i.e., 6 arterial and 6 venous), an optimized HPLC assay was used with two main improvements regarding the HPLC-column and the mobile phase (Nics et al., 2011). To obtain a robust assessment of radioactive metabolites, two fractions containing intact WAY-100635 and its metabolites were collected with a fraction collector and measured in the gamma counter. All activity measurements were corrected for radioactive decay and background activity.

The parent fraction of [*carbonyl*-¹¹C]WAY-100635 was then calculated as the ratio of intact radioligand to the total activity of both fractions. The time course of the unmetabolized radioligand was interpolated by fitting a Hill-type function (Gunn et al., 1998) to the six parent fractions for arterial and venous samples separately. The model parameters were estimated with a standard non-linear least squares algorithm as implemented in MatlabR2010a (The MathWorks, Natick, MA, USA). Since the radioligand experiences rapid metabolism during the first minutes, manual venous samples were preponed 15s in the analysis in order to account for different arrival times of the metabolites at different cannulation sites (a. radialis vs. v. cubitalis) (Ooue et al., 2007).

To obtain the arterial input function (AIF), automatic and manual whole-blood samples were combined and corrected for plasma to whole-blood ratio, radioactive metabolites and delay using only arterial samples. The delay (mean \pm SD = 12.1 \pm 4.9s) was determined by fitting the input function to the cerebellar white matter time activity curve for each subject and minimizing the sum of squared differences (Meyer, 1989; Ruotsalainen et al., 1997). The final plasma input function was interpolated with a sum of 3 exponentials from the peak onward (Parsey et al., 2005).

Image-derived input functions (IDIFs)

Image-derived input functions were obtained from the original (i.e., not spatially normalized) PET scans in several automated steps. First, cerebral blood vessels were delineated using linear discriminant analysis (LDA) (Hahn et al., 2010b). LDA is a supervised classification method which derives a discriminant function from a training set and assigns a (tissue) class to each voxel of the test set (i.e., the scans to be analyzed) (Hastie et al., 2009). Here, this training set was obtained from a tracer-specific template comprising an average of 36 healthy controls (Fink et al., 2009; Stein et al., 2008). Tissue classes (gray matter, white matter, cerebrospinal fluid) for the training set were defined from SPM5 probability atlases (Wellcome Trust Centre for Neuroimaging, London, UK; <http://www.fil.ion.ucl.ac.uk/spm/>). In addition, regions of interest (ROIs) for the carotid arteries were drawn manually within the PET template summed over the first minute. The individual PET scans were then scaled to the maximum intensity of the template, since classification was carried out using the voxel values rather than spatial location. Here, the maxima of the individual scans were scaled to the maximum of the template and all remaining voxels were adjusted proportionally. Classification into different tissue classes was carried out with the standard Matlab algorithm for linear discriminant analysis 'classify'. The input for LDA were voxel intensities for the training set (4 tissue groups: GM, WM, CSF, carotid arteries) and the test set (i.e., the scan to be analyzed). 'Classify' uses the training data to obtain a discriminant function, which in turn defines boundaries in multidimensional space of classification features. The features are given by the time points of the PET data. Since only the first minute of the PET scan was used, this approach may generally be considered as an adaptive thresholding technique. The blood vessel ROI resulting from LDA (Fig. S1) was then further refined. First, the peak activity and the corresponding frame when this maximum occurs were identified. The final blood vessel ROI was then restricted in order that each voxel exhibits 0.66 times the peak intensity within the identified time frame. This yields a blood pool with virtually homogenous kinetic characteristics.

To correct for spill-in from and spill-out to surrounding regions, the obtained vessel area was subjected to an ROI-based partial volume effect correction (PVC) as implemented in PMOD 3.3 (Rousset et al., 1998). The algorithm describes the spill-over between ROIs in a geometric transfer matrix (a system of linear equations) after convolution with the point spread function. The true activity for each ROI is then estimated by matrix inversion. The point spread function was defined according to the resolution of the reconstructed image by a 3D Gaussian function (4.36mm FWHM). The region surrounding the blood pool was defined as the ROI within a 4-voxel radius around the vessels (approximately 2.8 times the FWHM of the PET camera (Izquierdo-Garcia et al., 2009)). For the final input function, the peak was taken from the partial volume corrected IDIF, whereas the tail was defined by manual venous blood samples from 10min onward (IDIF+VIF). This is feasible since it may be difficult to obtain an accurate representation for both peak and tail from a single IDIF (Zanotti-Fregonara et al., 2011a) and venous samples showed only negligible differences to arterial ones after 10min (see results and figure 2). In 5 scans late venous samples (35 and 50min) were not available due to logistical problems (only one chemist available) and hence were replaced with arterial ones (see results and discussion). No scaling was applied to the IDIF (see discussion). Similar to the arterial input functions, IDIF+VIF were corrected for plasma to whole-blood ratio, radioactive metabolites and delay (mean \pm SD = 6.5 \pm 4.8s) but using only venous samples. Although in theory no delay correction is required for IDIF (Liptrot et al., 2004) this additional correction improved the model fits, most probably since IDIF were obtained from venous blood vessels. Again, the final input function was fitted with a sum of 3 exponentials.

Regions of interest and kinetic modeling

PET scans were spatially normalized to stereotactic space as defined by the Montreal Neurological Institute (MNI) with SPM8 (standard algorithm and parameters) using a tracer-specific template (Fink et al., 2009; Stein et al., 2008). For 5-HT_{1A} receptor quantification regions of interest were taken from an atlas (Stein et al., 2008): frontal, orbitofrontal, parietal, temporal, occipital and cingulate cortices, insula, amygdala-hippocampus complex, midbrain (including the dorsal raphe nucleus) as well as cerebellar gray (excluding vermis) and cerebellar white matter. These ROIs cover a great range of 5-HT_{1A} binding and include areas typically reported in psychiatric disorders (Drevets et al., 2007; Hahn et al., 2010a; Hirvonen et al., 2008; Lanzenberger et al., 2007; Parsey et al., 2010; Spindelegger et al., 2009). To improve model fits, the time activity curves of each ROI were resampled to 10x1min, 5x2min and 14x5min.

Quantification of the 5-HT_{1A} receptor binding potential (BP_P (Innis et al., 2007)) was carried out separately for AIF and IDIF+VIF with PMOD 3.3. A two-tissue compartment model was used, with K_1/k_2 fixed to that of cerebellar white matter (Hirvonen et al., 2007; Parsey et al., 2010). A cerebral blood volume component of 5% was assumed for all kinetic modeling procedures, using CBV for the whole-blood curve and 1-CBV for the tissue component (Gunn et al., 1998; Hirvonen et al., 2007; Parsey et al., 2010). In addition to ROI-based quantification, we computed voxel-wise binding potential maps to facilitate visualization of the results. A two-tissue compartment model with ridge regression was used to provide stable fits (Byrtek et al., 2005) with K_1/k_2 fixed to that of cerebellar white matter as obtained from the ROI analysis. Standard values of PMOD 3.3 ($\lambda = 10$ = penalty of factor 10) were chosen for ridge factors, which provided more stable parametric modeling estimates than the standard two-tissue compartment model. Taking into account potential uncertainties associated with variations in the cerebral blood volume component (CBV) (Gunn et al., 1998; Slifstein et al., 2000), this was included as fit parameter in an additional voxel-wise analysis.

To evaluate the performance in relation to a reference region model, 5-HT_{1A} receptor binding potentials were compared between the two-tissue compartment model with $BP_{ND} = (V_T - V_{ND})/V_{ND}$ and the multilinear reference tissue model 2 (MRTM2 (Ichise et al., 2003)). For the latter one, k_2' was estimated from time activity curves of a receptor rich and poor region (insula and cerebellar white matter, respectively) (Hahn et al., 2010a; Ichise et al., 2003) using the simplified reference tissue model (Lammertsma and Hume, 1996).

Statistical analysis

Comparisons between manual arterial (A) and venous (V) blood samples and input function parameters were carried out with paired- or two-sample t-tests where appropriate. Also, we calculated the variability (reproducibility) as $(A-V)/\text{mean}(A,V) \cdot 100$ (Hirvonen et al., 2007) and computed Bland-Altman plots. Direct comparison of 5-HT_{1A} BP_P obtained from AIF and IDIF+VIF was evaluated by linear regression analysis. Furthermore, to assess bias in 5-HT_{1A} binding obtained with the two different input functions, a repeated measures ANOVA was computed with method and ROI as fixed effects and subject as random effect (Ogden et al., 2010). All statistical tests were carried out two-tailed and calculated with MatlabR2010a or SPSS 18 (IBM, New York, USA).

RESULTS

For manual samples there was no significant difference in whole-blood activity between arterial and venous samples from 10min onward, variability was below 10% and absolute difference was less than 0.5kBq/ml ($p>0.4$). Similarly, no significant difference was found for plasma to whole-blood ratio between arterial and venous samples with a variability of 1.9% ($p>0.4$, Fig. S2). For radioactive metabolites, the first three venous samples (2, 5, 10min) showed significantly higher parent fractions but with absolute differences below 6% ($p<0.05$, Fig. 1). Also, maximum variability (24% at 5min) was in line with reported reproducibility values (Hirvonen et al., 2007; Parsey et al., 2000). Venous parent fractions obtained at later time points (20, 35, 50min) were not significantly different from arterial samples (variability $< 13%$, $p>0.12$). Bland-Altman plots generally confirm these results between arterial and venous manual blood samples (Fig. S3).

Automatically extracted regions of interest for IDIFs comprised 29.4 ± 18.3 voxels (mean \pm sd), of which only 0.9 ± 1.9 were located within the carotid arteries. Signal to noise ratio of uncorrected IDIF peaks to surrounding activity was 5.2 ± 0.8 . The magnitude of partial volume correction was consistent across subjects with a ratio of IDIF peaks after/before PVC of 1.75 ± 0.2 . Compared to image-derived input functions after PVC, the arterial input functions showed slightly but non-significantly lower peak values (mean difference $\Delta = -7.6\pm 16.9$ kBq/ml, $p>0.1$). However, the AIF peaks emerged significantly later ($\Delta = 4\pm 6.4$ s, $p<0.05$) and exhibited a higher full-width at half-maximum ($\Delta = 15.9\pm 5.2$ s, $p<0.001$, Fig. 2).

Direct comparisons of 5-HT_{1A} binding obtained with AIF and IDIF+VIF are given in Figures 3, Figure 5 and Table 1. For ROI-analysis, linear regression showed strong correlations between the two methods at baseline ($R^2=0.95$), after treatment ($R^2=0.93$) and when pooling all scans ($R^2=0.93$). Similarly, intercepts were close to zero (-0.05 to 0.16) and slopes close to unity (0.97 to 1.07, Table 1). The differences between baseline and treatment regression parameters were not significant for slopes ($p=0.87$), intercepts ($p=0.73$) nor correlation coefficients ($p=0.28$). Including only those 10 subjects where late venous sampling (35min and 50min) was fully available did not change the results ($R^2=0.94$, intercept=0.03, slope=1.03, table 1). Furthermore, there was no significant bias in 5-HT_{1A} BP_P between AIF and IDIF+VIF as assessed by repeated measures ANOVA ($F_{1,43} = 2.4$, $p>0.1$). Although individual model fits of the time activity curves were similar (Fig. 4), AIF showed slightly but significantly lower sum of squared differences ($F_{1,21} = 10.8$, $p<0.01$). Bland-Altman plots show no absolute or proportional errors, but a slightly increased variation with increasing binding potentials between the two methods (Fig. S4). Similarly, voxel-wise analysis showed excellent agreement between the two methods, where differences appeared only in areas

with lowest receptor binding (Fig. 5A and B). These differences almost vanished after inclusion of CBV as additional fit parameter (Fig. 5C and D).

The comparison of BP_{ND} values between the two-tissue compartment model and the MRTM2 was similar for AIF and IDIF+VIF. Although intercepts were close to zero (0.09 and 0.008), the agreement was weaker than within the two input function models when pooling all subjects ($R^2_{AIF}=0.823$ and $R^2_{IDIF+VIF}=0.818$). Slopes indicate a considerable underestimation by the reference tissue model (0.42 and 0.33), which is in line with previous results (Gunn et al., 1998). See table 1 and figure S5 for details.

DISCUSSION

This work demonstrates the applicability of image-derived input functions combined with venous blood samples to quantify serotonin-1A receptor binding using [*carbonyl*- ^{11}C]WAY-100635. Moreover, we were able to resolve essential issues for the use of IDIFs. Direct comparison showed that arterial samples can be substituted by venous ones for plasma to whole-blood ratios and parent fractions despite the fast metabolism of the radioligand. Hence, the combination of image-derived and venous input functions represents a promising quantification method which is entirely independent of arterial samples. Importantly, the approach yielded robust estimates of 5-HT_{1A} receptor binding at baseline and after 8 weeks of hormone treatment, which holds true for both ROI-based and voxel-wise quantification.

Although image-derived input functions have been evaluated for a variety of radioligands (see introduction), recent work demonstrated the limited applicability of IDIFs (Zanotti-Fregonara et al., 2011a). Potential problems include poor identification of cerebral blood vessels within the PET images, unreliable estimation of the input function shape, fast metabolism of the radioligand and differences between arterial and venous manual blood samples. Despite these issues, our results indicate that IDIFs combined with venous blood samples represent a promising approach for modeling of [*carbonyl*- ^{11}C]WAY-100635. The validation of IDIFs in clinical research protocols is a major step toward reduced invasiveness, however, to date only a few studies have used IDIFs as a routine tool (Zanotti-Fregonara et al., 2011a). Here, we investigate the application of IDIFs for both baseline and treatment measurements yielding robust 5-HT_{1A} binding estimates independent of hormone therapy. This combination of image-derived and venous input functions may provide a method that can be widely used in clinical studies, thereby offering a less invasive procedure for the patient. Still, the extrapolation to other radioligands requires further investigation especially for tracers with different plasma kinetics.

Manual blood samples, metabolites and kinetic modeling

Direct comparison of manual blood samples showed excellent agreement between arterial and venous data. For whole-blood samples it seems that arterio-venous equilibrium is reached at 10min post injection for [*carbonyl*-¹¹C]WAY-100635, which is a prerequisite for the complete avoidance of arterial cannulation (Zanotti-Fregonara et al., 2011a) unless a consistent relationship can be obtained to scale venous samples. This lack of equilibrium prior to 10min may at least in part explain the higher parent fraction observed in early venous samples (2, 5, 10min). Though, these differences are still within reported test-retest values of 26% (Hirvonen et al., 2007; Parsey et al., 2000).

Despite the aforementioned difference in the metabolite profile, linear regression analysis indicates a high degree of agreement of 5-HT_{1A} binding between IDIF+VIF and AIF based modelling ($R^2=0.93-0.95$). These values are comparable to previous studies using IDIFs for tracer kinetic modeling (Mourik et al., 2009; Sanabria-Bohorquez et al., 2003; Zanotti-Fregonara et al., 2011b). Notably, in the majority of these studies only the arterial whole blood time-activity curve was replaced by the image-derived input functions, but arterial blood samples were used for plasma to whole-blood ratios and metabolite correction. A residual variability of 5-7% between AIF and IDIF+VIF is well below previous test-retest values of 14% (Parsey et al., 2000) and 12% (Hirvonen et al., 2007) for 5-HT_{1A} binding.

Although the Logan plot (Logan et al., 1990) appears to be the preferred approach for assessing IDIFs (Mourik et al., 2009; Zanotti-Fregonara et al., 2011a; Zanotti-Fregonara et al., 2011b), we did not evaluate this method for two reasons. The fast metabolism of [*carbonyl*-¹¹C]WAY-100635 considerably decreases the area under the tail of the input function, which may complicate a robust estimation of 5-HT_{1A} binding due to potentially high variations in IDIF peaks (Zanotti-Fregonara et al., 2011a). Second, the two-tissue compartment model is considered as the model of choice for this radioligand when using input function modeling (Gunn et al., 1998; Hirvonen et al., 2007; Parsey et al., 2010). Individual rate constants may be difficult to estimate with IDIFs (Zanotti-Fregonara et al., 2011a), though, our results indicate that macroparameters such as binding potentials can be robustly identified with the combination of IDIFs and venous blood samples. This is also confirmed by the agreement between the two methods in 5-HT_{1A} binding obtained from both ROI-based and voxel-wise modeling. Moreover, the direct comparison between arterial and venous samples enables the application of venous blood for other non-invasive quantification techniques (Ogden et al., 2010).

Extraction of image-derived input functions

The radioligand [*carbonyl*-¹¹C]WAY-100635 showed a high signal contrast of cerebral vessel activity as compared to the surrounding tissue, which is another requirement when extracting IDIFs using blood vessel ROIs directly delineated from PET data (Zanotti-Fregonara et al., 2011a). The high signal to noise ratio also makes the algorithm robust against scaling errors induced by noise. Alternatively, the algorithm could be further improved by scaling individual scans not simply to the maximum but e.g., to the average of several maximum intensity voxels. Several techniques have been introduced for the definition of blood vessel ROIs, each comprising certain advantages. This includes simple manual delineation (Chen et al., 1998) as well as automatic methods such as clustering (Liptrot et al., 2004), fixed volumes of high intensity voxels (Mourik et al., 2008) and independent component analysis (Chen et al., 2007). We used linear discriminant analysis for a first definition of the cerebral blood vessels (Hahn et al., 2010b) followed by two additional restrictions (percentage of maximum in certain time frame). More generally, the algorithm automatically determines individually adaptive thresholds in several steps. Although it might be more intuitive to extract image-derived input functions from arteries (Zanotti-Fregonara et al., 2011a), the vast majority of our final ROIs comprised venous blood vessels. However, this freedom to let the algorithm choose may yield a higher signal-to-noise ratio for several reasons. Venous vessels showed higher tracer concentrations and the typical field of view of PET brain scans covers more voxels within venous vessels than arterial ones. The latter also indicates that venous cerebral vessels are larger than the carotid arteries, which in turn causes less pronounced partial volume effects. This may explain the similarly high IDIF peaks as compared to AIF, although manual venous blood samples showed lower activities than arterial ones. Alternatively, the slightly lower AIF peaks may result from dispersion caused by the automated blood sampling system or uncertainties in partial volume correction algorithm. Therefore, a thorough evaluation of issues such as dispersion correction as well as the definition of the point spread function and ROI size should be subject to future studies. Furthermore, it is theoretically possible that (depending on the transport across the blood brain barrier) the tracer concentration is more similar between arterial and venous blood in cerebral capillaries than at distal sites such as the hand. Nevertheless, it might be more important to focus on a homogenous blood pool for IDIF extraction rather than on its location (Naganawa et al., 2005; Turkheimer et al., 2007). Still, further evaluation is required for the extrapolation of the method to other radioligands and for the assessment of other modeling parameters such as individual rate constants.

Concerning peak recovery, recent work suggested that scaling of IDIFs with blood samples may provide better estimates than PVC solely based on image data (Zanotti-Fregonara et al., 2011a). However, the authors also acknowledged that IDIF methods are tracer specific and may not work equally well for other radioligands. Using an established scaling technique (Chen et al., 1998), we observed a high variability in IDIF peak values when compared to arterial input functions (data not shown), hence this approach was not further evaluated. Instead of scaling, partial volume corrected IDIFs were used for peaks only, whereas manual venous blood samples represented the tail of the input function. This is reasonable since a single IDIF may not give an accurate representation for both peak and tail of the input function (Zanotti-Fregonara et al., 2011a).

CONCLUSIONS

This study validates the use of image-derived input functions combined with venous blood data for the modeling of [*carbonyl*-¹¹C]WAY-100635. The direct comparison of manual arterial samples with venous ones enables the complete substitution of arterial cannulation, yielding a less-invasive procedure for the patient. Moreover, the evaluation of the method before and after treatment demonstrates its potential for routine use in clinical research protocols and encourages further investigation for other radioligands with different kinetics characteristics.

ACKNOWLEDGEMENTS

A. Hahn is a recipient of a DOC-fellowship of the Austrian Academy of Sciences (OeAW). This research was supported by a grant from the Austrian National Bank (OeNB12809). We are grateful to A. Höflich and P. Stein from the Department of Psychiatry as well as to the PET teams of the Department of Nuclear Medicine, especially to R. Dudczak, M. Schütz, B. Reiterits, R. Bartosch, I. Leitinger, S. Hartmann and M. Zeilinger for medical and/or technical support. This study is part of the doctoral theses of A. Hahn at the Medical University of Vienna (www.meduniwien.ac.at/clins) and L. Nics at the University of Vienna.

CONFLICT OF INTEREST

Without any relevance to this work, S. Kasper declares that he has received grant/research support from Eli Lilly, Lundbeck A/S, Bristol-Myers Squibb, Servier, Sepracor, GlaxoSmithKline, Organon, and has served as a consultant or on advisory boards for AstraZeneca, Austrian Science Found, Bristol-Myers Squibb, GlaxoSmithKline, Eli Lilly, Lundbeck A/S, Pfizer, Organon, Sepracor, Janssen, and Novartis, and has served on speakers' bureaus for AstraZeneca, Eli Lilly, Lundbeck A/S, Servier, Sepracor and Janssen. R. Lanzenberger received travel grants and conference speaker honoraria from AstraZeneca and Lundbeck A/S. M. Mitterhauser and W. Wadsak received speaker honoraria from Bayer.

Parts of this study were presented at the Xth International Conference on Quantification of Brain Function with PET (BrainPET), 2011, Barcelona, Spain.

REFERENCES

Byrtek, M., O'Sullivan, F., Muzi, M., Spence, A.M., 2005. An adaptation of ridge regression for improved estimation of kinetic model parameters from PET studies. *IEEE Transactions on Nuclear Science* 52, 63-68.

Chen, K., Bandy, D., Reiman, E., Huang, S.C., Lawson, M., Feng, D., Yun, L.S., Palant, A., 1998. Noninvasive quantification of the cerebral metabolic rate for glucose using positron emission tomography, 18F-fluoro-2-deoxyglucose, the Patlak method, and an image-derived input function. *J Cereb Blood Flow Metab* 18, 716-723.

Chen, K., Chen, X., Renaut, R., Alexander, G.E., Bandy, D., Guo, H., Reiman, E.M., 2007. Characterization of the image-derived carotid artery input function using independent component analysis for the quantitation of [18F] fluorodeoxyglucose positron emission tomography images. *Phys Med Biol* 52, 7055-7071.

Devanand, D.P., Mikhno, A., Pelton, G.H., Cuasay, K., Pradhaban, G., Dileep Kumar, J.S., Upton, N., Lai, R., Gunn, R.N., Libri, V., Liu, X., van Heertum, R., Mann, J.J., Parsey, R.V., 2010. Pittsburgh compound B (11C-PIB) and fluorodeoxyglucose (18 F-FDG) PET in patients with Alzheimer disease, mild cognitive impairment, and healthy controls. *J Geriatr Psychiatry Neurol* 23, 185-198.

Drevets, W.C., Thase, M.E., Moses-Kolko, E.L., Price, J., Frank, E., Kupfer, D.J., Mathis, C., 2007. Serotonin-1A receptor imaging in recurrent depression: replication and literature review. *Nucl Med Biol* 34, 865-877.

Fink, M., Wadsak, W., Savli, M., Stein, P., Moser, U., Hahn, A., Mien, L.K., Kletter, K., Mitterhauser, M., Kasper, S., Lanzenberger, R., 2009. Lateralization of the serotonin-1A receptor distribution in language areas revealed by PET. *NeuroImage* 45, 598-605.

Gunn, R.N., Sargent, P.A., Bench, C.J., Rabiner, E.A., Osman, S., Pike, V.W., Hume, S.P., Grasby, P.M., Lammertsma, A.A., 1998. Tracer kinetic modeling of the 5-HT1A receptor ligand [carbonyl-11C]WAY-100635 for PET. *NeuroImage* 8, 426-440.

Hahn, A., Lanzenberger, R., Wadsak, W., Spindelegger, C., Moser, U., Mien, L.-K., Mitterhauser, M., Kasper, S., 2010a. Escitalopram enhances the association of serotonin-1A autoreceptors to heteroreceptors in anxiety disorders. *J Neurosci* 30, 14482-14489.

Hahn, A., Savli, M., Spindelegger, C., Haeusler, D., Wadsak, W., Mitterhauser, M., Kasper, S., Lanzenberger, R., 2010b. Segmentation of [11C]DASB and [carbonyl-11C]WAY-100635 PET Brain Images using Linear Discriminant Analysis. *NeuroImage* 52 (S1), S155-S156.

Hammers, A., Panagoda, P., Heckemann, R.A., Kelsch, W., Turkheimer, F.E., Brooks, D.J., Duncan, J.S., Koepp, M.J., 2008. [11C]Flumazenil PET in temporal lobe epilepsy: do we need an arterial input function or kinetic modeling? *J Cereb Blood Flow Metab* 28, 207-216.

Hastie, T., Tibshirani, R., Friedman, J., 2009. *The Elements of Statistical Learning: Data Mining, Inference, and Prediction*. Springer, New York.

Hirvonen, J., Kajander, J., Allonen, T., Oikonen, V., Nagren, K., Hietala, J., 2007. Measurement of serotonin 5-HT_{1A} receptor binding using positron emission tomography and [carbonyl-(11)C]WAY-100635-considerations on the validity of cerebellum as a reference region. *J Cereb Blood Flow Metab* 27, 185-195.

Hirvonen, J., Karlsson, H., Kajander, J., Lepola, A., Markkula, J., Rasi-Hakala, H., Nagren, K., Salminen, J.K., Hietala, J., 2008. Decreased brain serotonin 5-HT_{1A} receptor availability in medication-naive patients with major depressive disorder: an in-vivo imaging study using PET and [carbonyl-11C]WAY-100635. *Int J Neuropsychopharmacol* 11, 465-476.

Hume, S.P., Myers, R., Bloomfield, P.M., Opacka-Juffry, J., Cremer, J.E., Ahier, R.G., Luthra, S.K., Brooks, D.J., Lammertsma, A.A., 1992. Quantitation of carbon-11-labeled raclopride in rat striatum using positron emission tomography. *Synapse* 12, 47-54.

Ichise, M., Liow, J.S., Lu, J.Q., Takano, A., Model, K., Toyama, H., Suhara, T., Suzuki, K., Innis, R.B., Carson, R.E., 2003. Linearized reference tissue parametric imaging methods: application to [11C]DASB positron emission tomography studies of the serotonin transporter in human brain. *J Cereb Blood Flow Metab* 23, 1096-1112.

Ichise, M., Meyer, J.H., Yonekura, Y., 2001. An introduction to PET and SPECT neuroreceptor quantification models. *J Nucl Med* 42, 755-763.

Iida, H., Rhodes, C.G., de Silva, R., Araujo, L.I., Bloomfield, P.M., Lammertsma, A.A., Jones, T., 1992. Use of the left ventricular time-activity curve as a noninvasive input function in dynamic oxygen-15-water positron emission tomography. *J Nucl Med* 33, 1669-1677.

Innis, R.B., Cunningham, V.J., Delforge, J., Fujita, M., Gjedde, A., Gunn, R.N., Holden, J., Houle, S., Huang, S.C., Ichise, M., Iida, H., Ito, H., Kimura, Y., Koeppe, R.A., Knudsen, G.M., Knutti, J., Lammertsma, A.A., Laruelle, M., Logan, J., Maguire, R.P., Mintun, M.A., Morris, E.D., Parsey, R., Price, J.C., Slifstein, M., Sossi, V., Suhara, T., Votaw, J.R., Wong, D.F., Carson, R.E., 2007. Consensus nomenclature for in vivo imaging of reversibly binding radioligands. *J Cereb Blood Flow Metab* 27, 1533-1539.

Izquierdo-Garcia, D., Davies, J.R., Graves, M.J., Rudd, J.H., Gillard, J.H., Weissberg, P.L., Fryer, T.D., Warburton, E.A., 2009. Comparison of methods for magnetic resonance-guided [18-F]fluorodeoxyglucose positron emission tomography in human carotid arteries: reproducibility, partial volume correction, and correlation between methods. *Stroke* 40, 86-93.

Lammertsma, A.A., Hume, S.P., 1996. Simplified reference tissue model for PET receptor studies. *NeuroImage* 4, 153-158.

Lanzenberger, R.R., Mitterhauser, M., Spindelegger, C., Wadsak, W., Klein, N., Mien, L.-K., Holik, A., Attarbaschi, T., Mossaheb, N., Sacher, J., Geiss-Granadia, T., Kletter, K., Kasper, S., Tauscher, J., 2007. Reduced serotonin-1A receptor binding in social anxiety disorder. *Biol Psychiatry* 61, 1081-1089.

Liptrot, M., Adams, K.H., Martiny, L., Pinborg, L.H., Lonsdale, M.N., Olsen, N.V., Holm, S., Svarer, C., Knudsen, G.M., 2004. Cluster analysis in kinetic modelling of the brain: a noninvasive alternative to arterial sampling. *NeuroImage* 21, 483-493.

Logan, J., Fowler, J.S., Volkow, N.D., Wang, G.J., Ding, Y.S., Alexoff, D.L., 1996. Distribution volume ratios without blood sampling from graphical analysis of PET data. *J Cereb Blood Flow Metab* 16, 834-840.

Logan, J., Fowler, J.S., Volkow, N.D., Wolf, A.P., Dewey, S.L., Schlyer, D.J., MacGregor, R.R., Hitzemann, R., Bendriem, B., Gatley, S.J., et al., 1990. Graphical analysis of reversible radioligand binding from time-activity measurements applied to [N-11C-methyl]-(-)-cocaine PET studies in human subjects. *J Cereb Blood Flow Metab* 10, 740-747.

Meyer, E., 1989. Simultaneous correction for tracer arrival delay and dispersion in CBF measurements by the H215O autoradiographic method and dynamic PET. *J Nucl Med* 30, 1069-1078.

Mintun, M.A., Raichle, M.E., Kilbourn, M.R., Wooten, G.F., Welch, M.J., 1984. A quantitative model for the in vivo assessment of drug binding sites with positron emission tomography. *Ann Neurol* 15, 217-227.

Mourik, J.E., Lubberink, M., Klumpers, U.M., Comans, E.F., Lammertsma, A.A., Boellaard, R., 2008. Partial volume corrected image derived input functions for dynamic PET brain studies: methodology and validation for [11C]flumazenil. *NeuroImage* 39, 1041-1050.

Mourik, J.E., Lubberink, M., Schuitemaker, A., Tolboom, N., van Berckel, B.N.M., Lammertsma, A.A., Boellaard, R., 2009. Image-derived input functions for PET brain studies. *Eur J Nucl Med Mol Imaging* 36, 463-471.

Naganawa, M., Kimura, Y., Ishii, K., Oda, K., Ishiwata, K., Matani, A., 2005. Extraction of a plasma time-activity curve from dynamic brain PET images based on independent component analysis. *IEEE Trans Biomed Eng* 52, 201-210.

Nics, L., Hahn, A., Zeilinger, M., Vranka, C., Ungersboeck, J., Haeusler, D., Hartmann, S., Wagner, K.-H., Dudczak, R., Lanzenberger, R., Wadsak, W., Mitterhauser, M., 2011. Quantification of the serotonin-1A receptor radioligand [carbonyl-11C]WAY-100635 and its radio-metabolites in human plasma: An improved HPLC-assay allowing two parallel patients. *Nuklearmedizin* Submitted.

Ogden, R.T., Zanderigo, F., Choy, S., Mann, J.J., Parsey, R.V., 2010. Simultaneous estimation of input functions: an empirical study. *J Cereb Blood Flow Metab* 30, 816-826.

Ooue, A., Ichinose-Kuwahara, T., Shamsuddin, A.K., Inoue, Y., Nishiyasu, T., Koga, S., Kondo, N., 2007. Changes in blood flow in a conduit artery and superficial vein of the upper arm during passive heating in humans. *Eur J Appl Physiol* 101, 97-103.

Parsey, R., Slifstein, M., Hwang, D.R., Abi-Dargham, A., Simpson, N., Mawlawi, O., Guo, N.N., Van Heertum, R., Mann, J.J., Laruelle, M., 2000. Validation and reproducibility of measurement of 5-HT_{1A} receptor parameters with [carbonyl-11C]WAY-100635 in humans: comparison of arterial and reference tissue input functions. *J Cereb Blood Flow Metab* 20, 1111-1133.

Parsey, R.V., Arango, V., Olvet, D.M., Oquendo, M.A., Van Heertum, R.L., John Mann, J., 2005. Regional heterogeneity of 5-HT_{1A} receptors in human cerebellum as assessed by positron emission tomography. *J Cereb Blood Flow Metab* 25, 785-793.

Parsey, R.V., Ogden, R.T., Miller, J.M., Tin, A., Hesselgrave, N., Goldstein, E., Mikhno, A., Milak, M., Zanderigo, F., Sullivan, G.M., Oquendo, M.A., Mann, J.J., 2010. Higher serotonin 1A binding in a second major depression cohort: modeling and reference region considerations. *Biol Psychiatry* 68, 170-178.

Rousset, O.G., Ma, Y., Evans, A.C., 1998. Correction for partial volume effects in PET: principle and validation. *J Nucl Med* 39, 904-911.

Ruotsalainen, U., Raitakari, M., Nuutila, P., Oikonen, V., Sipila, H., Teras, M., Knuuti, M.J., Bloomfield, P.M., Iida, H., 1997. Quantitative blood flow measurement of skeletal muscle using oxygen-15-water and PET. *J Nucl Med* 38, 314-319.

Sanabria-Bohorquez, S.M., Maes, A., Dupont, P., Bormans, G., de Groot, T., Coimbra, A., Eng, W., Laethem, T., De Lepeleire, I., Gambale, J., Vega, J.M., Burns, H.D., 2003. Image-derived input function for [¹¹C]flumazenil kinetic analysis in human brain. *Mol Imaging Biol* 5, 72-78.

Schroeder, T., Vidal Melo, M.F., Musch, G., Harris, R.S., Venegas, J.G., Winkler, T., 2007. Image-derived input function for assessment of ¹⁸F-FDG uptake by the inflamed lung. *J Nucl Med* 48, 1889-1896.

Slifstein, M., Laruelle, M., 2001. Models and methods for derivation of in vivo neuroreceptor parameters with PET and SPECT reversible radiotracers. *Nucl Med Biol* 28, 595-608.

Slifstein, M., Parsey, R.V., Laruelle, M., 2000. Derivation of [(11)C]WAY-100635 binding parameters with reference tissue models: effect of violations of model assumptions. *Nucl Med Biol* 27, 487-492.

Spindelegger, C., Lanzenberger, R., Wadsak, W., Mien, L.K., Stein, P., Mitterhauser, M., Moser, U., Holik, A., Pezawas, L., Kletter, K., Kasper, S., 2009. Influence of escitalopram treatment on 5-HT(1A) receptor binding in limbic regions in patients with anxiety disorders. *Mol Psychiatry* 14, 1040-1050.

Stein, P., Savli, M., Wadsak, W., Mitterhauser, M., Fink, M., Spindelegger, C., Mien, L.K., Moser, U., Dudczak, R., Kletter, K., Kasper, S., Lanzenberger, R., 2008. The serotonin-1A receptor distribution in healthy men and women measured by PET and [carbonyl-11C]WAY-100635. *Eur J Nucl Med Mol Imaging* 35, 2159-2168.

Turkheimer, F.E., Edison, P., Pavese, N., Roncaroli, F., Anderson, A.N., Hammers, A., Gerhard, A., Hinz, R., Tai, Y.F., Brooks, D.J., 2007. Reference and target region modeling of [11C]-(R)-PK11195 brain studies. *J Nucl Med* 48, 158-167.

Visvikis, D., Francis, D., Mulligan, R., Costa, D.C., Croasdale, I., Luthra, S.K., Taylor, I., Ell, P.J., 2004. Comparison of methodologies for the in vivo assessment of 18FLT utilisation in colorectal cancer. *Eur J Nucl Med Mol Imaging* 31, 169-178.

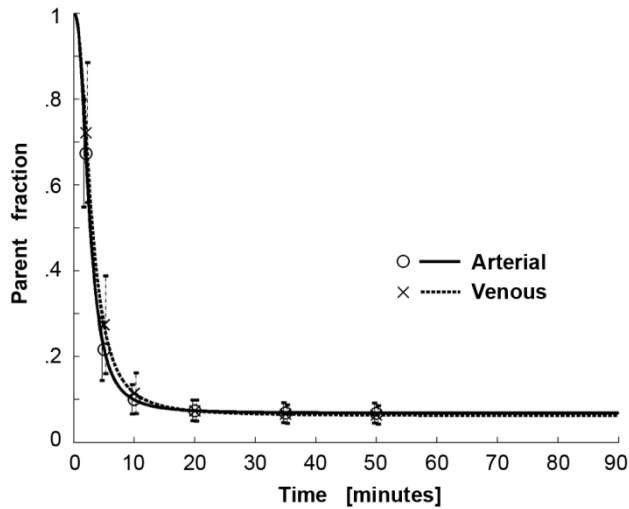
Wadsak, W., Mien, L.K., Ettliger, D.E., Lanzenberger, R., Haeusler, D., Dudczak, R., Kletter, K., Mitterhauser, M., 2007. Simple and fully automated preparation of [carbonyl-11C]WAY-100635. *Radiochimica Acta* 95, 417-422.

Zanotti-Fregonara, P., Chen, K., Liow, J.S., Fujita, M., Innis, R.B., 2011a. Image-derived input function for brain PET studies: many challenges and few opportunities. *J Cereb Blood Flow Metab* 31, 1986-1998.

Zanotti-Fregonara, P., Liow, J.S., Fujita, M., Dusch, E., Zoghbi, S.S., Luong, E., Boellaard, R., Pike, V.W., Comtat, C., Innis, R.B., 2011b. Image-derived input function for human brain using high resolution PET imaging with [C](R)-rolipram and [C]PBR28. *PLoS One* 6, e17056.

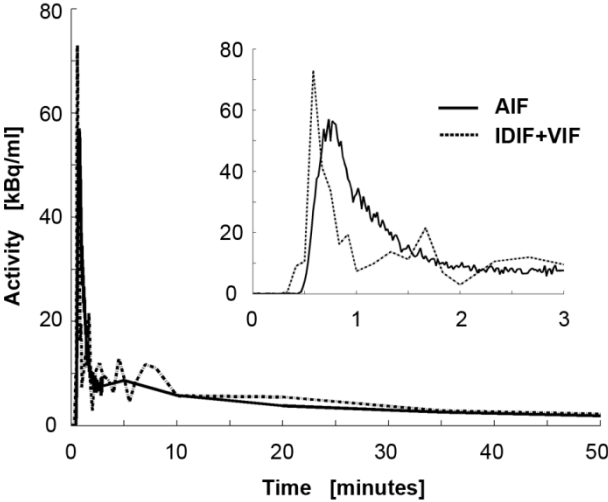
FIGURES

Figure 1



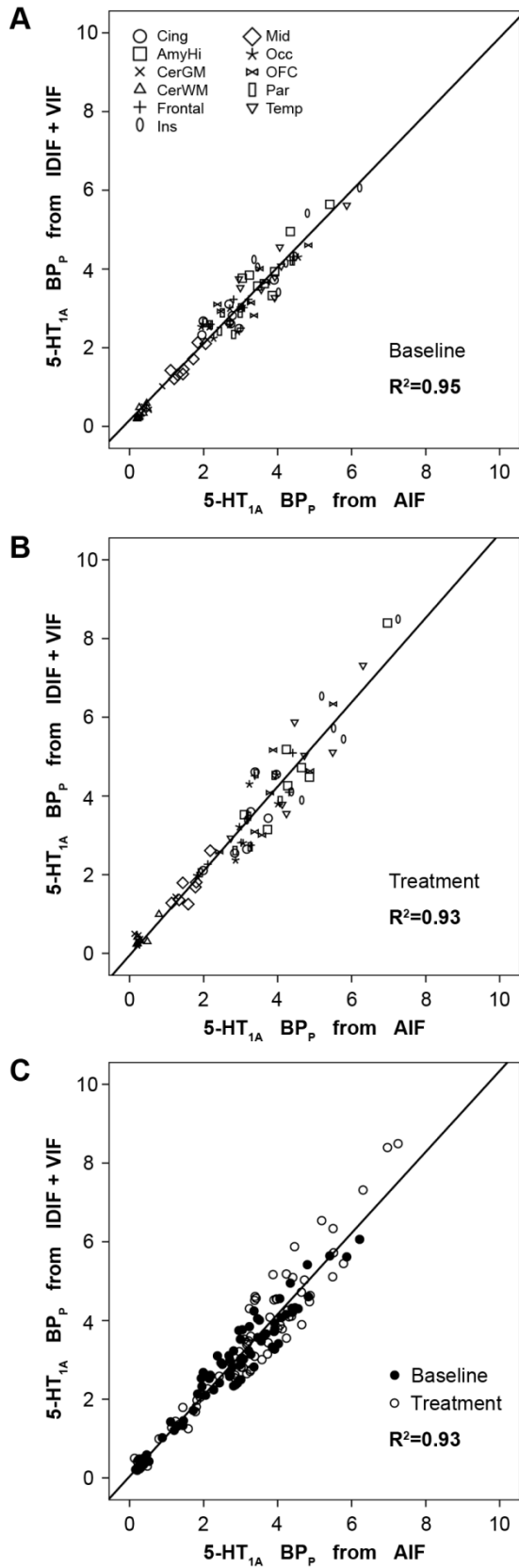
Parent fraction of [carbonyl-¹¹C]WAY-100635 (mean±SD of all 15 PET scans). The 6 arterial and 6 venous manual blood samples were taken at 2, 5, 10, 20, 35 and 50min post injection. Model fits were calculated with a Hill-type function (Gunn et al., 1998) for arterial (solid line, circles) and venous samples (dotted line, crosses) separately. Parent fraction was similar for both samples series with maximum variability of 24% at 5min. Bars denoting the standard deviation are shifted on abscissa to distinguish arterial and venous samples.

Figure 2



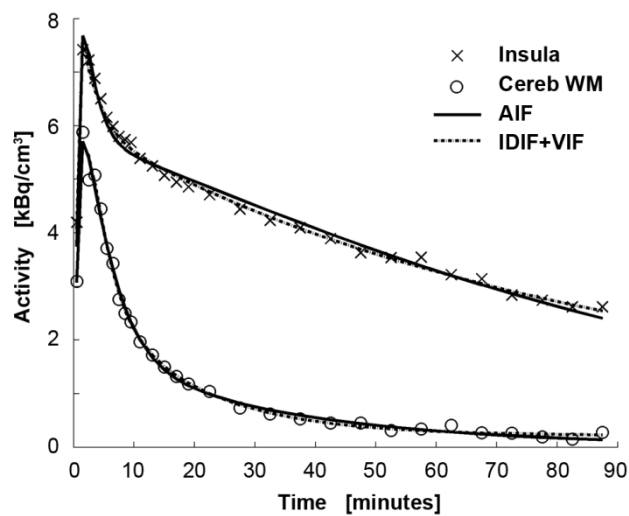
Whole-blood radioactivity concentrations of the two input functions used for kinetic modeling for a representative subject. Compared to the arterial input function (AIF, solid line), the image-derived input function (IDIF) shows good recovery of the initial peak after partial volume correction. The IDIF was combined with manual venous blood samples from 10min onward (IDIF+VIF, dotted line), resulting in similar tails for the two input functions. Zoom shows the first 3 minutes of the scan.

Figure 3



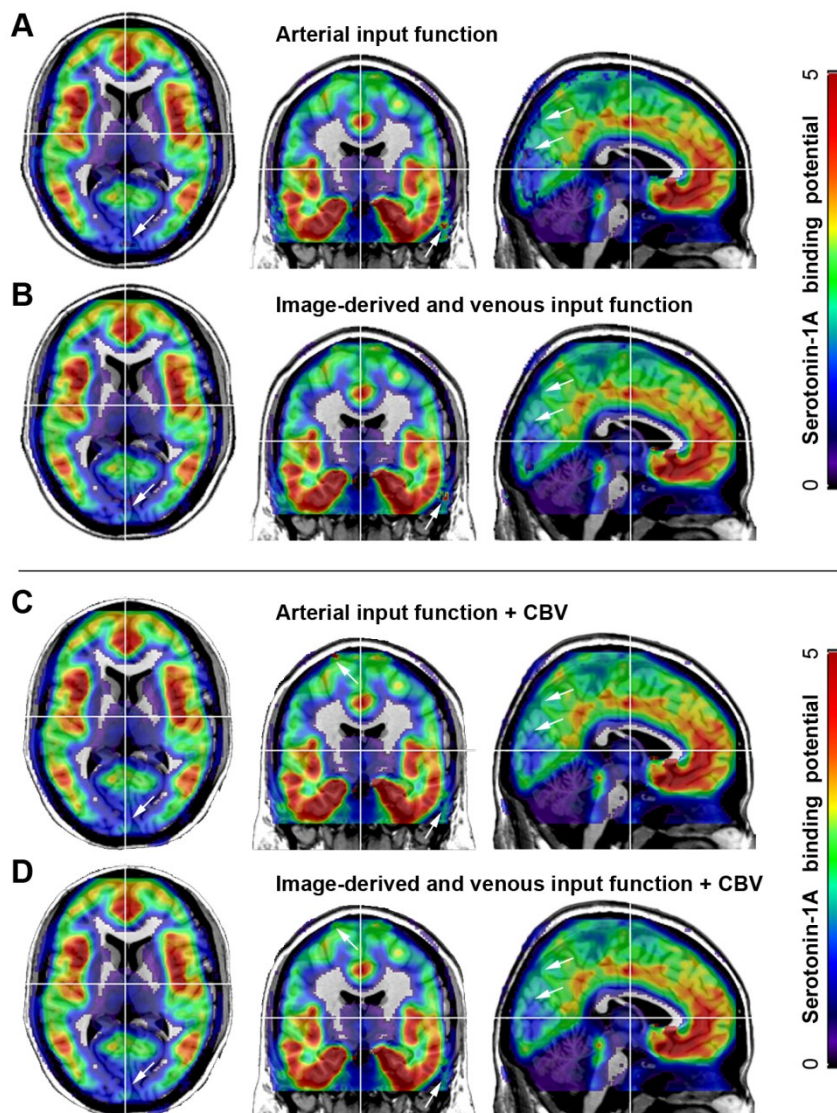
Direct comparison of serotonin-1A receptor (5-HT_{1A}) binding potential (BP_p). Receptor binding was obtained from arterial input functions (AIF) or the combination of image-derived and venous input functions (IDIF+VIF). Linear regression analysis shows strong agreement between these two independent approaches for PET measurements A) at baseline, B) after treatment and C) when pooling all scans (see table 1 for details). Symbols in A and B represent different regions of interest. Cing: cingulate cortex, AmyHip: amygdala-hippocampus complex, CerGM/CerWM: cerebellar gray/white matter, Ins: insula, Mid: midbrain, Frontal/OFC/Occ/Par/Temp: frontal, orbitofrontal, occipital parietal and temporal cortices.

Figure 4



Kinetic modeling of [*carbonyl*-¹¹C]WAY-100635. Time activity curves are shown for the insula (crosses) and cerebellar white matter (Cereb WM, circles) for a representative subject. Model fits calculated with a two-tissue compartment model resulted in similar fits when using the arterial input function (AIF, solid line) or the combination of the image-derived and venous input functions (IDIF+VIF, dotted line).

Figure 5



Voxel-wise quantification of [*carbonyl*-¹¹C]WAY-100635 for a representative subject. Maps were calculated with a two-tissue compartment model with ridge-regression fitting (Byrtek et al., 2005), with K_1/k_2 fixed to that of cerebellar white matter from ROI-based modeling. The model was applied with the cerebral blood volume (CBV) component fixed to 5% (**A**, **B**) and included as fit parameter (**C**, **D**). Serotonin-1A receptor binding potentials (BP_D) were computed with the arterial input function (AIF; **A**, **C**) and the combination of image-derived and venous input functions (IDIF+VIF; **B**, **D**) yielding virtually identical results. Of note, differences in binding potentials between the two methods were observed in some areas with lowest receptor binding (**A**, **B**; medial occipital cortex, extra-cerebral areas as indicated by white arrows). These differences almost vanished after inclusion of CBV as additional fit parameter (**C**, **D**).

TABLES

Table 1

Condition	n	R ²	Slope	Intercept
5-HT _{1A} BP _P AIF vs IDIF+VIF				
Baseline	8	0.95	0.97	0.16
Treatment	7	0.93	1.07	-0.05
Pooled	15	0.93	1.03	0.04
Late Venous	10	0.94	1.03	0.03
5-HT _{1A} BP _{ND} AIF vs MRTM2				
Pooled	15	0.82	0.42	0.09
5-HT _{1A} BP _{ND} IDIF+VIF vs MRTM2				
Pooled	15	0.82	0.33	0.01

Linear regression analysis was carried out for the direct comparison of serotonin-1A (5-HT_{1A}) receptor binding (BP_P) as quantified by arterial input functions (AIF) or the combination of image-derived and venous input functions (IDIF+VIF). Results showed good agreement between the two methods for PET measurements at baseline, after treatment and when pooling all scans (see also figure 3). Similar results were obtained when including only those 10 subjects where late venous sampling (35min and 50min) was fully available. Comparing two-tissue compartment models (AIF and IDIF+VIF) with the multilinear reference tissue model 2 (MRTM2, (Ichise et al., 2003)) gives weaker agreement and indicates an underestimation of receptor binding (BP_{ND}) with the latter (Gunn et al., 1998) (see also figure S5).

SUPPLEMENTARY FIGURES

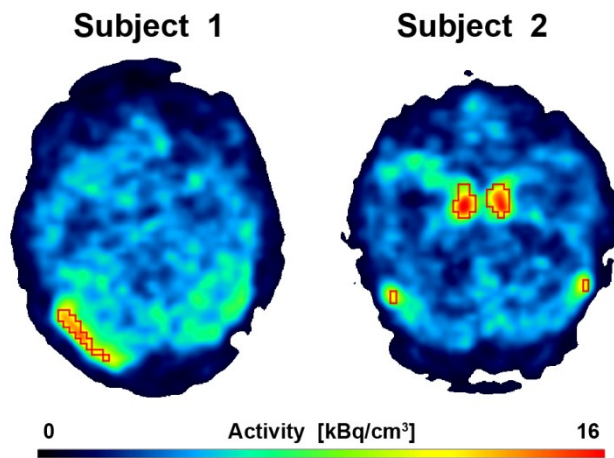


Figure S1: Result of automatic blood vessels region of interest (ROI) definition using linear discriminant analysis for 2 subjects. PET scans were averaged across the first minute. ROIs are denoted in red and outline the transversal sinus (both subjects) and the carotid arteries (subject 2).

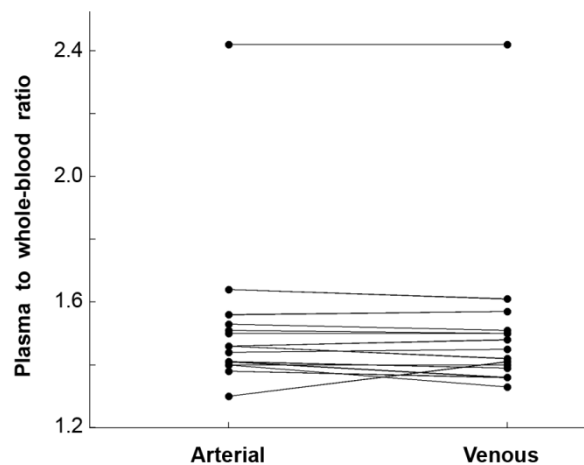


Figure S2: Plasma to whole-blood ratios for arterial and venous samples across subjects. Ratios were determined for manual samples taken at 5, 10 and 20min and averaged. The unexpected high plasma to whole-blood ratio in one subject could not be explained by routine blood tests or clinical parameters. Also, this did not affect estimation of 5-HT_{1A} receptor binding (see also comparison between two-tissue compartment and reference tissue models in figure S5).

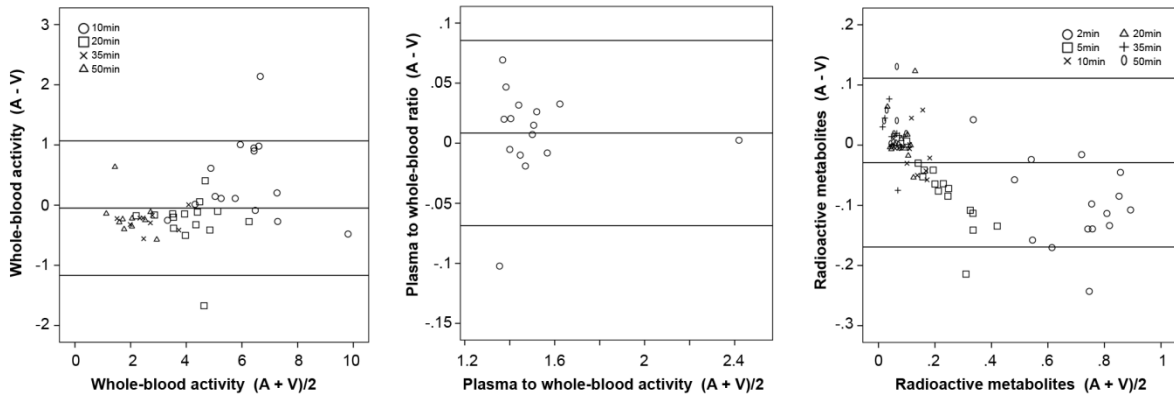


Figure S3: Bland-Altman plots comparing blood parameters obtained from arterial and venous manual blood samples. The unexpected high plasma to whole-blood ratio in one subject could not be explained by routine blood tests or clinical parameters. Also, this did not affect estimation of 5-HT_{1A} receptor binding (see also comparison between two-tissue compartment and reference tissue models in figure S5). Bars denote mean difference \pm 2*SD. Symbols represent different time points.

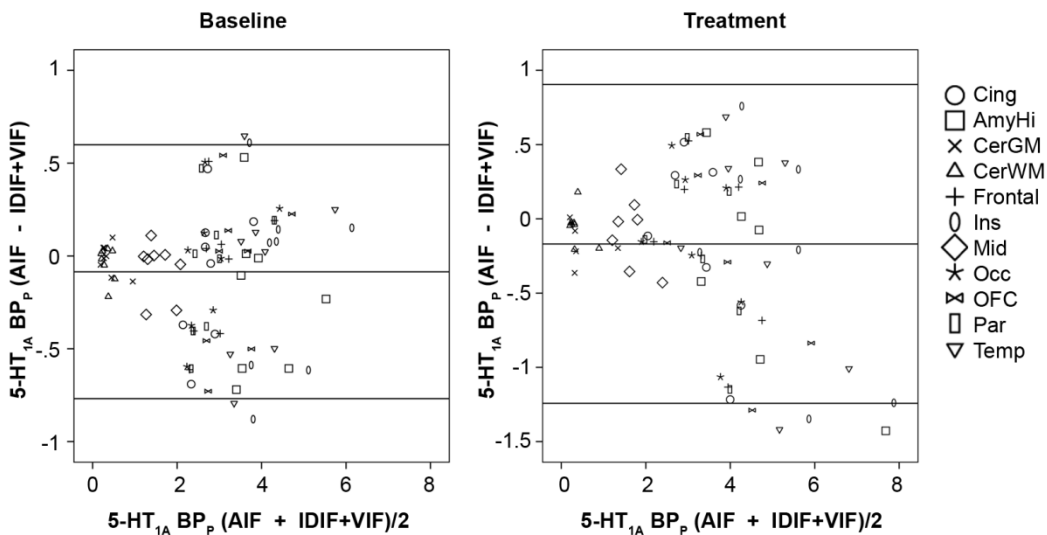


Figure S4: Bland-Altman plots comparing serotonin-1A (5-HT_{1A}) receptor binding potentials (BP_p) obtained from arterial input functions (AIF) and the combination of image-derived and venous input functions (IDIF+VIF). Bars denote mean difference \pm 2*SD. Symbols represent different brain regions. Cing: cingulate cortex, AmyHip: amygdala-hippocampus complex, CerGM/CerWM: cerebellar gray/white matter, Ins: insula, Mid: midbrain, Frontal/OFC/Occ/Par/Temp: frontal, orbitofrontal, occipital parietal and temporal cortices.

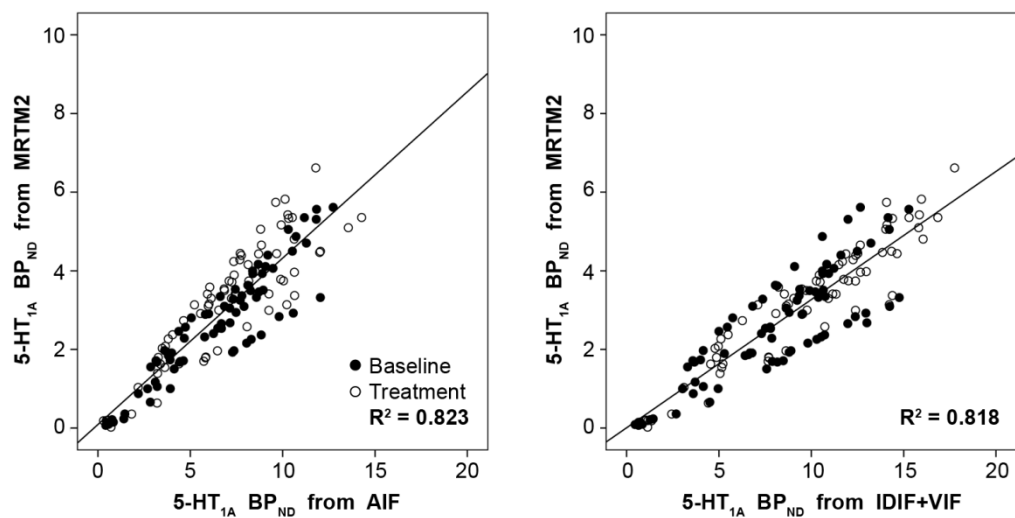


Figure S5: Comparison of serotonin-1A (5-HT_{1A}) receptor binding potentials (BP_{ND}) between the multilinear reference tissue model (MRTM2) and two-tissue compartment models using AIF and IDIF+VIF for all subjects. Intercepts were close to zero (0.09 and 0.008 for AIF and IDIF+VIF, respectively), but agreement was weaker ($R^2=0.823$ and 0.818) than within the two input function models. Furthermore, slopes indicate an underestimation with the reference region model.

Clinical application of image-derived and venous input functions in major depression using [*carbonyl*-¹¹C]WAY-100635

Andreas Hahn^a, Lukas Nics^b, Pia Baldinger^a, Wolfgang Wadsak^b, Markus Savli^a,
Christoph Kraus^a, Wolfgang Birkfellner^c, Johanna Ungersboeck^b, Daniela Haeusler^b,
Markus Mitterhauser^b, Georgios Karanikas^b, Siegfried Kasper^a, Richard Frey^a, Rupert Lanzenberger^{a*}

^a *Department of Psychiatry and Psychotherapy, Medical University of Vienna, Austria*

^b *Department of Nuclear Medicine, Medical University of Vienna, Austria*

^c *Center for Medical Physics and Biomedical Engineering, Medical University of Vienna, Austria*

For submission to: **European Journal of Nuclear Medicine and Molecular Imaging**

Word count	279	Abstract
	3682	Main section
Tables: 2, Figures: 2, References 58		

* Correspondence to: Rupert Lanzenberger, A/Prof. PD MD
Functional, Molecular and Translational Neuroimaging Lab
Department of Psychiatry and Psychotherapy
Medical University of Vienna
Waehringer Guertel 18-20, 1090 Vienna, AUSTRIA
Phone: +43-1-40400-3825
Fax: +43-1-40400-3099
rupert.lanzenberger@meduniwien.ac.at
<http://www.meduniwien.ac.at/neuroimaging/>

KEYWORDS

Image-derived input function, serotonin-1A receptor, depression, electroconvulsive therapy, venous input function, TrueX image reconstruction

ABSTRACT

Purpose

Image-derived input functions (IDIF) represent a promising non-invasive alternative to arterial blood sampling for quantification in positron emission tomography (PET) studies. However, routine application in patients and longitudinal designs are largely missing despite widespread attempts in healthy subjects. The aim of this study was to apply a previously validated approach to a clinical sample of patients with major depressive disorder (MDD) before and after electroconvulsive therapy (ECT).

Methods

Eleven scans from 5 patients with venous blood sampling were obtained with the radioligand [*carbonyl*-¹¹C]WAY-100635 at baseline, before and after 11.0±1.2 ECT sessions (5, 3 and 3 scans respectively). IDIFs were defined by two different image reconstruction algorithms (OSEM with subsequent partial volume correction (OSEM+PVC); reconstruction based modelling of the point spread function (TrueX)) and combined with manual venous samples from 10min onwards (IDIF+VIF). Serotonin-1A receptor (5-HT_{1A}) binding potentials (BP_P, BP_{ND}) were quantified with a two-tissue compartment (2TCM) and reference region model (MRTM2).

Results

Modelling 5-HT_{1A} BP_{ND} with IDIF+VIF from OSEM+PVC resulted in similar agreement with MRTM2 as reported previously ($R^2=0.82$, slope=0.31, intercept=0.17). Following ECT, decreased 5-HT_{1A} BP_{ND} and BP_P was found (23%-35%), except for one patient showing no change with the 2TCM but an increase with MRTM2. In contrast, IDIFs from TrueX showed lower peak values ($p<0.001$), decreased agreement in 5-HT_{1A} binding estimates ($R^2=0.57$) and markedly high test-retest variability for the same patient when using BP_{ND} (94%) but not BP_P.

Conclusions

Using image-derived and venous input functions defined by OSEM with subsequent PVC we confirm a decrease in 5-HT_{1A} binding (BP_{ND} and BP_P) in MDD patients after ECT. However, the observed discrepancies are not in favour of extracting IDIFs from reconstruction based modelling of the point spread function (TrueX).

INTRODUCTION

Quantification of neuronal binding sites such as receptors and transporters in positron emission tomography (PET) studies often requires measurement of an arterial input function for the kinetic modelling procedure [1-3]. Arterial cannulation is, however, an invasive technique and the analysis of manual blood samples can be a challenging task.

Image-derived input functions (IDIF) represent a promising alternative to obtain a non-invasive estimate of the input function since they can be extracted directly from cerebral blood vessels visible within the PET images. Although IDIFs have been applied for various radioligands in healthy subjects a widespread application in clinical routine is still missing (for review see [4]). The majority of patient studies with a successful implementation of IDIF concern tumour assessment. These include investigations where metabolite correction was omitted [5, 6] or modelled by population based approaches due to rather simple (e.g., monoexponential) metabolic characteristics [7-10]. Two further studies in the field of neuroscience used an IDIF extraction method for [^{18}F]FDG [11] to investigate patients with dream-enactment behaviour [12] and subjects genetically at risk for Alzheimer's disease [13]. Finally, Alzheimer has been studied using IDIF for quantification of [^{11}C]PIB, where a population-based metabolite correction could be successfully applied, too [14].

There is a particular interest to extend the use of these non-invasive approaches to patient populations and evaluate treatment effects [4] also with radioligands exhibiting more complex characteristics. One example for such an attempt is [^{11}C]PBR28 for the investigation of patients with multiple sclerosis [15]. However, quantification with IDIFs did not yield reliable binding estimates most probably due to the high metabolite fraction [4, 15]. Another radioligand which experiences a similarly fast metabolism is [*carbonyl*- ^{11}C]WAY-100635 for the quantification of serotonin-1A (5-HT_{1A}) receptors [16, 17]. It has been successfully applied for basic neuroscience investigations [18, 19] and studies of several psychiatric disorders including major depression (MDD) [20-22] and bipolar disorder [23, 24], anxiety disorders [25-27] as well as bulimia nervosa [28], alcohol dependence [29] and temporal lobe epilepsy [30]. However, the choice of outcome parameters derived from input function and reference region models may influence the results in longitudinal studies and when comparing different population groups [21, 22, 28]. This underlines the importance to establish less invasive but reliable techniques also in clinical research protocols. However, success rates for IDIFs may not only vary between radioligands but also for different scanners. Although high resolution scanners reduce partial volume effects [31-34], correction [35] or scaling was still required for accurate IDIF definition [36]. Therefore, recent advances such as modelling the point spread function (PSF) during image reconstruction may provide

an improved IDIF extraction due to further increased recovery also in small brain structures [33].

Recently, we validated an approach for the quantification of 5-HT_{1A} with [*carbonyl*-¹¹C]WAY-100635 in healthy subjects using a combination of image-derived and venous input functions [37]. The goal of this work was to extend the method to a patient population with major depression. In a longitudinal study design we aimed to evaluate test-retest variability at baseline and confirm recently reported effects of electroconvulsive therapy (ECT) on 5-HT_{1A} binding [38]. Finally, two different algorithms to correct for partial volume effects were compared to obtain accurate estimates of image-derived input functions on a high resolution PET scanner.

METHODS

Subjects and treatment

A subsample of five patients from a longitudinal treatment trial were included in this study (mean age \pm sd = 46.2 \pm 15.6 years, 3 female), which is described in full detail elsewhere [38]. All subjects suffered from severe unipolar depression (17-item Hamilton Rating Scale for Depression (HAMD₁₇) > 23) as assessed by the Structural Clinical Interview for DSM-IV (SCID). Further psychiatric, neurological or physical disorders as well as current or history of substance abuse were excluded by standard medical examination, electrocardiogram and laboratory tests. Patients were treatment-resistant to at least two pharmacotherapeutical trials with different antidepressants [39]. The current medication of the patients was continued at the same dosage during the study for ethical reasons and was in steady-state at least ten days before inclusion.

For this study, 11 PET scans with venous blood sampling were available, 5 at baseline, 3 before and 3 after electroconvulsive therapy (ECT). Hence, for 3 subjects test-retest data were available (i.e., baseline vs. pretreatment scans) and for 3 subjects the comparison before vs. after ECT was available (i.e., baseline or pre- vs. posttreatment scans). Electroconvulsive therapy was carried out by experienced psychiatrists and an anaesthesiologist [38]. Briefly, patients were administered anaesthetics (methohexital) and muscle relaxants (succinylcholine) before each therapy session and seizures were monitored by electroencephalography (EEG). ECT started unilaterally with electrode placement above the right frontotemporal lobe and was extended to bilateral treatment in case of no or minimal

clinical improvement after the fifth ECT session (n=4). On average, the 5 patients underwent 11.0 ± 1.2 treatment sessions. Subjects provided written informed consent after detailed explanation of the protocol and they received reimbursement for participation. The study was approved by the ethics committee of the Medical University of Vienna and the General Hospital of Vienna.

Positron emission tomography (PET)

Measurements were carried out using a Biograph 64 True Point PET/CT scanner (Siemens Medical, Erlangen, Germany) as described previously [38]. In short, the patient's head was placed in the scanner parallel to the orbitomeatal line by means of a laser beam system. A polyurethane cushion and straps around the forehead and chin were used to minimize head movement. Following a CT attenuation measurement, the 3D dynamic emission scan was started synchronously with the intravenous bolus injection of the radioligand [*carbonyl-¹¹C*]WAY-100635 (mean injected dose \pm SD = 253.6 ± 52.0 MBq). Radioligand synthesis was carried out as described previously [40]. PET scans lasted for 90min and were acquired in list-mode enabling different image reconstructions. To capture the initial peak of the image-derived input function the protocol comprised short time frames in the beginning of the scan (12x5s, 6x10s, 3x20s, 6x30s, 4x1min, 5x2min, 4x5min, 1x10min, 2x20min) [37]. For kinetic modelling a protocol with longer time frames was used for stable fits (15x1min, 5x5min, 1x10min, 2x20min) [38]. For image reconstruction two different algorithms were applied to assess the impact on IDIF extraction and peak recovery. First, an iterative ordered subsets expectation maximization (OSEM) algorithm was used, followed by partial volume correction (PVC, see image-derived input function section) for comparison with a previously established procedure of IDIF definition [37]. This yields a final image resolution of 4.2 x 4.2 x 4.7mm full-width at half-maximum (FWHM) 1cm next to the center of the field of view (340 x 340 x 220mm). Second, a Siemens-specific reconstruction algorithm was used, which includes the modelling of the point spread function during reconstruction (TrueX) [33, 41] resulting in a uniform image resolution of 2mm FWHM.

Blood sampling

Manual venous blood samples (V. cubitalis) of 3ml each were taken at 2, 5, 10, 20, 35 and 50min post injection. Blood samples were analyzed as described previously [37, 42]. Briefly, whole-blood activity was measured in a gamma counter (Wizard² 3" 2480, Perkin Elmer, Waltham, MA, USA) and plasma was separated by centrifugation (1800g, 7min) to determine individual plasma to whole-blood ratios. For metabolite analysis plasma aliquots of 830 μ l were precipitated with acetonitrile and spiked with unlabelled standards (WAY-100635 and its metabolites desmethyl-WAY-100635 and cyclohexanecarboxylic acid) to achieve a final

ratio of 42:58 (plasma/acetonitrile) [43]. After a second centrifugation step (23000g, 4min), 2ml of the supernatant were injected into a radio-high performance liquid chromatography system (radio-HPLC, Merck Hitachi, Sigma-Aldrich, St. Louis, MO, USA). For an accurate assessment of the radioactive metabolites, two fractions were collected with a fraction collector (one with metabolites, the second containing intact parent compound) and measured with the gamma counter. All measurements were corrected for radioactive decay and background activity.

The parent fraction of the radioligand [*carbonyl*-¹¹C]WAY-100635 was calculated as the ratio of unchanged compound to total activity of both fractions. The six time points of the unmetabolized radioligand were then interpolated with a Hill-type function [44] using standard non-linear least squares fitting of MatlabR2010a (The Mathworks, Natick, MA, USA). As described previously [37], venous samples were preponed 15s before interpolation to account for delay of metabolite arrival at the cannulation site (V. cubitalis).

Image-derived input functions

Image-derived input functions were extracted from the original (i.e., not spatially normalized) PET scans. The blood vessel region of interest (ROI) was defined separately for the OSEM and TrueX reconstruction settings. For ROI delineation the images were smoothed with a 6mm Gaussian kernel [31, 32, 36] due to increased scatter and noise in high resolution scanners [4]. Furthermore, the field of view was cranial and caudal restricted by 13.5mm (5 slices) and 27mm (10 slices), respectively. The remaining steps for ROI definition were carried out according to a validated procedure [37]. In short, cerebral blood vessels were delineated by linear discriminant analysis (LDA) using the first minute of the PET scan. The training set for the supervised classification was provided by the average tracer-specific template used in previous studies [45, 46]. The resulting blood vessel region of interest (ROI) was then further refined to obtain a blood pool with homogeneous kinetic characteristics. Following the identification of the frame where the maximum occurs, the ROI was restricted that each voxel comprises at least 0.66 times the peak activity within this particular time frame. After individual ROI definition, the further IDIF procedures (partial volume correction and IDIF extraction) were carried out with the non-smoothed original PET scans.

For the peak recovery of the image-derived input function, two different partial volume correction algorithms were evaluated to account for spill-in from and spill-out to surrounding brain regions. First, the IDIF peak was obtained similar to a previously introduced procedure [37]. Using the OSEM image reconstruction settings (see PET section) an ROI-based partial volume correction was applied as implemented in PMOD 3.3 [47] (OSEM+PVC). Here, the

point spread function was defined according to the resolution of the reconstructed image (4.2 x 4.2 x 4.7mm FWHM). Within the second approach, TrueX reconstruction was used where the IDIF was extracted directly from the above defined blood vessel ROI. Hence, no further corrections were applied since the TrueX algorithm includes the point spread function modelling in the reconstruction.

For the final input functions, the peak was defined by the partial volume corrected IDIFs (OSEM+PVC or TrueX) and the tail was given by the manual venous blood samples from 10min onwards (IDIF+VIF). This combination of different input functions is feasible since the IDIF alone may not yield an accurate estimate for peak and tail of the input function [4] and late venous samples are not different from arterial ones for the applied radioligand [37]. IDIF+VIFs were then corrected for plasma to whole-blood ratio, radioactive metabolites and delay. The obtained plasma input function was then fitted with a sum of 3 exponentials from the peak onward [48].

Regions of interest and kinetic modelling

All PET scans were spatially normalized to MNI (Montreal Neurological Institute) stereotactic space with SPM8 (standard algorithm and parameters, except for affine regularisation=average sized template) using a tracer- and study-specific template [38]. Regions of interest were taken from an AAL-based (automated anatomical labelling) atlas [45] and comprised frontal, orbitofrontal, parietal, temporal, occipital and cingulate cortices, insula, amygdala-hippocampus complex, midbrain (incl. dorsal raphe nucleus) as well as cerebellar gray (excl. vermis) and cerebellar white matter.

The serotonin-1A receptor binding potential ($BP_P = V_T - V_{ND}$ [49]) was quantified with IDIF+VIF as obtained separately from OSEM+PVC and TrueX reconstructions. Kinetic modelling was carried out in PMOD 3.3 using a two-tissue compartment model with K_1/k_2 fixed to that of cerebellar white matter and a cerebral blood volume component of 5% [22, 50]. For comparison with previous results [37, 38], 5-HT_{1A} BP_{ND} was also computed as $(V_T - V_{ND})/V_{ND}$ from the two-tissue compartment model and with the multilinear reference tissue model 2 (MRTM2 [51]). For the reference region model, k_2' was estimated with a receptor rich and poor region (insula and cerebellar white matter, respectively) [51, 52]. For visualization of the results voxel-wise binding potential maps were also calculated. Similar to ROI-based modelling, MRTM2 was used as the reference region model. For the quantification with IDIF+VIF a two-tissue compartment model with ridge regression [53] was applied as described previously [37].

Statistical analysis

Differences in IDIF peaks, width (FWHM) and time of maximum obtained from OSEM+PVC and TrueX image reconstruction were assessed by paired t-tests. The PVC magnitude was calculated as ratios of IDIF peaks after/before correction. Here, IDIF peaks after correction are obtained by OSEM+PVC and TrueX algorithms, whereas values before are given by peaks from OSEM reconstruction. In addition, fits of kinetic modelling procedures (sum of squared differences) were compared using repeated measures ANOVA with reconstruction algorithm and ROI as fixed effects and subject as random effect [37, 54]. Direct comparison of 5-HT_{1A} BP_{ND} between input function modelling and the reference tissue model was computed by linear regression analysis separately for OSEM+PVC and TrueX. To evaluate longitudinal changes in 5-HT_{1A} binding test-retest variability (i.e., baseline (BL) vs. pretreatment scans (PRE)) was calculated as $|(BL-PRE)|/\text{mean}(BL,PRE)*100$ [50] and treatment-induced effects (pre- vs. posttreatment scans (POST)) were assessed by $(POST-PRE)/PRE*100$ [38]. To provide results independent from a reference region, test-retest variability and ECT-induced changes were also computed from binding potentials relative to total radioligand in plasma (BP_P) [21, 22]. All statistical tests were carried out two-tailed and calculated with MatlabR2010a or SPSS18 (IBM, New York, USA).

RESULTS

IDIF peak values occurred at the same time ($p>0.1$) and exhibited a similar peak width FWHM ($p>0.2$) when comparing OSEM+PVC with TrueX reconstruction settings. However, IDIF peaks were significantly higher for OSEM+PVC (mean difference $\Delta=19.11\pm 9.05\text{ kBq/ml}$, $p<0.001$). This is also reflected by the magnitude of PVC with a mean ratio of 1.83 ± 0.17 and 1.41 ± 0.26 for OSEM+PVC and TrueX, respectively ($p<0.001$). Furthermore, IDIFs from OSEM+PVC showed a trend towards better model fits ($F_{1,27}=3.72$, $p=0.065$).

Direct comparison of 5-HT_{1A} BP_{ND} between input function and reference region modelling is given in figure 1 and tables 1-2. For OSEM+PVC linear regression analysis showed similar correlation ($R^2=0.82$) and underestimation by MRTM2 (slope=0.31, intercept=0.17, figure 1a) as determined previously ($R^2=0.82$, slope=0.33, intercept=0.01) [37]). In contrast, the agreement was weaker and bias more pronounced when using IDIFs obtained from TrueX algorithm ($R^2=0.57$, slope=0.26, intercept=1.18, figure 1b). Further analysis showed that this mismatch for input functions from TrueX was mostly caused by two patients (values without the two subjects: $R^2=0.83$, slope=0.38, intercept=0.5, figure 1c, see discussion).

Using input function modelling (IDIF from OSEM+PVC) we could replicate widespread decreases in 5-HT_{1A} BP_{ND} [38] and BP_P after ECT with ROI-based (23%-35%, table 1) and voxel-wise modelling (figure 2). However, one patient showed increased 5-HT_{1A} BP_{ND} when using MRTM2 (47%) but almost no change with IDIFs for OSEM+PVC (-2%) and a decrease with TrueX (-47%). In contrast, results with BP_P as outcome parameter were generally more consistent between IDIFs obtained from the two image reconstruction algorithms (OSEM+PVC and TrueX, table 1). The evaluation of 5-HT_{1A} test-retest variability was comparable between MRTM2 and OSEM+PVC for BP_{ND} (4%-21%) but slightly higher for BP_P (table 2). In contrast, using IDIF from TrueX showed markedly high variability in BP_{ND} values for one subject (94%) but not when using BP_P (20%). Subsequent analysis of this patient indicated that discrepancies in 5-HT_{1A} BP_{ND} as obtained with IDIF from TrueX emerged from a poor estimation of non-specific binding. V_{ND} was underestimated by a factor of 2.4 for the pretreatment scan (0.14ml/cm³ vs. 0.34±0.08ml/cm³ across the remaining patients), which in turn enters into the calculations of both ECT-effects and test-retest variability. In contrast, this was not the case for IDIF estimated with OSEM+PVC with V_{ND}=0.19ml/cm³ vs. 0.20±0.07ml/cm³.

DISCUSSION

This study validates the usefulness to apply the combination of image-derived and venous input functions [37] in a clinical sample of patients with major depression. More importantly, using input function modelling we confirm a widespread decrease in serotonin-1A receptor binding (approx. 25% BP_{ND} and BP_P) after treatment with ECT [38]. Furthermore, the evaluation of two different image reconstruction settings indicates that the conventional approach (OSEM algorithm followed by partial volume correction) yields a more stable IDIF definition compared to modelling of the point spread function during reconstruction (TrueX).

Image-derived and venous input functions in a clinical setting

Although several approaches with IDIFs have been validated for healthy subjects, the routine use in patient populations is mostly missing [4], especially for the application in neuroreceptor mapping with radioligands comprising challenging kinetics and metabolism. Therefore, one aim of this study was to validate a previously introduced approach of IDIF+VIF for the quantification of 5-HT_{1A} binding [37] in a clinical setting. The comparison of 5-HT_{1A} BP_{ND} between input function (IDIF from OSEM+PVC) and reference region models obtained here in MDD patients (R²=0.82, slope=0.31, intercept=0.17) were essentially the same as reported previously in healthy subjects (R²=0.82, slope=0.33, intercept=0.01 [37]).

The underestimation with the reference tissue model as indicated by the slope is also in line with previous results [43, 44]. In contrast, using 5-HT_{1A} BP_{ND} estimates obtained by TrueX reconstruction resulted in weaker agreement and increased bias. Although an improved match could be obtained when excluding two subjects, these two patients did not show any clinical, technical or methodological abnormalities which would justify study exclusion. Together with our previous study [37] the proposed method seems to provide stable results for quantification of [*carbonyl*-¹¹C]WAY-100635 independent of the population (healthy subjects and MDD patients), treatment (before/after pharmacological and electroconvulsive therapy) and scanner (GE Advance and Siemens high resolution tomograph) but not modelling of the point spread function (PVC vs. TrueX). The repeated successful applications of IDIF+VIF represent an important step for less invasive receptor quantification in routine clinical research protocols. Still, the approach needs to be validated for use with other radioligands with different kinetic characteristics.

Serotonin-1A receptor changes after electroconvulsive therapy

We have previously shown an almost global attenuation in 5-HT_{1A} BP_{ND} in MDD patients after ECT [38]. Here, this decreased binding was confirmed with input function modelling in a subsample of patients for both BP_{ND} and BP_P when defining IDIFs from OSEM+PVC with ROI-based and voxel-wise modelling. Interestingly, for one subject the results markedly diverged when comparing reference region and input function modelling. The MRTM2 showed increased BP_{ND} whereas IDIF from OSEM+PVC resulted in no change. In contrast, defining IDIF with TrueX yielded a decrease for BP_{ND} but an increase for BP_P. Subsequent analysis revealed that these discrepancies emerged from a two-fold underestimation of non-specific binding. Although such a high intersubject variability in non-specific binding indeed exists [50], this is not the case here. Instead, the observed mismatch was limited to BP_{ND} obtained from the TrueX algorithm (but not OSEM+PVC), caused by poor identification of non-specific binding. Comparing 5-HT_{1A} binding between OSEM+PVC and TrueX also showed more consistent results when using BP_P. This is in line with previous studies highlighting the importance for careful choice of the outcome parameter [21, 22, 28]. Clinically however, the differences between the models (MRTM2 and OSEM+PVC) for the one patient indicate that our previously reported effects on 5-HT_{1A} binding induced by ECT may at worst be underestimated [38].

Regarding test-retest variability, the values from OSEM+PVC were comparable or better to those from MRTM2, indicating good reliability in outcome parameters for IDIF+VIF. Again, this was not the case for BP_{ND} estimated with IDIF from TrueX for the one patient. Similar to 5-HT_{1A} changes after ECT, test-retest values were more consistent between OSEM+PVC

and TrueX when using BP_P instead of BP_{ND} . To summarize, the uncertainties observed with BP_{ND} are probably attributable to differences in the reconstruction algorithms and PSF modelling. This leads to variations in peak recovery of the input function which in turn causes unreliable estimation of modelling parameters.

Image reconstruction algorithms

Although IDIF peaks comprised a similar width and occurred at the same time, peak values from TrueX were significantly lower as compared to OSEM+PVC. This is in line with previous observations showing that, although to a lesser extent, activity concentrations are underestimated despite modelling of the PSF during reconstruction [55]. In other words, although high resolution scanners indeed reduce partial volume effects [31-34] corrections seem to be still required for sufficient IDIF extraction [15, 35]. Our findings suggest that such a correction realized with subsequent PVC seems to be more robust than modelling of the PSF during reconstruction. In contrast, Mourik et al. [56] successfully applied reconstruction based PVC for IDIF extraction on a HR+ scanner. However, transfer of the method to a high resolution scanner was only achieved after scaling IDIFs with manual arterial blood samples [36]. These discrepancies could be explained either by differences in the algorithms to model the PSF during reconstruction (Mourik's method vs. TrueX) or by uncertainties in the reconstruction based correction for high resolution scanners in general (e.g., due to increased noise and scatter [15]).

Limitations

One limitation of this study is that no arterial blood sampling was available. The approach of combining image-derived and venous input functions has however been validated with arterial input functions previously in healthy subjects before and after pharmacological treatment [37]. Furthermore, the comparison of IDIF+VIF with MRTM2 yields essentially the same agreement and underestimation by the reference region model in two independent populations (healthy participants [37] and MDD patients).

Another issue is the low number of subjects for the evaluation of 5-HT_{1A} test-retest variability and changes after ECT. However, blood samples were obtained in few subjects only for logistic reasons, but not due to any clinical, technical or methodological preferences. Hence, the patients included here provide a representative subsample of our previous study [38]. Furthermore, 11 scans were in total available for indirect validation of the method with a reference region model, which is a number similar to previous IDIF [35, 36, 54, 56-58] and test-retest studies [43, 50].

CONCLUSIONS

This study supports the use of image-derived and venous input functions also in clinical populations for the quantification of [*carbonyl*-¹¹C]WAY-100635. Using input function modelling our findings confirm the previously reported decrease of serotonin-1A receptor binding in patients with major depression after electroconvulsive therapy. Consistent with previous observations, binding potentials relative to nondisplaceable binding (BP_{ND}) are dependent on accurate use of reference regions or input function definition. Hence, for IDIF extraction conventional image reconstruction and subsequent partial volume correction may be preferred to modelling of the point spread function during reconstruction with TrueX.

ACKNOWLEDGEMENTS

A. Hahn is recipient of a DOC-fellowship of the Austrian Academy of Sciences (OeAW) at the Department of Psychiatry and Psychotherapy. This research was supported by a grant from the Brain and Behavior Research Foundation, USA (NARSAD, <http://bbrfoundation.org/>) to R. Lanzenberger and the Austrian National Bank (OeNB13219) to R. Frey. We are grateful to A. Höflich and C. Kraus from the Department of Psychiatry as well as to the PET teams of the Department of Nuclear Medicine, especially to R. Dudczak, Schmiedinger, P. Papesch, R. Aghamohammadi-Sareshgi, D. Senn, B. Straubinger, K. Salzmann, G. Wagner, M. Zeilinger and S. Hartmann for medical and/or technical support. This study is part of the doctoral theses of A. Hahn at the Medical University of Vienna (www.meduniwien.ac.at/clins).

CONFLICT OF INTEREST

Without any relevance to this work, S. Kasper declares that he has received grant/research support from Eli Lilly, Lundbeck A/S, Bristol-Myers Squibb, Servier, Sepracor, GlaxoSmithKline, Organon, and has served as a consultant or on advisory boards for AstraZeneca, Austrian Science Found, Bristol-Myers Squibb, GlaxoSmithKline, Eli Lilly, Lundbeck A/S, Pfizer, Organon, Sepracor, Janssen, and Novartis, and has served on speakers' bureaus for AstraZeneca, Eli Lilly, Lundbeck A/S, Servier, Sepracor and Janssen. R. Lanzenberger received travel grants and conference speaker honoraria from AstraZeneca and Lundbeck A/S. M. Mitterhauser and W. Wadsak received speaker honoraria from Bayer. R. Frey declares that he has received grant/research support from Bristol-Myers Squibb, AstraZeneca, Sandoz, Eli Lilly, and Janssen.

REFERENCES

1. Mintun MA, Raichle ME, Kilbourn MR, Wooten GF, Welch MJ. A quantitative model for the in vivo assessment of drug binding sites with positron emission tomography. *Ann Neurol.* 1984;15:217-27.
2. Slifstein M, Laruelle M. Models and methods for derivation of in vivo neuroreceptor parameters with PET and SPECT reversible radiotracers. *Nucl Med Biol.* 2001;28:595-608.
3. Ichise M, Meyer JH, Yonekura Y. An introduction to PET and SPECT neuroreceptor quantification models. *J Nucl Med.* 2001;42:755-63.
4. Zanotti-Fregonara P, Chen K, Liow JS, Fujita M, Innis RB. Image-derived input function for brain PET studies: many challenges and few opportunities. *J Cereb Blood Flow Metab.* 2011;31:1986-98.
5. Beer AJ, Grosu AL, Carlsen J, Kolk A, Sarbia M, Stangier I, et al. [18F]galacto-RGD positron emission tomography for imaging of alphavbeta3 expression on the neovasculature in patients with squamous cell carcinoma of the head and neck. *Clin Cancer Res.* 2007;13:6610-6.
6. Wang W, Lee NY, Georgi JC, Narayanan M, Guillem J, Schoder H, et al. Pharmacokinetic analysis of hypoxia (18)F-fluoromisonidazole dynamic PET in head and neck cancer. *J Nucl Med.* 2010;51:37-45.
7. Schiepers C, Chen W, Dahlbom M, Cloughesy T, Hoh CK, Huang SC. 18F-fluorothymidine kinetics of malignant brain tumors. *Eur J Nucl Med Mol Imaging.* 2007;34:1003-11.
8. Schiepers C, Chen W, Cloughesy T, Dahlbom M, Huang SC. 18F-FDOPA kinetics in brain tumors. *J Nucl Med.* 2007;48:1651-61.
9. Schiepers C, Hoh CK, Nuyts J, Seltzer M, Wu C, Huang SC, et al. 1-11C-acetate kinetics of prostate cancer. *J Nucl Med.* 2008;49:206-15.

10. Backes H, Ullrich R, Neumaier B, Kracht L, Wienhard K, Jacobs AH. Noninvasive quantification of ¹⁸F-FLT human brain PET for the assessment of tumour proliferation in patients with high-grade glioma. *Eur J Nucl Med Mol Imaging*. 2009;36:1960-7.
11. Chen K, Bandy D, Reiman E, Huang SC, Lawson M, Feng D, et al. Noninvasive quantification of the cerebral metabolic rate for glucose using positron emission tomography, ¹⁸F-fluoro-2-deoxyglucose, the Patlak method, and an image-derived input function. *J Cereb Blood Flow Metab*. 1998;18:716-23.
12. Caselli RJ, Chen K, Bandy D, Smilovici O, Boeve BF, Osborne D, et al. A preliminary fluorodeoxyglucose positron emission tomography study in healthy adults reporting dream-enactment behavior. *Sleep*. 2006;29:927-33.
13. Reiman EM, Chen K, Alexander GE, Caselli RJ, Bandy D, Osborne D, et al. Functional brain abnormalities in young adults at genetic risk for late-onset Alzheimer's dementia. *Proc Natl Acad Sci U S A*. 2004;101:284-9.
14. Lopresti BJ, Klunk WE, Mathis CA, Hoge JA, Ziolkowski SK, Lu X, et al. Simplified quantification of Pittsburgh Compound B amyloid imaging PET studies: a comparative analysis. *J Nucl Med*. 2005;46:1959-72.
15. Zanotti-Fregonara P, Liow JS, Fujita M, Dusch E, Zoghbi SS, Luong E, et al. Image-derived input function for human brain using high resolution PET imaging with [¹¹C](R)-rolipram and [¹¹C]PBR28. *PLoS One*. 2011;6:e17056.
16. Pike VW, McCarron JA, Lammertsma AA, Osman S, Hume SP, Sargent PA, et al. Exquisite delineation of 5-HT_{1A} receptors in human brain with PET and [¹¹C]WAY-100635. *Eur J Pharmacol*. 1996;301:R5-7.
17. Farde L, Ito H, Swahn CG, Pike VW, Halldin C. Quantitative analyses of carbonyl-carbon-11-WAY-100635 binding to central 5-hydroxytryptamine-1A receptors in man. *J Nucl Med*. 1998;39:1965-71.
18. Fisher PM, Meltzer CC, Ziolkowski SK, Price JC, Moses-Kolko EL, Berga SL, et al. Capacity for 5-HT_{1A}-mediated autoregulation predicts amygdala reactivity. *Nat Neurosci*. 2006;9:1362-3.

19. Hahn A, Wadsak W, Windischberger C, Baldinger P, Hoflich AS, Losak J, et al. Differential modulation of the default mode network via serotonin-1A receptors. *Proc Natl Acad Sci U S A*. 2012;109:2619-24.
20. Drevets WC, Frank E, Price JC, Kupfer DJ, Holt D, Greer PJ, et al. PET imaging of serotonin 1A receptor binding in depression. *Biol Psychiatry*. 1999;46:1375-87.
21. Hirvonen J, Karlsson H, Kajander J, Lepola A, Markkula J, Rasi-Hakala H, et al. Decreased brain serotonin 5-HT_{1A} receptor availability in medication-naive patients with major depressive disorder: an in-vivo imaging study using PET and [carbonyl-¹¹C]WAY-100635. *Int J Neuropsychopharmacol*. 2008;11:465-76.
22. Parsey RV, Ogden RT, Miller JM, Tin A, Hesselgrave N, Goldstein E, et al. Higher serotonin 1A binding in a second major depression cohort: modeling and reference region considerations. *Biol Psychiatry*. 2010;68:170-8.
23. Sullivan GM, Ogden RT, Oquendo MA, Kumar JS, Simpson N, Huang YY, et al. Positron emission tomography quantification of serotonin-1A receptor binding in medication-free bipolar depression. *Biol Psychiatry*. 2009;66:223-30.
24. Sargent PA, Rabiner EA, Bhagwagar Z, Clark L, Cowen P, Goodwin GM, et al. 5-HT_{1A} receptor binding in euthymic bipolar patients using positron emission tomography with [carbonyl-(¹¹C)]WAY-100635. *J Affect Disord*. 2010;123:77-80.
25. Lanzenberger RR, Mitterhauser M, Spindelegger C, Wadsak W, Klein N, Mien L-K, et al. Reduced serotonin-1A receptor binding in social anxiety disorder. *Biol Psychiatry*. 2007;61:1081-9.
26. Spindelegger C, Lanzenberger R, Wadsak W, Mien LK, Stein P, Mitterhauser M, et al. Influence of escitalopram treatment on 5-HT_{1A} receptor binding in limbic regions in patients with anxiety disorders. *Mol Psychiatry*. 2009;14:1040-50.
27. Nash JR, Sargent PA, Rabiner EA, Hood SD, Argyropoulos SV, Potokar JP, et al. Serotonin 5-HT_{1A} receptor binding in people with panic disorder: positron emission tomography study. *Br J Psychiatry*. 2008;193:229-34.

28. Bailer UF, Bloss CS, Frank GK, Price JC, Meltzer CC, Mathis CA, et al. 5-HTA receptor binding is increased after recovery from bulimia nervosa compared to control women and is associated with behavioral inhibition in both groups. *Int J Eat Disord*. 2011;44:477-87.
29. Martinez D, Slifstein M, Gil R, Hwang DR, Huang Y, Perez A, et al. Positron emission tomography imaging of the serotonin transporter and 5-HT(1A) receptor in alcohol dependence. *Biol Psychiatry*. 2009;65:175-80.
30. Assem-Hilger E, Lanzenberger R, Savli M, Wadsak W, Mitterhauser M, Mien LK, et al. Central serotonin 1A receptor binding in temporal lobe epilepsy: a [carbonyl-(11)C]WAY-100635 PET study. *Epilepsy Behav*. 2010;19:467-73.
31. Leroy C, Comtat C, Trebossen R, Syrota A, Martinot JL, Ribeiro MJ. Assessment of 11C-PE2I binding to the neuronal dopamine transporter in humans with the high-spatial-resolution PET scanner HRRT. *J Nucl Med*. 2007;48:538-46.
32. van Velden FH, Kloet RW, van Berckel BN, Buijs FL, Luurtsema G, Lammertsma AA, et al. HRRT versus HR+ human brain PET studies: an interscanner test-retest study. *J Nucl Med*. 2009;50:693-702.
33. Varrone A, Sjöholm N, Eriksson L, Gulyas B, Halldin C, Farde L. Advancement in PET quantification using 3D-OP-OSEM point spread function reconstruction with the HRRT. *Eur J Nucl Med Mol Imaging*. 2009;36:1639-50.
34. Schain M, Toth M, Cselenyi Z, Stenkrona P, Halldin C, Farde L, et al. Quantification of serotonin transporter availability with [11C]MADAM--a comparison between the ECAT HRRT and HR systems. *Neuroimage*. 2012;60:800-7.
35. Fung EK, Planeta-Wilson B, Mulnix T, Carson RE. A Multimodal Approach to Image-Derived Input Functions for Brain PET. *IEEE Nucl Sci Symp Conf Rec (1997)*. 2009;2009:2710-4.
36. Mourik JE, van Velden FH, Lubberink M, Kloet RW, van Berckel BN, Lammertsma AA, et al. Image derived input functions for dynamic High Resolution Research Tomograph PET brain studies. *Neuroimage*. 2008;43:676-86.

37. Hahn A, Nics L, Baldinger P, Ungersboeck J, Dolliner P, Frey R, et al. Combining image-derived and venous input functions enables quantification of serotonin-1A receptors with [carbonyl-11C]WAY-100635 independent of arterial blood sampling. *NeuroImage*. 2012;62:199-206.
38. Lanzenberger R, Baldinger P, Hahn A, Ungersboeck J, Mitterhauser M, Winkler D, et al. Global decrease of serotonin-1A receptor binding after electroconvulsive therapy in major depression measured by PET. *Mol Psychiatry*. 2012;In Press. doi:10.1038/mp.2012.93.
39. Bauer M, Bschor T, Pfennig A, Whybrow PC, Angst J, Versiani M, et al. World Federation of Societies of Biological Psychiatry (WFSBP) Guidelines for Biological Treatment of Unipolar Depressive Disorders in Primary Care. *World J Biol Psychiatry*. 2007;8:67-104.
40. Wadsak W, Mien LK, Ettliger DE, Lanzenberger R, Haeusler D, Dudczak R, et al. Simple and fully automated preparation of [carbonyl-11C]WAY-100635. *Radiochimica Acta*. 2007;95:417-22.
41. Casey M. Point spread function reconstruction in PET. Siemens Molecular Imaging; 2007.
42. Nics L, Hahn A, Zeilinger M, Vraka C, Ungersboeck J, Haeusler D, et al. Quantification of the radio metabolites of the serotonin-1A receptor radioligand [carbonyl-11C]WAY-100635 in human plasma: An HPLC-assay allowing two parallel patients. *Appl Radiat Isotopes*. 2012;Submitted.
43. Parsey R, Slifstein M, Hwang DR, Abi-Dargham A, Simpson N, Mawlawi O, et al. Validation and reproducibility of measurement of 5-HT1A receptor parameters with [carbonyl-11C]WAY-100635 in humans: comparison of arterial and reference tissue input functions. *J Cereb Blood Flow Metab*. 2000;20:1111-33.
44. Gunn RN, Sargent PA, Bench CJ, Rabiner EA, Osman S, Pike VW, et al. Tracer kinetic modeling of the 5-HT1A receptor ligand [carbonyl-11C]WAY-100635 for PET. *Neuroimage*. 1998;8:426-40.

45. Stein P, Savli M, Wadsak W, Mitterhauser M, Fink M, Spindelegger C, et al. The serotonin-1A receptor distribution in healthy men and women measured by PET and [carbonyl-11C]WAY-100635. *Eur J Nucl Med Mol Imaging*. 2008;35:2159-68.
46. Fink M, Wadsak W, Savli M, Stein P, Moser U, Hahn A, et al. Lateralization of the serotonin-1A receptor distribution in language areas revealed by PET. *Neuroimage*. 2009;45:598-605.
47. Rousset OG, Ma Y, Evans AC. Correction for partial volume effects in PET: principle and validation. *J Nucl Med*. 1998;39:904-11.
48. Parsey RV, Arango V, Olvet DM, Oquendo MA, Van Heertum RL, John Mann J. Regional heterogeneity of 5-HT_{1A} receptors in human cerebellum as assessed by positron emission tomography. *J Cereb Blood Flow Metab*. 2005;25:785-93.
49. Innis RB, Cunningham VJ, Delforge J, Fujita M, Gjedde A, Gunn RN, et al. Consensus nomenclature for in vivo imaging of reversibly binding radioligands. *J Cereb Blood Flow Metab*. 2007;27:1533-9.
50. Hirvonen J, Kajander J, Allonen T, Oikonen V, Nagren K, Hietala J. Measurement of serotonin 5-HT_{1A} receptor binding using positron emission tomography and [carbonyl-(11)C]WAY-100635-considerations on the validity of cerebellum as a reference region. *J Cereb Blood Flow Metab*. 2007;27:185-95.
51. Ichise M, Liow JS, Lu JQ, Takano A, Model K, Toyama H, et al. Linearized reference tissue parametric imaging methods: application to [11C]DASB positron emission tomography studies of the serotonin transporter in human brain. *J Cereb Blood Flow Metab*. 2003;23:1096-112.
52. Hahn A, Lanzenberger R, Wadsak W, Spindelegger C, Moser U, Mien L-K, et al. Escitalopram enhances the association of serotonin-1A autoreceptors to heteroreceptors in anxiety disorders. *J Neurosci*. 2010;30:14482-9.
53. Byrtek M, O'Sullivan F, Muzi M, Spence AM. An adaptation of ridge regression for improved estimation of kinetic model parameters from PET studies. *IEEE T Nucl Sci*. 2005;52:63-8.

54. Ogden RT, Zanderigo F, Choy S, Mann JJ, Parsey RV. Simultaneous estimation of input functions: an empirical study. *J Cereb Blood Flow Metab.* 2010;30:816-26.
55. Knausl B, Hirtl A, Dobrozemsky G, Bergmann H, Kletter K, Dudczak R, et al. PET based volume segmentation with emphasis on the iterative TrueX algorithm. *Z Med Phys.* 2012;22:29-39.
56. Mourik JE, Lubberink M, Klumpers UM, Comans EF, Lammertsma AA, Boellaard R. Partial volume corrected image derived input functions for dynamic PET brain studies: methodology and validation for [11C]flumazenil. *Neuroimage.* 2008;39:1041-50.
57. Liptrot M, Adams KH, Martiny L, Pinborg LH, Lonsdale MN, Olsen NV, et al. Cluster analysis in kinetic modelling of the brain: a noninvasive alternative to arterial sampling. *Neuroimage.* 2004;21:483-93.
58. Zanotti-Fregonara P, Maroy R, Peyronneau MA, Trebossen R, Bottlaender M. Minimally invasive input function for 2-(18)F-fluoro-A-85380 brain PET studies. *Eur J Nucl Med Mol Imaging.* 2012;39:651-9.

TABLES

Table 1

Subject	Changes before vs after ECT across ROIs [% difference]				
	MRTM2	IDIF+VIF OSEM+PVC		IDIF+VIF TrueX	
	BP _{ND}	BP _{ND}	BP _P	BP _{ND}	BP _P
1	-28.06 ± 4.76	-35.19 ± 9.28	-28.76 ± 10.20	-54.58 ± 6.96	-29.15 ± 10.85
2a	-23.12 ± 3.89	-22.99 ± 4.42	-29.08 ± 4.07	-19.68 ± 6.04	-26.04 ± 5.56
3	47.25 ± 6.09	-2.47 ± 6.14	6.56 ± 6.70	-46.81 ± 5.84	16.53 ± 12.80

Percentage change (mean±SD) of serotonin-1A receptor (5-HT_{1A}) binding before vs. after electroconvulsive therapy (ECT). Binding potentials (BP_{ND}) were obtained from the multilinear reference tissue model 2 (MRTM2 [51]) and the combination of image-derived and venous input functions (IDIF+VIF) using TrueX and OSEM image reconstructions (the latter followed by partial volume correction (OSEM+PVC)). Binding potentials relative to total radioligand in plasma (BP_P) are given for comparison. Input function modelling confirms a decrease in 5-HT_{1A} BP_{ND} and BP_P after ECT [38]. Interestingly, MRTM2 shows an increase in 5-HT_{1A} BP_{ND} for subject 3, whereas OSEM+PVC yields almost no change but TrueX gives a decrease. In contrast, BP_P values were more consistent for IDIFs obtained from the two image reconstructions algorithms.

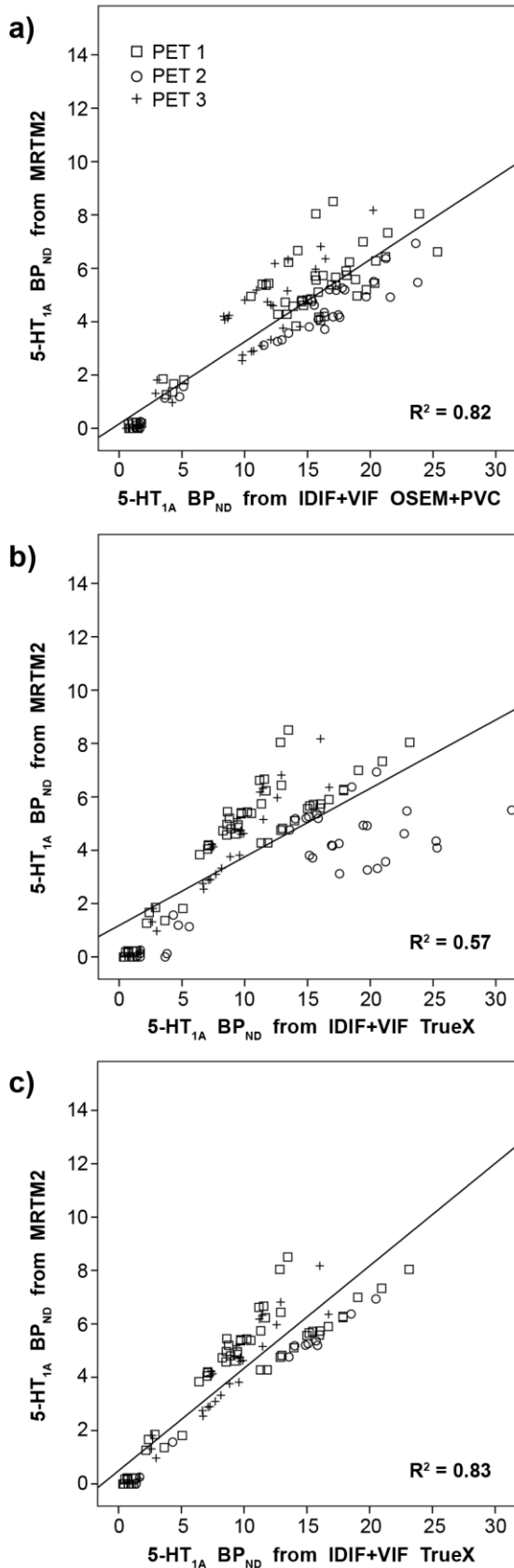
Table 2

Subject	Test-retest variability across ROIs [absolute % difference]				
	MRTM2	IDIF+VIF OSEM+PVC		IDIF+VIF TrueX	
	BP _{ND}	BP _{ND}	BP _P	BP _{ND}	BP _P
1	13.89 ± 2.66	14.87 ± 5.56	10.38 ± 5.57	25.24 ± 3.72	2.65 ± 2.78
2b	14.96 ± 6.32	3.56 ± 3.51	30.28 ± 5.00	12.12 ± 5.34	35.64 ± 5.18
3	21.21 ± 6.80	20.77 ± 3.47	35.57 ± 3.40	93.90 ± 5.98	20.34 ± 7.45

Percentage test-retest variability (absolute values, mean±SD) of serotonin-1A receptor (5-HT_{1A}) binding comparing two PET scans before electroconvulsive therapy (ECT). Variability in 5-HT_{1A} BP_{ND} using OSEM+PVC was comparable to MRTM2. In contrast, with TrueX reconstruction the BP_{ND} variability was considerably higher for 1 of the 3 subjects. Similar to ECT-induced changes (table 1), BP_P values were more consistent for IDIFs determined by the two different image reconstruction algorithms. For details on variable description see table 1. Subject 2b does not correspond to subject 2a in table 1 (because of availability of blood samples) but is named similarly for simplicity.

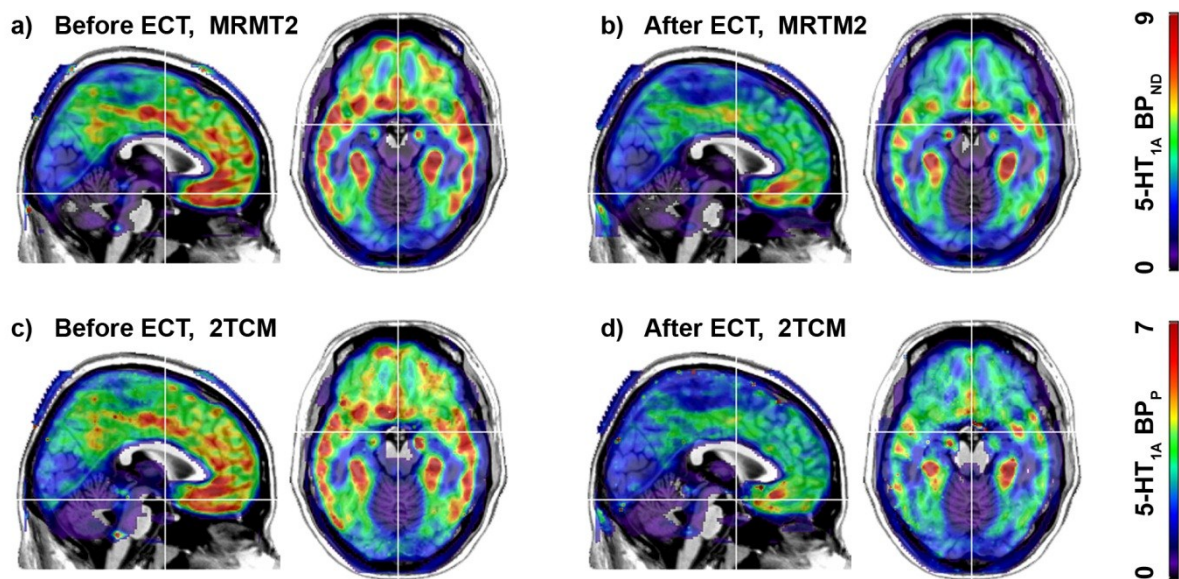
FIGURES

Figure 1



Comparison of serotonin-1A (5-HT_{1A}) receptor binding potentials (BP_{ND}) obtained from the combination of image-derived and venous input functions (IDIF+VIF) and the multilinear reference tissue model 2 (MRTM2 [51]). **a)** Extracting IDIFs from OSEM reconstruction followed by partial volume correction (OSEM+PVC) shows similar agreement ($R^2=0.82$) and bias (slope=0.31, intercept=0.17) as reported previously [37]. **b)** In contrast, IDIFs from TrueX reconstruction yields weaker agreement and considerable increased bias ($R^2=0.57$, slope=0.26, intercept=1.18). **c)** Excluding two subjects would resolve the mismatch for IDIFs obtained by TrueX ($R^2=0.83$, slope=0.38, intercept=0.5). Symbols represent the PET scans at baseline (PET 1), before (PET 2) and after ECT (PET 3). Multiple symbols indicate different regions of interest.

Figure 2



Serotonin-1A (5-HT_{1A}) receptor binding potentials from a representative patient (subject 2a in table 1). Voxel-wise maps were computed with **a-b)** the multilinear reference tissue model 2 (MRTM2 [51], BP_{ND}) and **c-d)** the 2-tissue compartment model with ridge regression (2TCM [53], BP_P). For the latter the combination of image-derived and venous input function was used as obtained from OSEM image reconstruction with subsequent partial volume correction (OSEM+PVC). The two models yield similar maps (**a-c** and **b-d**) and show a marked decrease of 5-HT_{1A} binding after electroconvulsive therapy (ECT, **b-d** vs. **a-c**). Note the different scaling of BP_{ND} (**a-b**) and BP_P (**c-d**) due to the different underlying calculations [49]. Crosshair at $x/y/z=1/0/-16\text{mm}$ MNI-space.

APPENDIX A – CURRICULUM VITAE

Andreas Hahn, MSc.
Functional, Molecular & Translational Neuroimaging Lab
Department of Psychiatry and Psychotherapy, Medical University of Vienna, Austria
<http://www.meduniwien.ac.at/neuroimaging/>
Phone: +43 1 40400 3825
Mobile: +43 650 2272742
Email: andreas.hahn@meduniwien.ac.at

Curriculum Vitae



Personal Data

Date & place of birth:	13 th February 1983, Vienna, Austria
Citizenship:	Austrian
Academic degree:	Master of Science in Engineering, MSc.
Community service:	Oct. 2002 – Sept. 2003, Austrian Red Cross
Current position:	Research associate/PhD-student Functional, Molecular and Translational Neuroimaging Lab Dept. of Psychiatry and Psychotherapy, Medical University of Vienna, Austria

Education

since Oct. 2008	Medical University of Vienna , Austria Doctoral program Clinical Neurosciences
Dec. 2007 until June 2008	Medical University of Vienna , Austria Dept. of Psychiatry and Psychotherapy Functional, Molecular & Translational Neuroimaging Lab – PET & fMRI Master's thesis: ROI-based comparison of molecular & functional data in multimodal neuroimaging using PET & fMRI
2006 – 2008	University of Applied Sciences Technikum Wien , Austria Masters's program Biomedical Engineering Sciences
Feb. – June 2006	Helsinki University of Technology , Finland Laboratory of Biomedical Engineering Bachelor's thesis: Detection of Dipyridamole induced myocardial ischemia with BSPM and MCG
Feb. – July 2005	Universidad Politécnic de Valencia , Spain Exchange semester Further courses in biomedical engineering
2003 – 2006	University of Applied Sciences Technikum Wien , Austria Bachelor's program Biomedical Engineering Bachelor's thesis: Evaluation of X-Ray CT's role in nuclear medical diagnostic; EEG for research & clinical application

Professional Experience

since Dec. 2007	Medical University of Vienna , Austria Dept. of Psychiatry and Psychotherapy Functional, Molecular & Translational Neuroimaging Lab – PET & fMRI Head: Prof. PD Dr. Rupert Lanzenberger Data processing and statistics, manuscript preparation, algorithm development
-----------------	--

Professional Experience (cont'd)

Feb. – Nov. 2007	University of Applied Sciences Technikum Wien , Austria Biomedical Engineering Sciences, Respiration laboratory Development and implementation of measurement techniques
Oct. – Dec. 2006 & Oct. – Dec. 2005	University of Applied Sciences Technikum Wien , Austria Tutor for basics in programming with C++
Feb. – Aug. 2006	Helsinki University of Technology , Finland Laboratory of Biomedical Engineering ECG und MCG data analysis, preparation for publication
July 2004 & Aug. 2005	Carl Reiner GmbH, Medical Instruments , Vienna, Austria Maintenance of respiration equipment, implementation of statistical analysis, measurements with respiration prototype

Special Training & Courses

June 10 th 2012	The Connectome – Educational Course 18 th OHBM Annual Meeting, Beijing, China
11 th – 22 nd July 2011	Neuroimaging Training Program Summer School University of California Los Angeles, California, USA
25 th May 2011	Scanners, Tracers and Quantification – Educational Course Preclinical and Clinical Applications – Educational Course 10 th BrainPET Conference, Barcelona, Spain
18 th – 21 st July 2010	PET Pharmacokinetics Course Drymen, Loch Lomond, Scotland, UK
31 st May - 4 th June 2010	fMRI Analysis Workshop with AFNI & SUMA CNR Research Campus, University of Pisa, Italy
23 rd June 2009	Advanced fMRI – Educational Course 15 th OHBM Annual Meeting, San Francisco, California, USA
27 th - 28 th March 2009	PMOD Training Workshop Zürich, Switzerland
10 th - 12 th Oct. 2008	Experimental Design and Practical Data Analysis in Positron Emission Tomography MRC Clinical Science Center, Imperial College London, UK

Additional Skills

Computer	Matlab, SPM, PMOD, AFNI & SUMA, FSL, MRIcro, Linux, C, C++, VBA, OrCad, SPSS, Adobe Photoshop, MS Office
Languages	German – native English – fluent Spanish – fluent Finnish – basic knowledge
Basic training in radiation protection; trained paramedic	

Grants & Fellowships: 4 projects, € 488,857

Principal investigator: 2 projects, € 63,000

Austrian Academy of Sciences (OeAW), Doctoral thesis fellowship (DOC): € 60,000

Jan. 2011 – Dec. 2013

Optimized non-invasive quantification of neuronal receptors in healthy condition and psychiatric disorders using positron emission tomography

Medical University of Vienna, Research grant: € 3,000

July – Dec. 2008

Multimodal Imaging: combining molecular and functional data as integrative analysis method

Co-investigator: 2 projects, € 425,857

Austrian Science Fund (FWF P24359): € 263,650

2012 – 2014

Influence of light exposure on cerebral monoamine oxidase A in seasonal affective disorder and healthy controls measured by PET

Austrian Science Fund (FWF P22981): € 162,207

2011 – 2013

Norepinephrine Transporter in Attention Deficit Hyperactivity Disorder investigated with PET

Honours & Awards

Researcher of the Month, Medical University of Vienna, Austria, Nov. 2012

Travel award ECNP Congress, Oct. 2012

Travel grant OeFG for NRM Congress, Aug. 2012

Travel grant OeFG for BrainPET and WFSBP Conferences, Mai/June 2011

Young scientists award “Alpenländerpreis” OeGN, DGN & SGNM, April 2011

PMOD beta-tester, since Dec. 2010

Research award in clinical psychiatry OeGPB, Nov. 2010

Best poster award (Nexus Scotland) NRM Congress, July 2010

Young investigator award (GSK) NRM Congress, July 2010

Travel grant OeFG for NRM Congress, July 2010

Erasmus mobility grant, AFNI & SUMA Workshop, June 2010

Travel award ECNP Congress, Sept. 2009

Young scientists award ECNP Congress, Sept. 2009

Associate membership ECNP, 2009-2013

Young scientists award WFSBP Congress, June/July 2009

Travel grant Pfizer for HBM Conference, June 2009

Travel grant OeFG for HBM Conference, June 2009

Travel grant ECNP Workshop, March 2009

Young scientists award OeGBMT, Master's Thesis, Nov. 2008

Master's degree with outstanding success, June 2008

Scholarship for excellent academic achievements within 2006/2007

Bachelor's degree with outstanding success, June 2006

Leonardo da Vinci mobility grant, February – May 2006

Exchange Scholarship Lower Austria, February – June 2005

Erasmus mobility grant, February – June 2005

Scholarship for excellent academic achievements within 2003/2004

University entrance examination with outstanding success, June 2002

List of Publications & Scientific Activities

Peer Reviewed Journals (accumulated IF: 88.802)

Hahn A., Wadsak W., Windischberger C., Baldinger P., Höflich AS., Losak J., Nics L., Philippe C., Kranz GS., Kraus C., Mitterhauser M., Karanikas G., Kasper S., Lanzenberger R. 2012. Differential modulation of self-referential processing in the default mode network via serotonin-1A receptors. *Proc Natl Acad Sci USA* 109(7): 2619-2624 [2011, IF: 9.681].

Hahn A., Lanzenberger R., Spindelegger C., Moser U., Mien L.-K., Mitterhauser M., Wadsak W., Kasper S. 2010. Escitalopram enhances the association of serotonin-1A auto- to heteroreceptors in anxiety disorders. *Journal of Neuroscience* 30 (43): 14482-89. [2011, IF:7.115].

Hahn A.*, Nics L.*, Baldinger P., Ungersböck J., Dolliner P., Frey R., Birkfellner W., Mitterhauser M., Wadsak W., Karanikas G., Kasper S., Lanzenberger R. 2012. Combining image-derived and venous input functions enables quantification of serotonin-1A receptors with [*carbonyl*-¹¹C]WAY-100635 independent of arterial sampling. *NeuroImage* 62 (1):199-206. [2011, IF: 5.895] *Contributed equally.

Hahn A.*, Stein P.*, Windischberger C., Weissenbacher A., Spindelegger C., Moser E., Kasper S., Lanzenberger R. 2011. Reduced resting state functional connectivity between amygdala and orbitofrontal cortex in social anxiety disorder. *NeuroImage* 56: 881-889. [2011, IF: 5.895] *Contributed equally.

Hahn A., Nics L., Baldinger P., Wadsak W., Savli M., Kraus C., Birkfellner W., Ungersböck J., Haeusler D., Mitterhauser M., Karanikas G., Kasper S., Frey R., Lanzenberger R. 2012. Clinical application of image-derived and venous input functions in major depression using [*carbonyl*-¹¹C]WAY-100635. *Eur J Nucl Med Mol Imaging* Submitted.

Lanzenberger R., Baldinger P., **Hahn A.**, Haeusler D., Mitterhauser M., Winkler D., Micskei Z., Stein P., Karanikas G., Wadsak W., Kasper S., Frey R. 2012. Global decrease of serotonin-1A receptor binding after electroconvulsive therapy in major depression revealed by PET. *Molecular Psychiatry* In Press [2011, IF: 13.668].

Kranz GS. **Hahn A.**, Savli M., Lanzenberger R. 2012. Challenges in the differentiation of midbrain raphe nuclei in neuroimaging. *Proc Natl Acad Sci USA* Epub 18th June 2012 [2011, IF: 9.681].

Kraus C., **Hahn A.**, Savli M., Kranz G., Baldinger P., Höflich A.S., Spindelegger C., Ungersboeck J., Haeusler D., Mitterhauser M., Windischberger C., Wadsak W., Kasper S., Lanzenberger R. 2012. Neuroplasticity is mediated by the serotonin-1A receptor as revealed by multimodal neuroimaging in human adults. *NeuroImage* In Press [2011, IF: 5.895].

Savli M., Bauer A., Mitterhauser M., Ding Y.-S., **Hahn A.**, Kroll T., Neumeister A., Haeusler D., Ungersböck J., Henry S., Isfahani SA., Rattay F., Wadsak W., Kasper S., Lanzenberger R. 2012. Normative database of the serotonergic system in healthy subjects using multi-tracer PET. *NeuroImage* In Press [2011, IF: 5.895].

Lanzenberger R., Kranz GS., Haeusler D., Akimova E., Savli M., **Hahn A.**, Mitterhauser M., Spindelegger C., Philippe C., Fink M., Wadsak W., Karanikas G., Kasper S. 2012. Prediction of SSRI treatment response in major depression based on serotonin transporter interplay between median raphe nucleus and projection areas. *NeuroImage* In Press [2011, IF: 5.895].

Fink M., Wadsak W., Savli M., Stein P., Moser U., **Hahn A.**, Mien L.-K., Kletter K., Mitterhauser M., Kasper S., Lanzenberger R. 2008. Lateralization of serotonin-1A receptor distribution in language areas with regards to sex and testosterone. *NeuroImage* 45 (2): 598-605. [2011, IF: 5.895].

Witte, AV., Flöel A., Stein P., Savli M., Mien L.-K., Wadsak W., Spindelegger C., Moser U., Fink M., **Hahn A.**, Mitterhauser M., Kletter K., Kasper S., Lanzenberger R. 2008. Aggression is related to frontal serotonin-1A receptor distribution revealed by positron emission tomography. *Human Brain Mapping* 30 (8): 2558-70. [2011, IF 5.880].

Lanzenberger R., Wadsak W., Spindelegger C., Mitterhauser M., Akimova E., Mien L.-K., Fink M., Moser U., Savli M., Kranz GS., **Hahn A.**, Kletter K., Kasper S. 2010. Cortisol plasma levels in social anxiety disorder patients correlate with serotonin-1A receptor binding in limbic brain regions. *The International Journal of Neuropsychopharmacology*. 13 (9): 1129-43. [2011, IF: 4.578].

Spindelegger C., Stein P., Wadsak W., Fink M., Mitterhauser M., Moser U., Savli M., Mien L.-K., Akimova E., **Hahn A.**, Willeit M., Kletter K., Kasper S., Lanzenberger R. 2011. Light-dependent alteration of serotonin-1A receptor binding in cortical and subcortical limbic regions in the human brain. *World Journal of Biological Psychiatry* Epub ahead of print (23rd Nov 2011). [2011, IF 2.385]

Fink M., Akimova E., Spindelegger C., **Hahn A.**, Lanzenberger R., Kasper S. 2009. Social Anxiety Disorder: Epidemiology, Biology and Treatment. *Psychiatria Danubina* 21 (4): 533-542. [2011, IF 0.444]

Kranz GS., **Hahn A.**, Baldinger P., Haeusler D., Philippe C., Kaufmann U., Wadsak W., Savli M., Höflich AS., Kraus C., Vanicek T., Mitterhauser M., Kasper S., Lanzenberger R. 2012. Cerebral serotonin transporter asymmetry in males and male-to-female transsexuals. *Brain Structure and Function* Submitted.

Nics L., **Hahn A.**, Zeilinger M., Vranka C., Ungersboeck J., Haeusler D., Hartmann S., Wagner K-H., Dudczak R., Lanzenberger R., Wadsak W., Mitterhauser M. 2012. Quantification of the radio metabolites of the serotonin-1A receptor radioligand [*carbonyl*-¹¹C]WAY-100635 in human plasma: A HPLC-assay allowing two parallel patients. *Applied Radiation and Isotopes* Submitted.

Höflich A., Moser U., Savli M., **Hahn A.**, Hofer-Irmler I., Kasper S., Lanzenberger R. 2010. Bildgebung in der Psychiatrie. *CliniCum neuropsy* 4/2010.

Invited Talks

Research award session, **12th OeGPB Conference**, Nov. 2010, Vienna.

Escitalopram enhances the association of serotonin-1A auto- to heteroreceptors in anxiety disorders.

Poster award session, **8th NRM Congress** July 2010, Glasgow.

Escitalopram enhances associations of pre-postsynaptic but not post-postsynaptic serotonin-1A receptor binding in anxiety disorders.

Young scientists award symposium **22nd ECNP Congress**, Sept. 2009, Istanbul.

Serotonin-1A Receptor Binding Potential in Dorsal Raphe Nuclei Predicts Orbitofrontal Reactivity in Healthy Subjects.

Oral Presentations

Oral session, **9th NRM Congress**, August 2012, Baltimore.

Serotonin-1A receptor-dependent modulation of the default mode network.

Oral session, **Winter Symposium of Biological Psychiatry**, March 2012, Oberlech.

Influence of the serotonin-1A receptor on the default mode network [in German].

Oral session, **11th ÖGfMRI Symposium**, Dec. 2011, Vienna.

Neuronal networks in psychiatric disorders [in German].

Free communication, **10th WFSBP Congress**, May/June 2011, Prague.

Reduced serotonin transporter association between raphe region and ventral striatum in major depressive disorder

Oral session, **XXVth ISCBFM & Xth BrainPET Conference**, May 2011, Barcelona.

Substitution of arterial blood-based quantification by combining image-derived input functions with venous blood data in neuroimaging with [*carbonyl*-¹¹C]WAY-100635.

Oral session, **Winter Symposium of Biological Psychiatry**, March 2011, Oberlech.

Pre- and postsynaptic serotonin-1A receptors under escitalopram therapie [in German].

Free communication, **19th EPA Conference**, March 2011, Vienna.

Attenuated serotonin transporter association between midbrain and nucleus accumbens in major depression.

Oral session **6th YSA Symposium**, June 2010, Vienna.

Alterations of the amygdalar functional connectivity network in patients with anxiety disorders.

Young scientists award session **9th WFSBP Congress**, June/July 2009, Paris.

Amygdala hyperactivity in social anxiety disorder induced by facial attractiveness.

Oral session **5th YSA Symposium**, June 2009, Vienna.

Serotonin-1A Receptor Binding Potential in Dorsal Raphe Nuclei Predicts Orbitofrontal Reactivity in Healthy Subjects.

Junior speaker **ECNP Workshop for Young Scientists**, March 2009, Nice.

Serotonin-1A Receptor Binding Potential in Dorsal Raphe Nuclei Predicts Orbitofrontal Reactivity in Healthy Subjects.

Thesis Supervision & Teaching

Oct. 2011 – May 2012

Sebastian GANGER, **Master's thesis and internship**

Resting state and task specific connectivity assessed with functional MRI

Nov. 2011 – May 2012

Raquel SOLÁ, **Master's thesis**

Evaluation of metabolic connectivity in temporal lobe epilepsy using [¹⁸F]FDG

April 2011 – Oct. 2011

Sylvia ZGUD, **Diploma thesis**

Serotonin-1A receptor distribution in pre- and postmenopausal women quantified by PET and [¹¹C]WAY

International Peer Review

Neuropsychopharmacology

Psychoneuroendocrinology

International Journal of Neuropsychopharmacology

Brain Connectivity

Conference Boards

Program committee member, 13th OeGPB Conference, Nov. 2011

Conference Participation

18th HBM Conference, June 2012, Beijing, China.

Winter Symposium of Biological Psychiatry, March 2012, Oberlech, Austria.

11th OeGfMRI Symposium, Dec. 2011, Vienna, Austria.

13th OeGPB Conference, Nov. 2011, Vienna, Austria.

7th PhD Symposium Medical University of Vienna, June 2011, Vienna, Austria

10th WFSBP Congress, May/June 2011, Prague, Czech Republic.

10th BrainPET Conference, May 2011, Barcelona, Spain.

NuklearMedizin 2011, April 2011, Bregenz, Austria.

Winter Symposium of Biological Psychiatry, March 2011, Oberlech, Austria.

19th EPA Congress, March 2011, Vienna, Austria.

12th OeGPB Conference, Nov. 2010, Vienna, Austria.

23rd EANM Congress, Oct. 2010, Vienna, Austria.

8th NRM Congress, July 2010, Glasgow, UK.

6th PhD Symposium Medical University of Vienna, June 2010, Vienna, Austria.

22nd ECNP Congress, Sept. 2009, Istanbul, Turkey.

9th WFSBP Congress, June 2009, Paris, France.

15th HBM Conference, June 2009, San Francisco, CA, USA.

5th PhD Symposium Medical University of Vienna, May 2009, Vienna, Austria.

6th ECNP Workshop for Young Scientists, March 2009, Nice, France.

14. Update in Psychiatrie, May 2008, Vienna, Austria.

3. Wiener Biomaterialsymposium, Nov. 2008, Vienna, Austria.

Abstracts & Conference Proceedings

22 first author, 70 co-author